The Pennsylvania State University

The Graduate School

Intercollege Graduate Degree Program in Materials Science and Engineering

ELECTROCHEMICAL STUDY OF CORROSION PROCESSES IN HIGH SUBCRITICAL AND SUPERCRITICAL AQUEOUS SYSTEMS

A Thesis in

Materials Science and Engineering

by

Xueyong Guan

Submitted in Partial Fulfillment
of the Requirements
for the Degree of

Doctor of Philosophy

May 2007

The thesis of Xueyong Guan was reviewed and approved* by the following:

Digby D. Macdonald
Distinguished Professor of Materials Science and Engineering
Thesis Advisor
Chair of Committee

Long-Qing Chen
Professor of Materials Science and Engineering

Paul R. Howell
Professor of Metallurgy

Fan-Bill Cheung
Professor of Mechanical & Nuclear Engineering

James Runt
Professor of Polymer Science
Chair of Intercollege Graduate Degree Program in Materials Science and Engineering

*Signatures are on file in the Graduate School

ABSTRACT

Severe corrosion damage occurs in high temperature aqueous systems and few materials can withstand these harsh working conditions. In this work, electrochemical emission spectroscopy (EES) is used to identify corrosion mechanisms and to analyze the effect of pressure on corrosion reactions in high subcritical and supercritical aqueous systems.

Two corrosion mechanisms, "chemical oxidation" (CO) and "electrochemical oxidation" (EO), have been proposed to describe the corrosion processes in high temperature aqueous systems, depending upon the density and dielectric constant of the systems. EO corrosion processes are featured by partial charge transfer reactions such as the metal dissolution and the reduction of oxygen. On the other hand, CO processes are dominated by direct molecular processes such as the direct reaction of the metal with aggressive species on one site. EES method is used to differentiate two corrosion mechanisms by postulating that only the electrochemical mechanism gives rise to spontaneous fluctuations in current and potential. Experiments show that the electrochemical mechanism is the dominant corrosion mechanism when the temperatures are below 350 ^{o}C and that it becomes of progressively lower importance as the temperature increases above the critical temperature (T_c = 374.15 ^{o}C). The energy of activation of corrosion of Type 304 SS and titanium in 0.01 M HCl at the temperature range of 50 – 250 ^{o}C has been estimated. The result shows that titanium is more corrosion resistant than Type 304 SS in HCl solution due to the formation of the strong protective passive film on the surface of titanium.

A model is developed to study the effect of pressure on corrosion rates of metals in high temperature aqueous systems, with emphasis on contributions from the activation, the degree of dissociation of aggressive species, and the system isothermal compressibility. EES was applied to estimate the pressure

dependencies of the electrochemical corrosion rates of Type 304 SS and nickel in high temperature HCl solutions. The study shows that the volume of activation of corrosion processes is pressure dependent in high temperature aqueous systems. And the magnitude of the volume of activation decreases with increasing pressure in both high subcritical and supercritical conditions. The contribution from the volume of activation plays a dominant role on the relative dissociation is found to be more important to the relative corrosion rate at supercritical conditions.

TABLE OF CONTENTS

LIST OF FIGURES

LIST OF TABLES

ACKNOWLEDGEMENTS

I would like to thank my advisor, Dr. Digby D. Macdonald for all of his guidance, enthusiasm, and help. I would also like to thank the other members in the committee, namely Dr. Fan-Bill Cheung, Dr. Long-Qing Chen, Dr. Paul R. Howell, and Dr. Earle R. Ryba for their helpful comments and suggestions.

I am grateful to Li Miao for her consistent support and encouragement. Many thanks also go to my friends and colleagues at Penn State, principally Brian & Lisa Edge, Martin & Susan Friedman, Anne Friedman, Sarah Dilts, Chad Eichfeld, Molly Barsic, Brandon Ribic, Mike Ruffin, Paul Cha, NingYu Liu, Rhys Ulerich, Dr. Murry Small, Brian Marx, John, Dr. Z. F. Zhou, and Dr. J. H. Ai.

Most importantly, I would like to thank my family for their unlimited support, encouragement, and love.

Chapter 1

GENERAL INTRODUCTION

1.1. Overview

High temperature water (HTW) has been widely used in many chemical and engineering applications as a reaction medium for chemical synthesis, materials synthesis, biomass processing, and waste destruction due to its unique properties such as nontoxic, high fluidity, low-cost, and easy separation from many products [1,2]. For example, supercritical water oxidation (SCWO) is a promising technology for destroying highly toxic organic waste (including physiological agents) and for reducing the volume of low-level nuclear waste. The essence of SCWO is that the waste is heated with water to the temperature up to 600 ^{o}C at a pressure of 500 bar in the presence of a high fugacity of oxygen and/or concentration of hydrogen peroxide. The final products of SCWO are simple nontoxic compounds. The SCWO process offers a number of advantages over other wastes destruction technologies, such as high destruction efficiencies and zero emissions to the environment. However, the harsh working environments of those high temperature aqueous systems can be very aggressive toward reactor fabrication materials and lead to mass corrosion that few materials can withstand [3,4]. For instance, if the wastes in SCWO contain heteroatoms, such as sulfur, phosphorous, and chlorine, the corresponding inorganic acids will be formed and those highly reactive chemicals would attack reactors severely [5].

1.2 Corrosion in High Subcritical and Supercritical Aqueous Systems

Corrosion of metals in high subcritical and supercritical aqueous systems (SCAS) highly correlates with the properties of SCAS such as density, dielectric constant, and degree of dissociation of attacking species. The density of high temperature water (HTW) exists between those of gas-like values and liquid-like values. For example, $\rho = 0.6255$ g·cm^{-3} at T = 350 ^{o}C, P = 250 bar and $\rho =$ 0.0897 g·cm^{-3} at T = 500 ^{o}C, P = 250 bar. The change of the dielectric constant of high temperature water corresponds to the density change in a way that the dielectric constant decreases with increasing temperature and decreasing density. Strong electrolytes (such as HCl and H_2SO_4) under the ambient conditions may become only partially ionized in low-density supercritical aqueous systems due to the low dielectric constant. Consequently, the corrosion of metals in high temperature aqueous systems is significantly influenced by the working temperature and pressure of the systems.

Passive films are reaction-produced films formed on the metal/alloy surfaces to protect underlying metals from corrosive environments. Corrosion resistance of metals highly depends on the stability, structure, and thickness of the passive films because the films may block the movement of charges carriers during transient coupling processes. Moffat et al [6]. reported that the corrosion rate of Fe-Cr alloy decreases with increasing thickness of chromium oxide passive film due to the exponentially decreasing of electron-transfer rate. Because of the harsh working conditions, the dissolution of passive films in high temperature aqueous systems can be fast and a high corrosion rate is expected in SCAS [7]. In addition, the transpassive dissociation of passive films in high temperature aqueous systems such as $2Cr^{3+} + 7H_2O \rightarrow Cr_2O_7^{2-} + 14H^+ + 6e^-$ further degrades the protective character of the films [8]. Strong acids (H^+) or bases (OH^-) are formed in high subcritical aqueous systems due to the relatively high density and high dielectric constant. Therefore, the high corrosion rate is

expected because of the high solubility of protective passive films in the high subcritical systems. On the other hand, electrochemical corrosion rate is low in supercritical aqueous systems due to the low dielectric constant and low degree of dissociation of aggressive species.

Fe based austenitic Stainless Steel, Ni-based Inconels, and Ti-based alloys are the most commonly used alloys as the reactor fabrication materials for the high temperature aqueous systems. Experiments demonstrate that it is almost impossible for a single metal/alloy material to sustain all existing aggressive high temperature aqueous systems. A specific alloy may possess acceptable corrosion resistance for one type of solution, but it is unacceptable for different types of solutions. For instance, titanium exhibits a high corrosion resistance against high temperature oxidizing HCl. However, it shows a low corrosion resistance in H_2SO_4 and H_3PO_4 at temperatures above 400 ^oC [9].

Stainless steel alloys show a fairly good corrosion resistance in deionized water at temperature range of 300 - 500 ^oC. However, severe corrosion has been observed when they were exposed to high temperature acidic solutions, such as the corrosion rate of Type 316 SS can reach to a few dozen mmpy in 0.5 m HCl at supercritical conditions [10]. Drews et al. reported that the most severe corrosion of Type 316 SS in HCl solutions happens at the high subcritical temperature range with the pitting corrosion in dominant [10].

Nickel based alloys are probably the most studied alloys for high temperature applications due to its extensive usage. Nickel based alloys such as Alloy 625 (minimum Ni 58%) and C-276 (Ni 57%) exhibit high corrosion resistance when exposed to supercritical deionized water (450 ^oC - 500 ^oC) and to high temperature alkaline solutions because of the formation of protective oxide passive films on the surfaces. Kritzer et al [11]. reported that only slight intergranular corrosion (IGC) could be observed on Alloy 625 in HCl solution

when temperatures < 130 ^{o}C. Cl^{-} induced pitting corrosion happens at the temperature range of 250 - 300 ^{o}C. And at even higher temperatures, the entire surface is corroded and general corrosion can be observed due to the transpassive dissolution of protecting oxide passive film. They also reported that the severe corrosion of nickel based alloys happens in high-subcritical temperatures and corrosion is much less significant in the supercritical conditions [11]. IGC has been detected on Alloy 625 in H_2SO_4 solutions at the temperature range of 150 - 200 ^{o}C [12]. At temperatures > 250 ^{o}C, the whole surface are corroded and general corrosion are observed because of the dissolution of protecting oxide passive film in H_2SO_4 solutions. Alloy 625 shows much higher corrosion rate (in the order of 10 magnitudes) in acidic HNO_3 solutions than in HCl and H_2SO_4 solutions due to the enhanced solubility of the corrosion products in nitric acid [13].

Titanium alloys have relatively low corrosion rates (in the order of a few mmpy) when they are exposed in high subcritical and supercritical acidic HCl and H_3PO_4 solutions. On the other hand, severe corrosion could be observed when the titanium alloys are in the supercritical H_2SO_4 solutions [14]. The good corrosion resistance of titanium alloys in high temperature HCl solutions can be attributed to the formation of the protective titanium oxide passive film on titanium surfaces. Experiments show that the passivity characteristics can be observed for titanium alloys in both high subcritical and supercritical HCl solutions [15].

1.3 Corrosion Mechanisms and Kinetics

Because high temperature aqueous systems have properties that range from those that are characteristic of a gas phase at low pressure (low dielectric constant) to those that are characteristic of a condensed liquid phase (moderate density and higher viscosity) at high pressure, two competing corrosion

mechanisms can be envisioned: “chemical oxidation” (CO) and “electrochemical oxidation” (EO) mechanisms, depending upon the density and dielectric constant of the medium. A corrosion process involving partial interfacial charge transfer process, as envisioned by the Wagner-Traud hypothesis [16], in relatively high-density subcritical and supercritical solutions is called an “electrochemical oxidation (EO)” process. Unlike EO mechanism in which corrosion typically involves two or more coupled redox reactions at different sites of corroding metal surfaces, the CO mechanism is a result of direct reactions of metals with aggressive species, such as oxygen, on one site. Discriminating between the two corrosion mechanisms is the key to developing appropriate techniques for corrosion protection of metallic reactors. In those cases where the electrochemical mechanism dominates, various cathodic protection strategies might be effective as corrosion control techniques. On the other hand, if the chemical mechanism dominates, the most effective methods of corrosion control would be to lower the maximum operating temperature and the oxygen fugacity.

Corrosion processes in high subcritical and supercritical aqueous systems (SCAS) highly correlates with the density of solutions, the degree of dissociation of attacking species, and the stability of protective passive film. Those parameters are all influenced by the temperature and pressure of the systems. According to activation complex theory, the rate constant k for an elementary reaction, such as $aA + bB + \cdots \leftrightarrow M^{\neq} \rightarrow$ products, can be expressed by $k = k^0 \exp(-\Delta G^{\neq} / R_g T)$, in which R_g is the gas constant and $\Delta G^{\neq}$ is the free energy of activation [1]. Based on reaction rate law, the corrosion rate can be expressed as $R = k[C_{agre}]$, in which R is the corrosion rate, k is the reaction rate constant, $[C_{agre}]$ is the concentration of aggressive species in the solutions. As both the reaction rate constant and the concentration of aggressive species are function of temperature and pressure, the kinetics of corrosion processes in high

temperature aqueous systems are highly correlated with the working temperature and pressure of the systems.

In summary, the research objectives of this thesis focus on corrosion mechanisms and corrosion kinetics in high subcritical and supercritical aqueous systems. The subsequent chapters are devoted to the following topics:

Chapter 2: Background Study

Chapter 3: The Chemical Properties of High Temperature Aqueous Systems

Chapter 4: Corrosion Mechanisms and Kinetics of Corrosion in High Temperature Aqueous Systems

Chapter 5: Polarization Study and Monitoring Instantaneous Corrosion Rate

Chapter 6: Effect of Pressure on Kinetics of Corrosion of Metals in High Temperature Aqueous Systems

References

1. P. Savage, S. Gopalan, T. Mizan, C. Martino, E. Brock, “Reactions at Supercritical Conditions: Applications and Fundamentals”, *AIChE Journal*, **41**, 1723 (1995)

2. H. Weingartner, E. Franck, “Supercritical Water as a Solvent” *Angew.Chem.Int. Ed*. **44**, 2672 (2005)

3. P. Kritzer, N. Boukis, E. Dinjus, “Corrosion of Alloy 625 in Aqueous Solutions Containing Chloride and Oxygen”, *Corrosion,* **54**, 824 (1998)

4. R. M. Latanision, R. W. Shaw, “Corrosion in supercritical water oxidation systems, Workshop Summary”, MIT The Energy Laboratory, Workshop Summary, Massachusetts Institute of Technology, Boston, MA. (1993)

5. D. D. Macdonald, L.B. Kriksunov, “Probing the chemical and electrochemical properties of SCWO systems” *Electrochimica Acta*, **47**, 775 (2001)

6. T. Moffat, H. J. Yang, F. –F. Fan, and A. Bard, “Electron-transfer reactions on passive chromium” *J. Electrochem. Soc.* **139,** 3158 (1992)

7. L. B. Kriksunov, D. D. Macdonald, “Potential-pH diagrams for iron in supercritical water” *Corrosion* **53**, 605 (1997)

8. P. Kritzer, N. Boukis, E. Dinjus, “Factors controlling corrosion in high-temperature aqueous solutions: a contribution to the dissociation and solubility data influencing corrosion processes” *J. of Supercritical Fluids* **15**, 205 (1999)

9. P. Kritzer, E. Dinjus; “An assessment of supercritical water oxidation (SCWO) existing problems, possible solutions and new reactor concepts” *Chemical Engineering Journal* **83**, 207 (2001)

10. M. J. Drews, M. Williams, and M. Barr; “The corrosion of Sol-Gel-coated type 316 SS in chlorinated SC water” *Ind. Eng. Chem. Res*. **39,** 4772 (2000)

11. P. Kritzer, N. Boukis, and E. Dinjus “Corrosion of alloy 625 in aqueous solutions containing chloride and oxygen” *Corrosion* **54,** 824 (1998)

12. P. Kritzer, N. Boukis, E. Dinjus “Corrosion of alloy 625 in high-temperature, high-pressure sulfate solutions” *Corrosion*, **54, 689** (1998)

13. P. Kritzer, N. Boukis, E. Dinjus “The corrosion of nickel-base alloy 625 in sub- and supercritical aqueous solutions of HNO_3 in the presence of oxygen” *J. of Materials science letters* **18,** 771 (1999)

14. C. Friedrich, P. Kritzer, N. Boukis, G. Franz, E. Dinjus “The corrosion of tantalum in oxidizing sub- and supercritical aqueous solutions of HCl, H_2SO_4 and H_3PO_4” *J. of Materials Science* **34**, 3137 (1999)

15. Ph. Botella, C. Frayret, Th. Jaszay, M. H. Delville; “Experimental study, via current-potential curves, of the anodic behavior of Alloy C-276 and T60 titanium in chlorinated and oxygenated aqueous media under sub- to supercritical conditions” *J. of Supercritical Fluids* **25**, 269 (2003)

16. K. Wagner, W. Traud, Z. *Elektrochem* **44**, 391 (1938)

Chapter 2

BACKGROUND STUDY

2.1 Introduction

Severe corrosion damage occurs in high subcritical and supercritical aqueous systems (SCAS), and few materials can withstand those harsh working conditions. Because the SCAS has properties that range from those that are characteristic of a gas phase at low pressure conditions to those that are characteristic of a liquid phase at high pressure conditions, two competing corrosion mechanisms can be envisioned: “chemical oxidation” (CO) and “electrochemical oxidation” (EO) to describe the corrosion processes in high temperature aqueous systems. Differentiating corrosion mechanisms is the key step in order to develop appropriate techniques for corrosion protection of reactors of high temperature aqueous systems.

The corrosion of SCAS reactor fabrication materials is typically evaluated by surface observation and gravimetric tests. Those methods seldom provide detailed information about corrosion processes, such as corrosion mechanisms (electrochemical vs. chemical), differential corrosion kinetics, and the activation parameters. Electrochemical methods, such as the linear polarization method (LPM), electrochemical impedance spectroscopy (EIS), and electrochemical emission spectroscopy (EES) can be used to study and monitor corrosion processes *in-situ*. A reference electrode is required for the LPM and EIS methods, but may not be required for EES, depending upon the version of the technique adopted, In a recent review of the subject, Macdonald et al. concluded

that no generally applicable, accurate, reference electrode technology for measuring potentials in high subcritical and supercritical aqueous solutions exists at the present time [1].

Before detailed analysis of corrosion mechanisms and corrosion kinetics in high subcritical and supercritical aqueous systems can be carried out, the properties of high temperature water (HTW) has been reviewed in this chapter. Electrochemical emission spectroscopy (EES), as the electrochemical measurement method in this study, has also been introduced in this chapter.

2.2 Properties of High Temperature Water

2.2.1 Overview

Liquid phase and gas phase of water can co-exist at equilibrium conditions. As the working temperature and pressure increasing up to critical point, the density of the liquid phase decreases due to thermal expansion and the density of gas phase increases as the pressure rising. Eventually, when the critical point is reached, the densities of the liquid phase and the gas phase become identical and the differences between the two phases disappear and it is called supercritical water (SCW). A state of SCW at relatively high pressure can be treated as a liquid phase with normal density or gas phase with high density. A state of SCW at relatively low pressure can be treated as a gas phase with normal density or liquid phase with low density. At temperatures higher than the critical temperature, distinct two-phase equilibrium does not exist and thus the gaseous state cannot be liquefied by isothermal compressions at temperatures higher than critical temperature.

Supercritical water (SCW) is widely used as a reaction/transport medium due to its unique properties such as nontoxic, polarity, low-cost, and easy separation from many products. The critical temperature (T_c) of water is 374.15 ^oC, the critical pressure (P_c) is 221 bar, and the critical density is 0.322 $g.cm^{-3}$. Thermodynamically, supercritical fluids are considered to be a state different from the solid, liquid and gaseous states. Because water has only one phase under supercritical conditions, the system has two degrees of freedom based on Gibbs' phase rule. Consequently, the pressure and temperature may be varied independently while maintaining the same single phase under the supercritical conditions.

2.2.2 Hydrogen bonds of high temperature water

As the name "hydrogen bond" implies, one part of a hydrogen bond involves a hydrogen atom. Hydrogen bonds occur when the partially positively charged hydrogen atoms lying between the partially negatively charged elements such as oxygen or nitrogen atoms [2]. The typical hydrogen bond is much weaker than both the ionic bond and the covalent bond [2]. Many important properties of a solvent such as its structure and dielectric constant can be attributed to the hydrogen bonding. A cluster of hydrogen-bonded molecules may exist in a solvent as the hydrogen bonding happened in a form of a network connecting water molecules. At ambient conditions, the structure of water is prevailed with the hydrogen bonds where each molecular is tetrahedrally coordinated to each other [2]. Many unique properties of water such as the high boiling temperature can be attributed to the existence of network of hydrogen bonds [2].

Hydrogen bonds in water are highly sensitive to working temperature and pressure in a way that the tetrahedral network is partially broken in the high temperature working conditions. It is important to estimate to what extent

hydrogen bonding persists in the high temperature water (HTW) to determining other properties of high temperature water such as dielectric constant. Guardia et al. reported that one water molecule has average 3.7 hydrogen bonds at ambient conditions [3]. The value drops to 1.6 bonds per molecule at the temperature of 400 ^{o}C and density of 0.49 g.cm^{-3}. And it diminishes to 0.8 bonds per molecule at the temperature of 500 ^{o}C and density of 0.26 g.cm^{-3}. Mizan et al. observed that the cluster size of high temperature water is less than five molecules per cluster at the low density state($\rho = 0.257$ g.cm^{-3}) as water molecules exist either as small clusters or single entities at the supercritical conditions [4]. Two mechanisms have been proposed by Okada et al. to explain the disruption of hydrogen bonding of water with increasing temperature, i.e. the decreasing of the number of molecules in the first coordination shell with decreasing density and the increasing of thermal agitation activities with increasing temperature [5]. In general, hydrogen bonds exist in a form of small clusters of water molecules in high temperature water. The size of those clusters diminishes with decreasing density and increasing temperature. High temperature water has many different properties from those that of ambient liquid water because of the weakening hydrogen bonding in high temperature conditions. On the other hand, high temperature water still holds some liquid-like properties due to the remaining hydrogen bonds in it.

2.2.3 Density of high temperature water

The density of water at the ambient condition can not be modified easily. However, the density of high temperature water can vary from liquid-like values to gas-like values by changing working temperature and pressure. The density of high temperature water (HTW) exists between those of gas-like values and liquid-like values as shown in Figure 2.1**.** For example, the density is approximately 0.1g·cm^{-3} at 450 ^{o}C and 250 bar and it is comparable to the

density of nitrogen gas at 25 ^{o}C and 100 bar [6]. Therefore, supercritical water can be described as a “dense gas” from the volumetric point of view. The significant drop of the density of high temperature water has dramatically weakened the persistence of hydrogen bonding present in water. It further influences many properties of supercritical water such as dielectric constant, solubility, and diffusion coefficient as those properties highly correlate with the density. As shown in Figure 2.1, the density of high temperature water is a strong function of temperature and pressure in a way that the density of high temperature water decreases with increasing temperature and decreasing pressure.

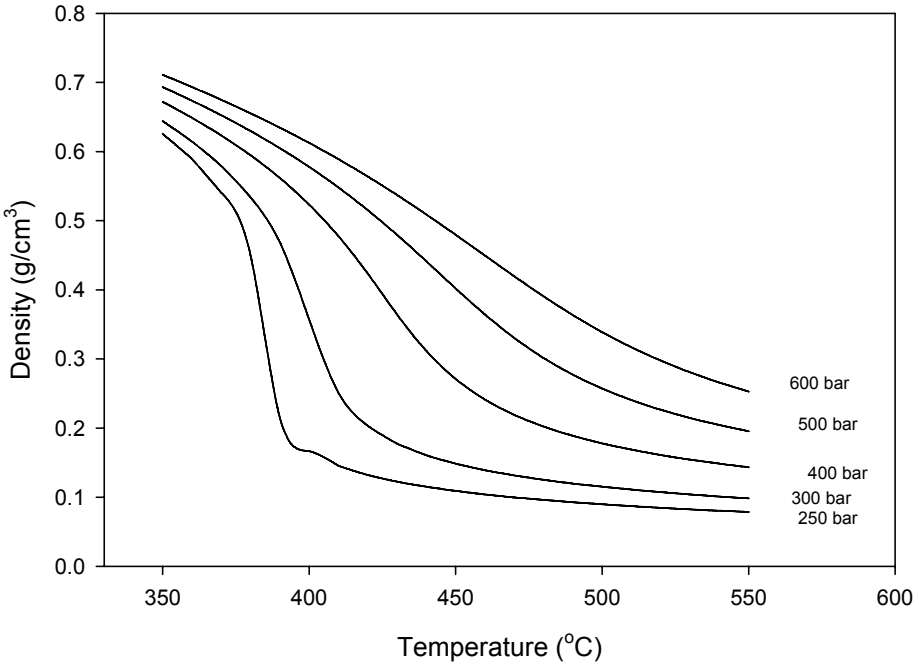

Figure 2.1: Plots of density vs. temperature for high temperature water as a function of pressure

2.2.4 Dielectric constant of high temperature water

The dielectric constant of a solvent is a relative measure of its polarity. The dielectric constant ε of high temperature water (HTW) determines the extent to which ions are stabilized in a condensed medium. Since the solute-solvent electrostatic interactions are prevailing interactions for ionic reactions or polar non-ionic reactions, the dielectric constant has been widely used to indicate the solubility of solvents and the degree of dissociation of electrolytes.

The change of dielectric constant of HTW corresponds to the variation of hydrogen bonding in the way that the dielectric constant decreases with increasing temperature and decreasing density as indicated by Figure 2.2. The dielectric constant of water at ambient conditions (T = 25 ^{o}C, p = 1 atm) is 78 and this relative high value results from preferred dipole orientations in the water structure. This high value allows ionic components such as HCl, H_2SO_4, and NaCl to fully dissolve in the ambient conditions. For relatively high-density HTW, the value of dielectric constant ε is at the range of 10 through 25, such as ε = 21 at T = 300 ^{o}C and ρ =0.75g.cm^{-3}. The values of ε in this range allow both non-polar components miscible and ionic solutes dissolving in the solution. With increasing temperature at constant pressure (decreasing density), the dielectric constant of the supercritical water decreases rapidly to a value that is typical of an organic solvent at low density limit, such as a dielectric constant value of 4.1 at T = 500 ^{o}C and ρ =0.30g.cm^{-3}. Consequently, strong electrolytes under ambient conditions are very poorly ionized and generally exist as contact pairs in low density supercritical water systems, and hence are generally insoluble. On the other hand, many inorganic gases and simple organic compounds that display almost no solubility in water under ambient conditions (e.g. benzene) are fully miscible with water at supercritical temperatures.

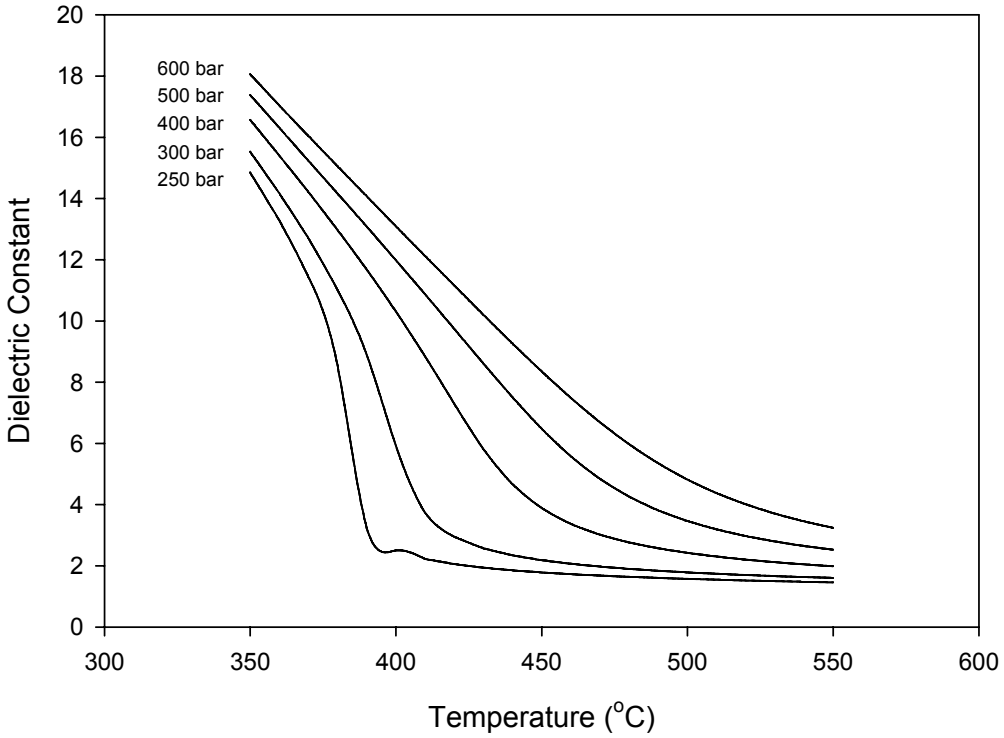

Figure 2.2: Plots of dielectric constant vs. temperature for high temperature water as a function of pressure

Due to the high isothermal compressibility of high temperature water, a small change in pressure would have a big influence on the density of high temperature water and thus influences its dielectric constant. Figure 2.3 displays the dielectric constant of supercritical water as a function of pressure. As shown by the figure, the dielectric constant of high temperature water decreases with decreasing pressure as density decreasing.

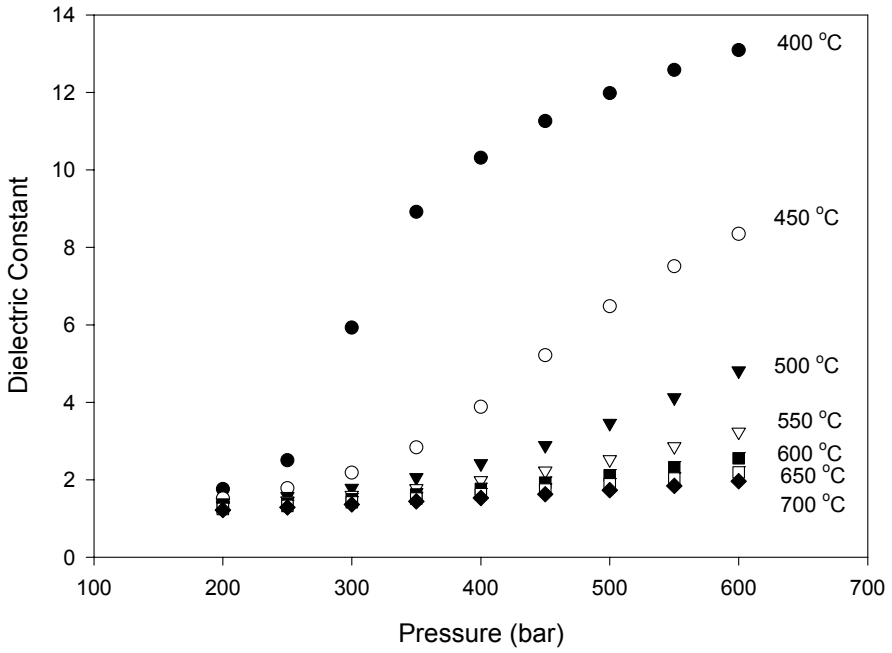

Figure 2.3: Plots of dielectric constant vs. pressure for high temperature water as a function of temperature [6]

2.2.5 Transport coefficients

The transport properties of a medium control the rate of corrodents (e.g. O_2 and H^+) movements in the solvent. Therefore, the maximum corrosion rates for mass transport-controlled corrosion processes are determined by those properties. For dilute ionic solutions, the mass transport diffusion rate can be expressed by the following Stokes-Einstein relation [7],

$$D = \frac{k_B T}{6\pi\eta r} \tag{2.1}$$

where D is the diffusion coefficient of species of interest, η is the dynamic viscosity of the medium, and r is the effective Stokes-Einstein radius.

Weingartner et al.[7,8] suggested that the effective Stokes-Einstein radius is a fairly constant value at densities > 0.322 g.cm^{-3} (critical density). Thus the Walden product can be treated as a constant value in this density range and it is defined as $D\eta =$ constant. As expressed by Walden product, an inversed relationship exists between the diffusion coefficient D and the dynamic viscosity η. It shows that if the viscosity of a medium descends, the diffusivities of interested species and mass transport-controlled reaction rates are expected to increase. On the other hand, the first shell solvent is more strongly attracted to the ion at supercritical conditions (ρ < 0.322 g.cm^3). Therefore, the local viscosity in ion-solvent shell is larger than that in the bulk solution. In addition, the effective Stokes-Einstein radius decreases with decreasing density in the supercritical conditions due to the desolvation. Consequently, a different correlation between the D and η is expected for the low-density gaseous phase (ρ < 0.322 g/cm^3) such as $D\rho/\eta$ =constant [7].

At a constant pressure, the viscosity of a low-density gas-like medium increases slightly as temperature increases, which can be explained by kinetic theory of gases. As for a high-density medium, the η decreases sharply with increasing temperature due to the collosional momentum transfer as indicated by Figure 2.4. It is reported that the viscosity η is roughly independent from the temperature and density at a density range of 0.6 g.cm^{-3} through 0.9 g.cm^{-3} and has a value of one order of magnitude less than its value at the ambient temperature and pressure [7].

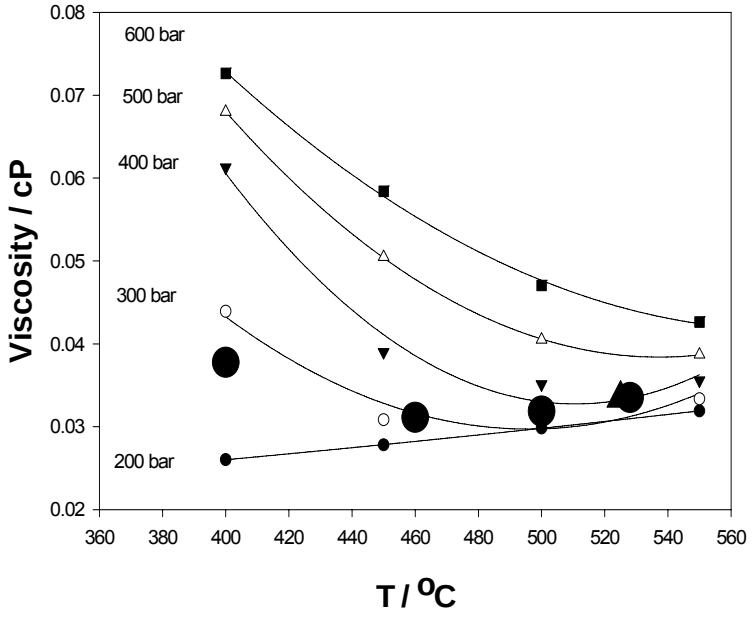

Figure 2.4: Plots of viscosity vs. temperature for supercritical water as a function of pressure. The large filled circles indicate the 0.01 m HCl solution [6]

2.2.6 Degree of dissociation of electrolytes in high temperature water

Liquid water at the ambient conditions has relatively high dielectric constant values. Therefore, it is an excellent solvent for many ionic electrolytes and polar components. On the other hand, water at supercritical conditions, especially at low density, shows low solvation ability for ionic components and high miscibility for non-polar components [9]. Solubility in the high temperature water is depended on the solvation ability of the solvent and on the volatility of the solutes. The solvation ability of a solvent is determined by its ability to

diminish the long-range electrostatic interaction through dielectric screen (dielectric constant), which highly correlates with the density of the solvent. The volatility of solutes corresponds with the working temperatures. Since the density of high temperature water is a strong function of pressure and temperature, a small variation of pressure would influence its solvation abilities. Based on transition state theory, Chialvo et al.[10] suggested that the temperature and density have an opposite impacts on the degree of dissociation of ions in dilute supercritical water such as the degree of dissociation decreases with increasing temperature and decreasing density.

Johnson et al. [11] have predicted the trend of equilibrium dissociation constants of HCl (K_{HCl}) under supercritical working conditions by solving the equilibrium reaction constant, mass balance, and charge balance equations. The analytic results showed that K_{HCl} decreases with decreasing density monotonically in a way that dissociation constant for HCl has dropped by 13 orders of magnitude from 25 ^{o}C to the critical temperature of water at 374.15 ^{o}C. And thus HCl becomes a weaker acid at low density and high temperature supercritical working conditions. The above result has also been confirmed by Mesmer et al. [12]. Figure 2.5 presents the relationship of degree of dissociation of 0.01 m HCl as a function of pressure and temperature. The figure shows that 0.01 m HCl is fully dissociated and is a strong acid when temperatures below 325 ^{o}C. At high subcritical and supercritical conditions, the degree of dissociation of HCl is highly correlated with supercritical water density due to the shielding effect (dielectric constant). As shown by Figure 2.5, the degree of dissociation of HCl decreases with decreasing density as the dielectric constant decreases with the decreasing density. The undissociated HCl exists as pairing ions in supercritical conditions.

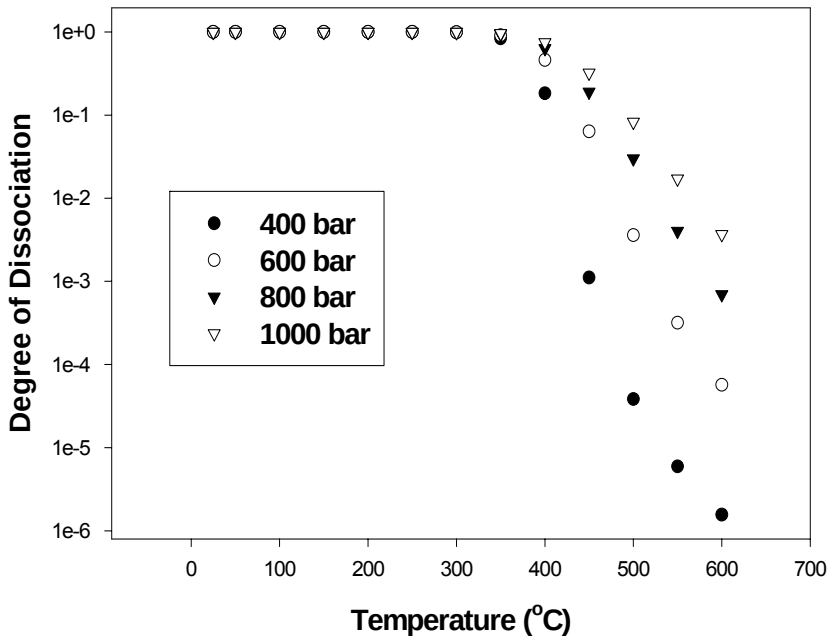

Figure 2.5: Plots of calculated degree of dissociation of 0.01 m HCl as a function of temperature and pressure [6]

2.2.7 Solubility of salts in high temperature aqueous systems

Because of the non-polar properties of supercritical water, salts display low solubility and are readily precipitated as solid phases when supercritical conditions are achieved; this is in contrast with the majority of gas-water and water-organic systems, where in which the components are fully miscible. Salt-water systems can be classified into two types based on whether critical behavior is observed in saturated solutions [47]. Type 1 systems exhibit high salt solubility in the vicinity of the critical temperature of water, whereas Type 2

systems have low salt solubility. Classical examples of Type 1 and 2 are NaCl-H_2O and Na_2SO_4-H_2O system, respectively (Figure 2.6 and Figure 2.7).

There are several interesting features in Figure 2.6: 2 lines of S-L-V (solid-liquid-vapor) equilibrium (solidus) at 450 ^oC and 720 ^oC between which there is no liquid phase present, the critical curves separating the liquid and liquid+vapor phase(L/V+L), and the saturation lines separating the liquid and liquid+solid phase (L/L+S). It is more convenient to select several concentrations to explain the phase changes that occur with increasing temperature. For the 20 w% (weight percentage) NaCl-H_2O system, starting from the lowest temperature shown in the diagram, the system maintains a single phase (an unsaturated NaCl solution) until it crosses the critical curve where it becomes a 2-phase system: a vapor phase (supercritical fluid) and a liquid phase (NaCl saturated solution). After that, as the temperature is increased further, the system moves along the critical curve, with the NaCl concentration in the liquid progressively increasing, until the critical temperature of the saturated liquid is reached. At this point (450 ^oC and ≈ 48 w% NaCl), a 'eutectic-like' reaction occurs in the system with the formation of a 'dry salt' and supercritical water containing a very low concentration of NaCl. For the 40 w% (weight percentage) NaCl case, the system starts as a saturated solution with precipitated solid salt and, as the temperature increases, the NaCl solubility in the liquid solution also increases until the saturation line is met at about 300 ^oC. At higher temperatures, the liquid phase is unsaturated and no solid salt exists in the system. However, at a still higher temperature the system intersects the critical line resulting in two phases; a supercritical water ("vapor") phase and a salt solution, as described above. The concentration of the salt solution increases with further increases in temperature until the critical curve intersects the 3-phase line at 450 ^oC, at which point solid NaCl precipitates. Starting at 80 wt% NaCl system is basically the same as the previous case, except that the solution at subcritical temperatures never becomes unsaturated and a solid NaCl phase always exists in the system.

At the temperature of 720 ^{o}C, another eutectic reaction occurs when the system produces a supercritical water phase containing a finite concentration of NaCl and a liquid comprising molten salt containing a certain amount of H_2O. Note that water depresses the melting temperature of NaCl.

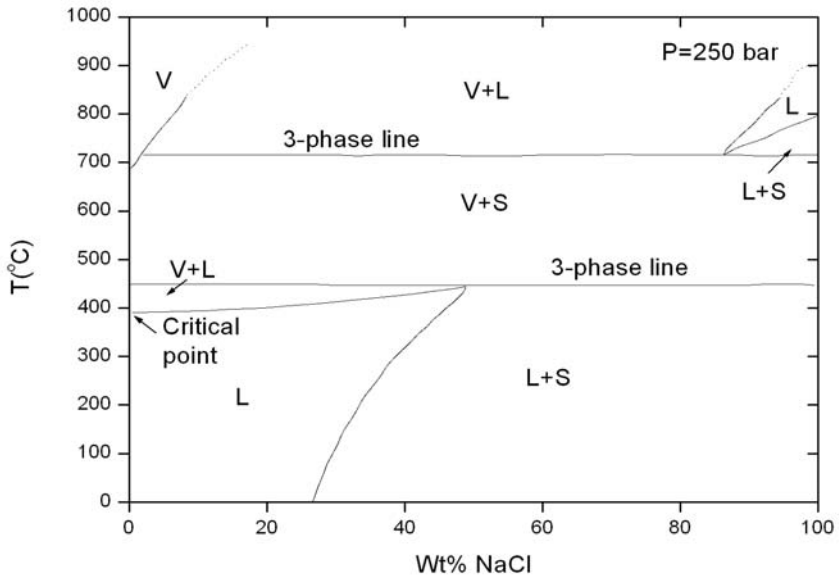

Figure 2.6: Temperature-composition phase diagram for NaCl-H_2O at 250 bar [47]

For the Na_2SO_4-H_2O system (Figure 2.7), one obvious distinction is the lack of low-temperature intersection of the L+S saturation line with the S-L-V curve in the phase diagram; instead the saturated fluid displays a continuous transition from liquid-like to gas-like behavior as the temperature increases. Note also the two turning points on the saturation line at the lower part of the diagram; the solubility of Na_2SO_4 begins a slow decrease at the first point (T ≈ 40 ^{o}C) and decreases dramatically above the second point (approximately 200 ^{o}C) until T=374 ^{o}C, where the system is separated into 2 phases: supercritical fluid and solid salt.

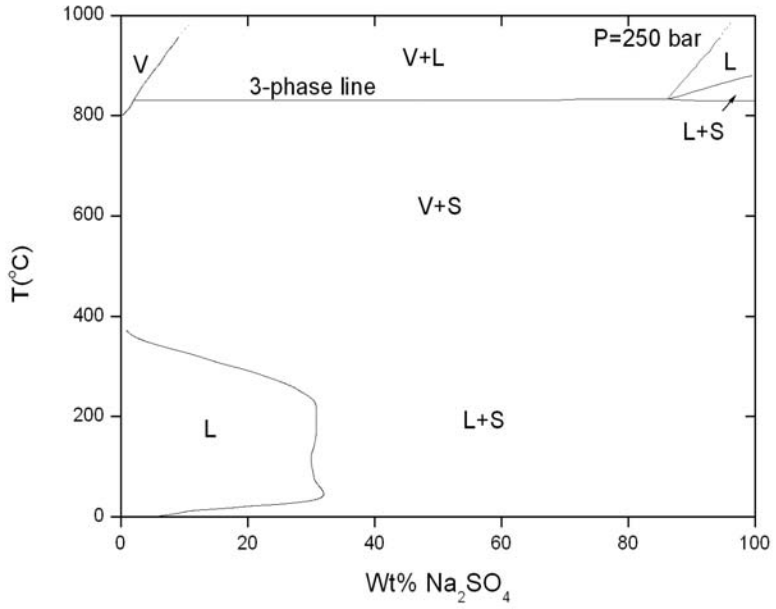

Figure 2.7: Temperature-composition phase diagram for Na_2SO_4-H_2O at 250 bar [47]

2.3 Chemical Reactions in High Temperature Water

The low-density high temperature water has properties of low dielectric constant and low viscosity. The low dielectric constant improves dissolution abilities of non-polar organic materials and the low viscosity helps to enhance mixing processes as a result of increasing solutes mass-transfer rates. If a reaction is a mass-transfer controlled reaction, it will have a much faster reaction rate in high temperature solutions because of the high diffusivity and excellent transport properties of the solvents. The chemical reaction rates are highly depended on the reaction conditions such as the working temperature and pressure. For instance, many reactions that require a high concentration of acid or base in ambient conditions can proceed very fast in very low acid or base

concentration solutions under supercritical conditions due to high thermal energy of supercritical water.

The ion product ($K_w = a(H^+)a(OH^-)$ of water is a strong function of temperature and density such as it increases with increasing temperature up to 255 ^oC (ρ = 0.83 g.cm^{-3}) and a maximum of three orders of magnitude higher K_w (compared to its value at the ambient condition) is obtained at the constant pressure of 250 bar. After that, K_w stays in the same level up to the critical temperature. Then K_w decreases sharply as the temperature transitions the critical value, such that the value is reduced by nine orders of magnitude at the temperature of 550 ^oC and pressure of 250 bar (ρ = 0.08 g.cm^{-3}) compared to its value at ambient temperature and pressure [13]. Since the dielectric constant and density of high temperature water are function of temperature and pressure at high subcritical and supercritical range, high temperature water can be used as a medium for either ionic or free radical reactions depending on the reaction conditions. For example, the ionic reaction is the favored mechanism in dense high temperature water (HTW) as the ion product of water is relative high ($K_w \geq 10^{14}$) and the free-radical chemistry is the dominant mechanism at high-temperature, low-density supercritical water (< 0.1 g.cm^{-3}) as the ion product of water is low ($K_w << 10^{14}$) [14]. Ionic reactions are reactions which take place among ions in an aqueous solution and it can be classified into two reaction types: ionogenic and iso-coulombic ionic reactions. Ionogenic reaction is a process that dissociates neutral molecules into charged species and its reaction rate increase with increasing dielectric constant (shielding effect). On the other hand, dielectric constant has less effect on kinetics of iso-coulombic type of reactions due to the conservation of number of charges in the iso-coulombic process [15]. Free radical is a molecule or atom that contains an unpaired electron but is neither positively nor negatively charged. Due to a significant amount of energy is required for homolytic cleavage processes, free radicals are

difficult to form. On the other hand, free radicals are very unstable and react quickly with other compounds because of the low activation energy. When a free radical reacts with a molecule or atom, it tries to capture the needed electron to gain stability and thus produce another free radical, which begins a chain reaction. Note that since all free radicals are electrically neutral and very little force is required to get the atoms close enough to react, it results in extremely fast reaction rate and kinetics.

The interactions between the solvents and solutes have significant effects on kinetics of reactions in high subcritical and supercritical conditions in a way that the reaction rate constant k can be affected by solvent-solute interactions through changes of free activation energy $\Delta G^{\neq}$ and transmission coefficient κ. The solvent-induced impacts on activation energy are termed equilibrium solvation effect, and the solvent-induced impacts on transmission coefficient are called non-equilibrium solvation effect [16]. It is suggested that the equilibrium solvation effect is prevailing when the solvent molecules is fast enough to correspond the changes in the reaction systems and thus maintain the equilibrium solvent structure [14]. Non-equilibrium solvation effect is more important for processes related to a large change of reactants electronic structures. The transmission coefficient κ is less than unity in non-equilibrium solvation processes due to the 'slow' adjustment speed of solvent to the changing reactions processes. In summary, solvent solubility, dielectric constant, ionic strength of medium, and 'cage' effect of solvent are four solvent properties that can influence kinetics of chemical reaction in supercritical conditions [9].

Beside acts as a medium, high temperature water (HTW) may participate in chemical reactions as a reactant such as in hydrolysis and hydration processes. In addition, individual water molecules can also be used as catalysts in chemical reactions such as water as a source of an acid or base catalyst [16]. HTW has properties that range from those that are characteristic of a gas phase

at low pressure (low dielectric constant) to those that are characteristic of a condensed liquid phase (moderate density and higher viscosity) at high pressure. Therefore, the chemical reactions in HTW can be treated as reactions in liquid phase or gas phase depending on reaction conditions.

2.4 Electrochemical Emission Spectroscopy

2.4.1 Introduction

Noise in electronic circuits is generally defined as any unwanted electrical or magnetic signals. There are three main noise-generating processes in electronic devices: thermal noise, shot noise, and flick noise: thermal noise is generated by thermal agitation of charge carriers; shot noise results from the fact that the electric current carried by charge is quantized; and flick noise may be due to various defects motions and the power spectra density of the flick noise is a function of frequency [17, 18, 19].

Electrochemical noise (EN) is defined as a series of electrochemical voltage/current transient events and it is measured as fluctuations of potential noise and current noise of electrochemical processes. Iverson first introduced electrochemical noise measurements in corrosion studies around three decades ago and it has become one of the very promising methods for monitoring and characterizing of corrosion processes since then [20, 21]. Different from other electrochemical corrosion monitoring techniques (such as polarization method and electrochemical impedance spectroscopy), electrochemical emission spectroscopy (also known as electrochemical noise analysis) is carried out in freely corroding systems such as no external disturbing electrical signals are needed and the natural evolution of corrosion systems is guaranteed. The

nature of EN generated by corrosion processes is not fully understood yet. At the same time, it is uncertain whether certain noise signals are stochastic process (a random, unpredictable process), deterministic process (a predictable process) or a combination of the two [22]. For instance, transient fluctuations happened in localized corrosion may generate from both random process and deterministic process in a way that the initiative of pitting is a stochastic process and the propagation of pits is a deterministic process [23]. The possible sources of electrochemical noise in corroding systems are listed as follows [17, 24],

(1)Partial faradaic currents and corrosion potential fluctuation
(2)Occurrence of transient events produced by nucleation, growth, and death of metastable pits at the duration of the order of a few seconds
(3)The results of mechanical effects, such as propagation of stress corrosion cracking and corrosion fatigue
(4)Passive films breakdown due to particles impact
(5)Nucleation and detachment of bubbles, such as evolution and detachment of hydrogen in acidic solutions
(6)Fluctuation in mass transfer process, such as turbulent mass transport
(7)Chemical adsorption/desorption process

The uniform corrosion is referred as an evenly corrosive attacking process over the entire metal surface areas and it is characterized by frequently alternation of microscopic anodic sites and cathodic sites. Therefore, the noise generated by uniform corrosion is defined as “white noise” and its amplitude is typically small comparing with other localized corrosion. The nucleation, growth, and death processes of metastable/stable pits are short-lived transient events as pitting is a repetitive passivation and reactive process. Different from uniform corrosion, the pitting process is characterized by relative large charge values and low frequency of transient events. Crevice corrosion is a pitting process with restricted oxygen access to the crevice. Since the crevice corrosion has similar initiation and propagation processes as the pitting corrosion, the noise transient

of crevice corrosion exhibits similar characteristics as the pitting process except with much extended living time up to many hours. The collision of solid particles or gas bubble on electrodes surfaces may either increase transient current due to the breaking of passive film or decrease the transient current because of the shielding effect. The collision process has similar effect as metastable pitting. Corrosion in acids with hydrogen evolution will increase the transient events (noise) due to the formation and detachment of hydrogen bubbles. Turbulent flow is a flow regime characterized by semi-random, stochastic properties changes and it has noise-like properties. Consequently, electrochemical noise resulting from turbulence mass transport is expected [17].

It has been reported that the shape and size of the noise transients, among other characteristics of the EN data, are directly dependent on the type and severity of corrosion in the system. Consequently, electrochemical emission spectroscopy can be used to study corrosion processes, as well as to distinguish different types of corrosion [17, 25, 26].

2.4.2 Electrochemical noise measurement

The most commonly applied electrochemical noise sensors (ENS) comprise three electrodes in a way that the two electrodes are nominally identical working electrodes and the third one is a reference electrode. The electrochemical current noise is measured between the two identical working electrodes by a zero resistance ammeter (ZRA) as the same potential level can be kept between the two identical working electrodes. The electrochemical potential noise is measured between the coupled working electrodes and the reference electrode. If working conditions permit, a true reference electrode, such as a saturated calomel electrode (SCE) or Ag/AgCl electrode, is recommended as the reference electrode in ENS. Otherwise, a third working

electrode is applied as a pseudo reference electrode and potential noise can be measured between the paring working electrodes and the pseudo reference electrode. Babrielli et al [27]. reported that the noise power spectral density (PSD) of electrochemical noise produced by commercially available reference electrodes, such as a SCE or a saturate sulfate electrode (SSE), is comparable with the PSD of instrumental noise (only slightly larger) and those reference electrodes can be treated as “noiseless” reference electrodes. In the case of applying a pseudo reference electrode in ENS, two uncorrelated noise powers, which are produced by the coupling-working electrodes and the pseudo reference electrode respectively, would be measured such as $\Psi_{measure} = \Psi_{working} + \Psi_{pseudo-refer}$. In order to avoid an extra unknown value generated by a pseudo reference electrode, a nominally identical third working electrode can be used as the pseudo reference electrode in ENS such as $\Psi_{working} = \Psi_{pseudo-refer}$.

Beside three-electrodes ENS, many different electrodes arrangements such as two-electrodes ENS and four-electrodes ENS have been applied for noise measurement. The current and potential noises are measured simultaneously between two identical working electrodes in the two-electrodes ENS. The current noise is measured between the two electrodes and potential noise is measured between the rest two electrodes in the four-electrodes ENS.

The surface areas of working electrodes and their locations with respect to the reference electrode affect noise measurement significantly. The larger working electrodes area may affect current noise measurement because of lower signal/noise ratio caused by the lower impedance of the larger working electrodes. On the other hand, it is much difficult to recognize corrosion events if the working electrodes are too small [17]. Distance between the working electrode and the reference electrode influences electrochemical noise measurement in a way that it should not be too short in order to detect the

corresponding electrochemical noises [28]. If the solution resistance is negligible comparing with the impedance of the working electrode, the location of reference electrode would not affect the noise measurement.

The noise signals are analog signals in real world and the analog signals are continuous in both time and amplitude. When we acquire those analog signals through computers, the signals are measured as discrete-time digital signals. The process converting a signal from continuous to discrete time is called sampling process. It is important to notice that the measured noise power depends on the range of frequencies included in the measurement and it is decided by sampling rate and total measuring time. Because at least two samples are required within each cycle of a given frequency to define the amplitude of a sine wave, the sampling process limited the maximum frequency that can be represented in the time records [29]. The sampling theory sets the upper and lower limits for sampling frequencies. The maximum frequency, also know as Nyquist critical frequency, is defined as $f_{\max} = 1/(2\Delta t)$ where Δt is the sampling interval. The lowest frequency is decided by total duration of measuring time T as $f_{\min} = 2/T$. If the signals produced in frequencies out of Nyquist limit present in the sampled data, those signals will reappear in the lower frequency range in the following data analysis. This process is known as aliasing and it causes difference between the reconstructed signal and the original signal. Aliasing is a problem inherent to the signal acquisition and the aliased data cannot be extracted from “real data” because they are inseparable once recorded. It is important to note that once the signal being sampled consists of some frequencies outside of limit of sampling frequencies, further increases in the sampling frequency do not improve the quality of the reconstructed signal. The aliasing can be avoided by filtering process before the sampling process. The most commonly used filtering techniques include the application of analog low-pass filter and digital filtering process [30]. The digital filtering process can be described as: the time domain data is first transferred to Fourier domain by

Fast Fourier Transform (FFT); then the output of FFT transformation is multiplied by a filter function; after that, the data can be transferred back to time domain by an inverse FFT [29]. The commonly applied sampling rate in electrochemical emission spectroscopy is in the order of 1 Hz as most noise transient events are in the low frequencies range of 10^{-3}Hz to 1Hz [17]. It is also suggested that the noise generated in high frequency are mainly due to the instrumental noise [28].

2.4.3 Data analysis methods

Electrochemical noise signals are collected discretely in the time domain and they can be analyzed in both time and frequency domains based on different analyzing perspectives. Time domain parameters such as mean and standard deviation are time-varying quantities and most of them are independent with their sampling sequence. The characteristic features of a specific corrosion can be analyzed in time domain. For example, the initiation/death of pitting and propagation of SCC can be observed as the independent transient events in time domain. The analysis in the frequency domain is also known as the spectral estimation. Typically, power is presented as a function of frequency in the frequency domain analysis. Different from the time domain analysis, the data analysis in the frequency domain is depended on sampling sequence.

2.4.3.1 Statistical analyses

Statistical techniques interpret noise data in terms of statistical parameters such as mean, standard deviation, root mean square (RMS), skew, and kurtosis. Random (stochastic) processes can be classed either as stationary or nonstationary processes. One precondition of application of many common statistic methods is that the stochastic process should be a stationary process.

Mean is the first order moment and variance is the second order moment. The instantaneous potential noise E_E is defined as $E_E = E_{measure} - \overline{E}$, in which $E_{measure}$ represents the measured potential noise and $\overline{E}$ is the mean potential noise. Standard deviation of potential noise, σ_E, is defined as square root of variance such as $\sigma_E = \left(\overline{E_E^2}\right)^{1/2}$, in which $\left(\overline{E_E^2}\right)$ is the variance of the potential noise. Similarly, standard deviation of the current noise, σ_i, is defined as $\sigma_i = \left(\overline{E_i^2}\right)^{1/2}$. Standard deviation of potential and current noises can be applied to monitor the intensity of corrosion process as it has been reported that the amplitudes of current noise are related with the corrosion rates, with a high current noise associates with a high corrosion rate [31].

Skew is a third order statistic and is a parameter describing asymmetry of the probability distribution of a random variable. Skew distribution can be related to characteristic of uni-directional transient events in asymmetric electrodes systems [17]. Kurtosis is a fourth order statistic and has characteristic of the "peakness" of the probability distribution of a random variable. Kurtosis can be used to identify localized corrosion as the relatively infrequent transient fluctuations tend to have a high kurtosis [32].

2.4.3.2 Spectra analyses

EN data are collected in the time domain. Those data can be transformed to the frequency domain by transformation functions such as fast fourier transform (FFT) and maximum entropy method (MEM). The spectra analyses have been introduced to understand the corrosion mechanisms and to monitor corrosion processes. In many practical situations, the time records are

contaminated with external signals at certain frequencies (such as effects of AC power at 60 Hz and its harmonics) and those external noise signals are impossible to filter out in the time domain but can be subtracted at the appropriate frequencies in the frequency domain. Another advantage of operating in the frequency domain is that data can be deconvoluted much easier in the frequency domain than in the time domain [33]. The corrosion noise data in the time domain might be difficult to analyze due to the overlapping of transient fluctuations. However, spectra analyses can provide detailed corrosion information in the frequency domain. For example, periodic signals clearly give rise to a peak at a certain frequency in the power spectrum and those rising may be related to crevice or pitting corrosion.

In spectral analysis, the noise signals are presented as power spectral density (PSD) in frequency domain. The PSD is defined as the power per unit frequency and it is proportional to the square of the amplitude of a value at given frequency. Mathematically, PSD is defined as the Fourier transform of the autocorrelation sequence of the time series and it has a dimension of power/Hz such as, V^2/Hz and A^2/Hz. The power spectral density (PSD) for a Poisson process is defined as [34],

$$\Psi(f) = \kappa\left|F(\omega)\right|^2 = 2\lim_{T\to\infty}\frac{N(T)\left|F(\omega)\right|^2}{T} = 2\lim_{T\to\infty}\frac{\lambda\cdot S\cdot T\left|F(\omega)\right|^2}{T} = 2\lambda\cdot S\left|F(\omega)\right|^2 \quad (2.2)$$

where $F(\omega)$ is Fourier transform of the voltage transients and $F(\omega)=\int_{-\infty}^{+\infty}V(t)\exp(-j\omega t)dt$, κ is intensity of the Poisson process, T is sampling time, $N(T)$ is total number of transients, λ is average number of transient per unit area, S is total surface area, and ω is angle frequency($\omega = 2\pi f$). The mathematical transformation can be used to transform noise data from the time domain (a time series) into the frequency domain. The equation has shown that the noise spectrum contains information related with transient events rate and

other relevant transient variables. In order to decrease the error of the estimation, values can be averaged by several closed frequencies in one spectrum or by ensemble a number of spectra [35].

Parseval's theorem expresses that the total power of signal is the same whether it is in the time domain or in the frequency domain [29],

$$\text{Total power} \equiv \int_{-\infty}^{+\infty} \sigma^2(t)dt = \int_{-\infty}^{+\infty} \Psi(f)df \qquad (2.3)$$

Similar to the standard deviation of current noise, the power spectral density can be used as the corrosion intensity indicator in the frequency domain in a way that the corrosion rate is expected to increase with increasing power spectral density. For example, the magnitude of the plateau of PSD in low frequencies is sometimes considered to indicate the corrosion rate [17]. It is important to note that precautions should be taken before make any theoretical interpretation of those plateaus since artificial plateaus can be generated at low frequencies by data processes such as trend removal, windowing process, or extrapolating MEM below to the frequencies range defined by sampling theory.

2.4.3.3 Drifts removal and windowing process

Drift is defined as a change of mean potential or current during the data acquisition period and it can be induced by instability of working electrodes during the measurement. In many cases, time-record corrosion noise data moves continuously toward one direction (positive or negative against zero) due to the preferential corrosion. Drift has properties of "quasi-dc" value and it may be attributed to transient events happen in lower frequencies range (much lower than $1/t$).

The existence of drift implies that data is non-stationary. Consequently, the drift should be removed from the noise data because many statistic analysis methods such as standard deviation and PSD are applicable only for stationary data. Two commonly used drift removal techniques are digital filtering technique (linear regression, exponential decays function, and polynomial fitting) and analog high frequency pass filtering technique. Digital filtering technique has drawbacks such as data contamination. On the other hand, long stability time and large-capacitance capacitors are required for analog high-pass technique.

Discontinuities at the beginning and at the end of sampling process may cause incorrect estimation of PSD. Window functions can be applied to avoid those discontinuities and to minimize edge effects caused by spectral leakage in the FFT spectrum [29]. Theoretically speaking, a window function has the property that its value and all its derivatives are zero at the ends in order to keep data smoothly at the ends. There are a variety of windowing functions, such as Rectangle, Hanning, Hamming Gaussian, and Kaiser. Hanning windowing function probably is the most commonly used for noise data analysis because of its high frequency resolution and moderate side lobes [36]. Cottis recommended that the drift should be removed from time-record noise data and following windowing function should be applied on the data in order to decrease the artifact errors in PSD [17].

2.4.4 Electrochemical noise resistance

2.4.4.1 Polarization resistance

For charge transfer controlled (anodic and cathodic) corrosion processes, experiments shows that a relationship exists between electrochemical overpotential and current density [37],

$$i_{app} = i_{corr}\left(\exp\left[\frac{2.3(E-E_{corr})}{b_a}\right]-\exp\left[\frac{2.3(E-E_{corr})}{b_c}\right]\right) \qquad (2.4)$$

where i_{app} is applied current density, i_{corr} is corrosion current density, E is applied potential, and E_{corr} is corrosion potential. Experiments show that the corrosion current density, i_{corr}, is in a linear relationship with over potential $\Delta E = (E - E_{corr})$ when applied potentials are within ± 5 mV to ± 10 mV range of corrosion potential. The slope of this linear relationship, $\Delta E / i_{app}$, is defined as the polarization resistance R_p and it can be used to determine the instantaneous interfacial reaction rates such as corrosion rates and exchange current densities [38].

$$R_p = \left[\frac{\Delta E}{\Delta i_{app}}\right]_{(E-E_{corr})\to 0} = \left(\frac{b_a b_c}{2.3 i_{corr}(b_a + b_c)}\right) \qquad (2.5)$$

Stern-Gary relationship can be obtained by rearranging Eq. 2.5

$$i_{corr} = \frac{1}{(2.3R_p)}\left(\frac{b_a b_c}{b_a + b_c}\right) = \frac{B}{R_p} \qquad (2.6)$$

where B is the Stern-Gary constant. b_a is anodic Tafel slope and b_c is cathodic Tafel slope. The polarization resistance R_p in Eq. 2.6 can be obtained by linear

polarization techniques and b_a & b_c can be estimated by experimental data fitting processes. Hence, the corrosion rate can be estimated. In the more complex cases such as existence of non-negligible solution resistance R_s, the polarization resistance R_p can be determined by electrochemical impedance method. For example, the impedance of a charge transfer control corrosion process can be written as follows [37],

$$Z(\omega) = R_s + \frac{R_p}{\left(1+\omega^2 R_p^2 C_{dl}^2\right)} - \frac{j\omega C R_p^2}{\left(1+\omega^2 R_p^2 C_{dl}^2\right)} \tag{2.7}$$

where R_s is solution resistance, R_p is polarization resistance and it equals to charge transfer resistance R_{ct}, and C_{dl} is parallel double layer capacitor in equivalent electrical circuit. At the low frequency limit, $Z_{w\to 0}(\omega) = R_s + R_p$ as the impedance of double layer capacitor becomes infinity. At the high frequency limit, $Z_{w\to\infty}(\omega) = R_s$ as the impedance of double layer capacitor decreases to zero. Therefore, R_p can be calculated by $R_p = \left(|Z(\omega\to 0)| - |Z(\omega\to\infty)|\right)$.

2.4.4.2 Electrochemical noise resistance and noise impedance

The electrochemical noise resistance (R_n) is defined as the standard deviation of potential noise divided by standard deviation of current noise [39],

$$R_n = \frac{\sigma_E}{\sigma_i} \tag{2.8}$$

It is reported that there is a direct relationship between the noise resistance R_n and the polarization resistance R_p based on assumptions that the electrochemical current noise is produced by a large number of independent transient sources and potential noise is produced by application of the current

noise on the polarization resistance of a working electrode [40, 41]. However, Scully [37] suggested that the relationship between the noise resistance R_n and the polarization resistance R_p is more complex because the measured R_n is susceptible to influence of rapid fluctuations (high frequency) of noises and the R_p is typically measured at the low frequency range of ~10^{-2} Hz as R_p is defined as impedance at zero frequency limiting.

A rigorous theoretical analysis of relationship between R_n and R_p in the frequency domain was carried out by Bertocci et al [28]. The analysis presents the current noise source model and potential noise source model independently. Therefore, the noise processes can be either potential fluctuation initiative or current fluctuation initiative. Based on Parseval's theorem (the total power of signals in the time domain is equal to the total power of signals in the frequency domain), the noise resistance can be expressed as follows,

$$R_n = \frac{\sigma_v}{\sigma_i} = \left(\frac{\int_0^{+\infty} \Psi_v(f) df}{\int_0^{+\infty} \Psi_i(f) df} \right)^{1/2} \tag{2.9}$$

where $\Psi(f)$ is power spectral density of signals. Spectral noise impedance $R_{sn}(f)$, which has the dimension of resistance, is defined as follows,

$$R_{sn}(f) = \left(\frac{\Psi_v(f)}{\Psi_i(f)} \right)^{1/2} \tag{2.10}$$

According to the sampling theory, the transformation of PSD is limited in a frequency bandwidth of ($f_{\min}$, $f_{\max}$), consequently we have

$$R_n = \left(\frac{\int_{f_{\min}}^{f_{\max}} \Psi_i(f) R_{sn}^2(f) df}{\int_{f_{\min}}^{f_{\max}} \Psi_i(f) df} \right)^{1/2} \tag{2.11}$$

If $R_{sn}(f)$ in Eq. 2.11 is independent of frequency, R_n is equal to $R_{sn}(f)$, i.e. $R_n = R_{sn}(f)$.

Polarization resistance R_p is defined as the cell impedance at the zero-frequency limiting and $Z(f)$ is defined as the impedance of an electrode. Therefore, modulus of $Z(f)$ at zero-frequency limit is equal to R_p if the solution resistance is negligible, i.e. $|Z(f=0)| = R_p$. U. Bertocci et al. [28] proposed a correlation (Eq. 2.12) between $R_{sn}(f)$ and $|Z(f)|$ for the model with the current noise sources,

$$R_{sn}^2(f) = \frac{\left|Z_1\left[Z_2 + R_s(1-x)\right]\right|^2 \Psi_{i_1} + \left|Z_2\left(Z_1 + R_s x\right)^2\right| \Psi_{i_2}}{\left|Z_1\right|^2 \Psi_{i_1} + \left|Z_2\right|^2 \Psi_{i_2}} \qquad (2.12)$$

where Z_i is the impedance of working electrodes, Ψ_i is the PSD of the noise level of each electrode, R_s is the resistance of solutions, and x is the fraction of solution resistance between the reference electrode and one working electrode. If the electrochemical cell is consisted of two identical working electrodes (with identical impedance modulus) and a noiseless reference electrode, and if the solution resistance is negligible, $R_{sn}(f)$ is equal to the working electrode impedance $|Z(f)|$ such as $R_{sn}(f) = |Z(f)|$. Consequently, a correlation between the noise resistance R_n and the polarization resistance R_p can be obtained in the sufficient low frequency range such as,

$$R_n = R_{sn}(f \to 0) = |Z(f=0)| = R_p \qquad (2.13)$$

It is important to noted that Eq. 2.13 is valid for any sources of noises, such as noises generated by localized corrosion, uniform corrosion, bubble detachment, and mass transfer. It is suggested that the noise resistance R_n may

be much lower than the polarization resistance R_p for passive or coated electrodes, unless very long time record are taken [42]. If the two working electrodes have different electrodes impedances, which is very common even for two identical working electrodes with same initial conditions because corroding electrodes incline to develop differently, the relationship between $R_{sn}(f)$ and impedance of electrodes can be written as follows,

$$R_{sn}^2(f) = \frac{|Z_2|^2 \Psi_{i_1} + |Z_1|^2 \Psi_{i_2}}{\Psi_{i_1} + \Psi_{i_2}} \tag{2.14}$$

where $|Z_1|$ and $|Z_2|$ are impedance modulus of two working electrodes and $|Z_1| \neq |Z_2|$, Ψ_i is the PSD of the noise level of each electrode. As demonstrated by Eq. 2.14, the value of $R_{sn}(f)$ exists between the $|Z_1|$ and $|Z_2|$. And if $|Z_1|$ equals to the polarization resistance R_{P1} and $|Z_2|$ equals to the polarization resistances R_{P2} at the low frequency limit, $R_{sn}(f)$ exists in between the R_{P1} and R_{P2}. Eq. 2.14 shows that the value of $R_{sn}(f)$ is close to the impedance of the less noise electrode (small Ψ). Thus those asymmetric corrosion cell can be described as that one electrode (with large Ψ) acts as a source signal for the measurement of the impedance of another electrode (with small Ψ) [42]. In the case of Ψ_{i_1} = Ψ_{i_2}, $R_{sn}^2(f) = \left(|Z_1|^2 + |Z_2|^2\right)/2$.

If the electrochemical cell consists three identical electrodes (with identical electrode impedance modulus) and if the solution resistance is negligible, the relationship between $R_{sn}(f)$ and $|Z(f)|$ becomes,

$$R_{sn}(f) = |Z(f)| \left(1 + \frac{4\Psi_{i_3}}{\Psi_{i_1} + \Psi_{i_2}}\right)^{1/2} \tag{2.15}$$

If three electrodes are assumed to generate identical noises, the above equation can be simplified as $R_{sn}(f) = \sqrt{3}|Z(f)|$.

The above theoretical analysis of relationship between the spectral noise impedance $R_{sn}(f)$ and the electrode impedance modulus $|Z|$ has been confirmed by experiments [28]. It is also suggested that $R_{sn}(f \to 0)$ can be represented by a long low frequency plateau when the voltage and current PSD have similar $1/f^{\alpha}$ behavior.

2.4.5 Differentiate corrosion types by noise processes

Because different corrosion processes have different characteristic transient events frequencies due to the kinetics processes underlying the corrosion processes, the characteristics of electrochemical noises such as characteristic charge q, characteristic frequency f_n, slope of PSD (roll-off slope), and low-frequency plateau have been proposed to identify the transient shape and thus to differentiate corrosion types. For instance, electrochemical noise data in time domain can be used to differentiate the general and localized corrosions such as the noises level generated by the uniform corrosion is relatively flat (no visible fluctuations). On the other hand, localized corrosion produces distinct transient events such as spikes in time-record noise data.

Shot noise results from the stochastic emission of quantized charge pulses and it is a white noise (frequency independent). If the transient events (noise) are independent from other events, the power spectral density of the current noise can be written as, $\Psi_I = 2qI = 2f_n q^2$, in which q is the charge on charge carrier, I is the mean current, and f_n is the mean frequency of charge emission. Based on the

assumptions of (1) noises generated by corrosion are short duration of transient events in low frequency range; (2) transient events (noises) are independent from other events and are stochastic processes; (3) noise is produced by anodic processes (such as meta-stable pitting), whereas cathodic reactions are noise-free; (4) the potential noise results from the application of current noise on the polarization resistance of a working electrode, Cottis et al [43]. applied shot noise analysis to model and to interpret corrosion processes. Two characteristic parameters, i.e. characteristic charge q and characteristic frequency f_n, have been introduced to describe the corrosion processes and those two parameters are related by average corrosion current I_{corr}, such as $I_{corr} = qf_n$. The q and f_n can be obtained by the following Eq. 2.16 and Eq. 2.17 ,

$$q = \frac{\sqrt{\Psi_{E,meas}\Psi_{i,meas}}}{B} \tag{2.16}$$

$$f_n = \frac{I_{corr}}{q} = \frac{B^2}{\Psi_{E,meas}} \tag{2.17}$$

where B is the Stern-Gary constant, $\Psi_{E,meas}$ is the low frequency limit of the power spectral density of potential noise, and $\Psi_{i,meas}$ is the low frequency limit of power spectral density of current noise. The values of q and f_n are the average values as the shot noise analysis is a statistic process. It is natural to relate a large value of frequency f_n (>1 KHz/cm^2) with uniform corrosion and a low value of f_n with localized corrosion as many transient events occur for the uniform corrosion and less transient events are expected for localized corrosion. Characterization charge q can be used to indicate the magnitude of the individual events. It is suggested that a relative large q with a small f_n may indicate the onset of localized corrosion [43].

Electrochemical noise signals generated by fluctuations of transient events indicate the underlying corrosion kinetics. Therefore, power spectral density graphs of corrosion noises such as the shape of PSD, roll-off slope, and roll-off frequency have been applied to identify the corrosion types. Typically, power spectra density falls with increasing frequency at the high frequency range such as $\Psi(f) \propto 1/f^n$, in which n is a constant. Gabrielli et al. [44] suggested that the roll-off slope of $1/f^2$ is related with transient events with the sudden birth/sudden death and the roll-off slope of $1/f^4$ is related with slow birth of transient events following a slow repassivation processes. Cheng et al [34]. reported that the PSD of metalstable pitting is independent from frequency (white noise) at the low frequency range and it has a feature of $1/f^2$ at the higher frequency range because the transient events of metastable pitting processes have a characteristic of sudden birth/slow decay or slow birth/sudden decay. The spectrum of a passive state is 'white noise' in the low frequency range and has roll-off slope of $1/f^4$ in the higher frequency range. They also concluded that the noise spectrum in the high frequencies range is more depended on the transient shape rather than on the types of corrosion. Therefore, it is unreliable to identify the corrosion type by roll-off slope alone [34]. Cottis [17] questioned the validity of correlations between roll-off slope and corrosion types and he concluded that the different type of corrosion cannot be reliably identified by PSD roll-off slope alone.

The roll-off frequency is defined as the frequency where the low frequency plateau ends and the PSD plot begins to drop (the cross point of 'white' noise and $1/f^n$). It is suggested that the roll-off frequency is related to the time constant of repassivation, which is connected to the aggressiveness of the environment inside pits [19]. The low-frequency plateau is commonly observed in PSD of corrosion processes and the magnitude of the plateau is sometimes considered to indicate the rate or severity of corrosion such as a higher plateau

height can be linked to significant localized attack if the plateau is generated by a corrosion process rather than an artifact effect.

Many other parameters such as the coefficient of variation of current noise (ratio of the standard deviation of current noise over its mean), localization index (standard deviation of current divided by RMS of current), and skew have been proposed to predict the extent of corrosion localization [45]. Mansfeld et al [46] questioned the reliability of both coefficient of variation of current and localization index as the indicators for localized corrosion. Experimental data of mild steel in NaCl system was analyzed and the results demonstrated that the localization index can not be used to identify corrosion types.

2.5 Conclusions and Summary

In summary, the properties of high temperature water have been addressed in this chapter, with emphasis on the effect of pressure and temperature on those properties. A non-perburbative electrochemical technique, electrochemical emission spectroscopy (EES), has been introduced in this chapter in order to exploring its applications in corrosion studying of high temperature, high pressure aqueous systems.

References

1. Macdonald, D. D., T. Zhu, and X. Guan, “Current State-of-the-Art in Reference Electrode Technology for Use in High Subcritical and Super Critical Aqueous Systems”, *Corrosion*, submitted (2006).

2. D. S. Eisenberg, W. Kauzmann, The Structure and Properties of Water, Oxford, New York, 1969.

3. E. Guardia, J. Marti, “Density and temperature effects on the orientational and dielectric properties of supercritical water”, *Physical Review* **E 69**, 011502 (2004).

4. T. I. Mizan, P. E. Savage, R. M. Ziff, “Temperature Dependence of Hydrogen Bonding in Supercritical Water” *J. Phys. Chem.* **100,** 403 (1996).

5. K. Okada, Y. Imashuku, M. Yao, “Microwave spectroscopy of supercritical water” *J. Chem. Phys.* **107**, 9302 (1997).

6. D. D. Macdonald, L. B. Kriksunov, “Probing the chemical and electrochemical properties of SCWO systems” *Electrochimica Acta* **47,** 775 (2001).

7. H. Weingartner, E. U. Franck, “Supercritical water as a solvent” *Angew. Chem. Int Ed.*, 44, 2672 (2005)

8. P. B. Balbuena, K. P. Johnston, P. J. Rossky, J-K Hyun, “Aqueous Ion Transport Properties and Water Orientation Dynamics from Ambient to Supercritical Conditions” *J. Phys. Chem*. **B 102**, 3806 (1998).

9. P. E. Savage, S. Gopalan, T. I. Mizan, C. J. Martino, E. E. Brock, “Reactions at Supercritical Conditions: Applications and Fundamentals” *AICHE Journal* **41**, 1723 (1995)

10. A. A. Chialvo, P. T. Cummings, J. M. Simonson, R. E. Mesmer "Thermodynamics and kinetics of ion speciation in supercritical aqueous solutions: a molecular-based study" *Fluid Phase Equilibria* **150-151,** 107 (1998)

11. K. P. Johnson, J. B. Chlistunoff, "Neutralization of acids and bases in subcritical and supercritical water: acetic acid and HCL" *J. Supercritical Fluids* **12**, 155 (1998)

12. R. E. Mesmer, W. L. Marshall, D. A. Palmer, J. M. Simonson, H. F. Holmes "Thermodynamics of aqueous association and ionization reactions at high temperatures and pressures, *J. Solution Chem*. **17**, 699 (1988).

13. M. Hodes, P.A. Marrone, G.T. Hong, K.A. Smith, J.W. Tester. "Salt precipitation and scale control in supercritical water oxidation-Part A: fundamentals and research*" J. Supercritical Fluids* **29**, 265 (2004).

14. References referencing in N. Akiya, P. E. Savage "Roles of water for chemical reactions in high-temperature water", *Chem. Rev*. 102, 2725 (2002).

15. P. B. Balbuena, K. P. Johnson, P. J. Rossky, "Molecular dynamics simulation of electrolyte solutions in ambient and supercritical water. 2. Relative acidity of HCl" *J. Physical Chem. Res.* **100,** 2716 (1996)

16. N. Akiya, P. E. Savage, "Roles of Water for Chemical Reactions in High-Temperature Water" *Chem. Rev.* **102,** 2725 (2002).

17. R. A. Cottis, "Interpretation of electrochemical noise data" *Corrosion* **57**, 265 (2001).

18. J. Liu, "Electrochemical Emission and Impedance Spectroscopies of Passive Iron and Carbon Steel". Ph.D thesis. University Park, PA: Pennsylvania State University (2002).

19. U. Bertocci, F. Huet, “Noise analysis applied to electrochemical systems” *Corrosion*, **51**, 131 (1995)

20. W. P. Iverson, J. Electrochem. Soc. 115, 6, P617 (1968) and more}

21. A. Legat “The effect of electrolyte stirring and laminar flow on measured electrochemical noise” *Materials and Corrosion* **55** 761 (2004)

22. R. A. Cottis, M.A. Al-Ansari, G. Bagley and A. Pettiti, “Electrochemical noise measurements for corrosion studies” *Material Science Forum* **289-292**, 741 (1998).

23. www.corrosion-docs.org

24. C. Jeyaprabha, S. Muralidharan, G. Venkatachari and M. Raghavan, “Application of electrochemical noise measurements in corrosion studies: a review” *Corrosion review* **19**, 301 (2001).

25. M. Leban, A. Legat, V. Dolecek, V. Kuhar “Electrochemical noise as a possible method for detecting stress-corrosion cracking” *Material Science Forum* **289-292**, 157 (1998).

26. H.A.A.Al-Mazeedi, R. A. Cottis “A practical evaluation of electrochemical noise parameters as indicators of corrosion type” *Electrochimica Acta* **49**, 2787 (2004)

27. C. Gabrielli, F. Huet, nad M. Keddam, *Electrochim. Acta*, **31**, 1025 (1986)

28. U. Bertocci, C. Gabrielli, F. Huet, and M. Keddam, “Noise resistance applied to corrosion measurements I. theoretical analysis” *J. Electrochem. Soc*. **144**, 31 1997).

29. W. Press, S. Teukolsky, W. Vetterling, B. Flannery, Numerical Recipes in C++, Cambridge University Press, 2002

30. I. N. Bastons, F. Huet, R. P. Nogueira, and P. Rousseau, “Influence of Aliasing in Time and Frequency Electrochemical Noise Measurements” *Journal of Electrochem. Soc.* **147**, 671 (2000).

31. X. Y. Zhou, S. N. Lvov, X. J. Wei, L. G. Benning, D. D. Macdonald, “Quantitative Evaluation of General Corrosion of Type 304 Stainless Steel in Subcritical and Supercritical Aqueous Solutions via Electrochemical Noise Analysis”, *Corrosion Science,* **44**, 841 (2002)

32. E. E. Barr, R. Goodfellow, and L. M. Rosenthal, NACE 2000, Paper No. 414

33. M. Smith, “Wavelet analysis of electrochemical electrochemical noise data for monitoring corrosion in nuclear waste storage containers” M.S thesis. University Park, PA: Pennsylvania State University (2005).

34. Y. F. Cheng, J.L. Luo, and M. Wilmott, “Spectral analysis of electrochemical noise with different transient shapes*” Electrochimica Acta* **45,** 1763 (2000).

35. Bendat, J.S., and Piersol, A.G. "Engineering Applications of Correlation and Spectral Analysis." New York: Wiley, 1980.

36. U. Bertocci, J. Frydman, C. Gabrielli, F. Huet, and M. Keddam, “Analysis of electrochemical noise by power spectral density applied to corrosion studies” *J. Electrochemical. Soc*. **145**, 2780 (1998).

37. J. Scully, “Polarization resistance method for determination of instantaneous corrosion”, *Corrosion* **56**, 199 (2000)

38. M. Stern, A. L. Geary, *J. Electrochem. Soc*. **105,** 638 (1958).

39. D. A. Eden, K. Hladky, D. B. John, and J. L. Dawson, “Electrochemical noise-simultaneous monitoring of potential and current noise signals from corroding electrodes” CORROSION’91 No. 274, Houston, NACE (1991)

40. F. Mansfeld and H. Xiao, “Electrochemical noise analysis of iron exposed to NaCl solutions of different corrosivity”*J. Electrochem. Soc*. **140** 2205 (1993).

41. J. F. Chen and W. F. Bogaerts “Physical meaning of noise resistance**”** *Corrosion Science* **37,** 1839 (1995).

42. A. Aballe, A. Bautista, U. Bertocci, and F. Huet, “Measurement of the noise resistance for corrosion application” *Corrosion*, **57**, 35 (2001).

43. R. A. Cottis, S. Turgoose, “Electrochemcial noise measurements – A theoretical basis” *Materials Science Forum* **192-194**, 663 (1995).

44. C. Gabriellli, M. Keddam, “Review of applications of impedance and noise analysis to uniform and localized corrosion” *Corrosion* **48**, 794 (1992)

45. D. A. Eden, “Corrosion’98” NACE, Paper no. 386

46. F. Mansfeld, Z. Sun, C. H. Hsu and A. Nagiub, “Concerning trend removal in electrochemical noise measurements” *Corrosion Science* **43**, 341 (2001)

47. Marc Hodes, Philip A. Marrone, Glenn T. Hong, Kenneth A. Smith and Jefferson W. Tester “Salt precipitation and scale control in supercritical water oxidation—Part A: fundamentals and research” Journal of

supercritical fluids, **29**, 265 (2004)

Chapter 3

THE CHEMICAL PROPERTIES OF HIGH TEMPERATURE AQUEOUS SYSTEMS

3.1 Introduction

Supercritical water (SCW) is used as a solvent in many chemical processes and waste destruction technologies due to its unique properties such as high fluidity and low density. For example, hazardous and toxic organic wastes can be oxidized to harmless products via the supercritical water oxidation (SCWO) processes. Many properties of SCW, including density, dielectric constant, and viscosity are strongly correlated with the working temperature and pressure. Therefore the chemical/electrochemical reaction rates in SCW can be controlled through the manipulation of temperature and pressure.

The dielectric constant of SCW decreases with increasing temperature and increases with increasing pressure under supercritical conditions. The consequence of this dielectric constant change is that strong electrolytes under ambient conditions are very poorly ionized and generally exist as contacting pairs in low density supercritical water systems [1]. Therefore, the chemical properties of high temperature aqueous systems such as pH and dissociation constant are function of temperature and pressure in the supercritical conditions.

3.2 Dissociation Constant in High Temperature Aqueous Systems

Equilibrium dissociation constant K and ion product K_w of the water dissociation equilibrium $H_2O \Leftrightarrow H^+ + OH^-$ are defined as:

$$K = \frac{a(H^+)a(OH^-)}{a(H_2O)} \tag{3.1}$$

$$K_w = a(H^+)a(OH^-) \tag{3.2}$$

where $a(H^+)$ and $a(OH^+)$ are the activities of H^+ and OH^- respectively. Ion product $K_w = 1\times10^{-14}$ at the ambient conditions. At temperatures < 250 ^oC, the value of K_w is determined by the opposite effects of the temperature and density in a way that K_w increases with increasing temperature and decreases with increasing density as illustrated by Table 3.1. The value of K_w at constant pressure of 250 bar increases with increasing temperature up to 250 ^oC (ρ = 0.82 g.cm^{-3}) and a maximum of three orders of magnitude higher K_w (compared to its value at the ambient conditions) is obtained at the temperature range of 255 ^oC to 374 ^oC. After that, K_w decreases sharply with increasing temperature when the temperatures are above the critical temperature. For example, the K_w is reduced by nine orders of magnitude at the temperature of 550 ^oC (ρ = 0.08 g.cm^{-3}) compared to its value at the ambient conditions [2]. This sharp decrease in K_w further prove the non-polar nature of supercritical water at low density. Weingartner et al [3]. reported that the K_w of supercritical water at temperature of 1000 ^oC and liquid-like density is at least six orders of magnitude higher than its value at the ambient conditions.

Table 3.1: K_w as function of temperature at 250 bar

Temperature (°C)	Density (g.cm^{-3})	Dielectric constant	K_w
25	1.008	79.32	1.25E-14
50	0.9986	70.78	6.45E-14
100	0.9696	56.37	6.61E-13
150	0.9303	44.92	2.89E-12
200	0.8813	35.71	6.86E-12
250	0.8209	28.11	9.55E-12
300	0.743	21.47	7.18E-12
350	0.6255	14.85	1.68E-12
400	0.1665	2.504	3.68E-20
450	0.109	1.782	2.55E-22
500	0.08974	1.572	3.88E-23
550	0.07852	1.458	1.24E-23
600	0.07072	1.383	5.40E-24

Johnson et al [4]. reported that the equilibrium dissociation constant of HCl decreases with decreasing density monotonically in a way that the dissociation constant of HCl has dropped by 13 orders of magnitude from 25 °C to the critical temperature of water at 374 °C. Therefore, HCl becomes a weaker acid at low density and high temperature supercritical working conditions. Based on the transition state theory, Chialvo et al. [1] predicted that the temperature and density have opposite effects on ion dissociation processes in a way that the degree of dissociation decreases with increasing temperature and increases with increasing density at the high temperatures. Since the strength of coulomb interaction of ions is highly depend on the dielectric constant of the solvent, a

variety of ion configurations (anion-cation distance) range from a high ion association to high ion dissociation can happen in supercritical water [5].

Electrical conductance measurement is a widely used method to determine the dissociation constant in aqueous systems. The electrical conductance Λ of salts such as Λ(KCl) is the sum of ionic conductance of cations and anions resulting from the hydrodynamic migration of these ions. As for the acids/bases electrical conductance, excess ionic conductance due to the hydrogen transfer in hydrogen-bonded bulk water should be added to the electrical conductance on the top of the contributions from the hydrodynamic migration of ions. Hydrodynamic ionic conductance is controlled by temperature, pressure, medium dielectric constant and its viscosity. Whereas, the excess ionic conductance generated by the hydrogen transfer is the function of temperature, pressure, and solution concentration [6]. Ho et al. reported that the dissociation constants of K_{KCl} and K_{KOH} decrease with decreasing density and increases with decreasing temperature based on the measurement of molar conductance of Λ_0(KCl) and Λ_0(KOH) for dilute KCl and KOH solutions (concentration < 0.001 mol/kg) at supercritical temperatures (>375 ^oC) [6].

3.3 pH of High Temperature Aqueous Systems

3.3.1 Theoretical background

The dielectric constant of high temperature water decreases with increasing temperature. Therefore, the strong electrolytes such as HCl and NaOH that are essentially fully ionized at the ambient conditions are poorly ionized in supercritical conditions. The concentration of hydrogen ions (molal concentration, mol/kg H_2O) in the HCl solution can be estimated by combing the

HCl dissociation reaction (Eq. 3.3) along with water dissociation reaction (Eq. 3.4) [7].

$$HCl = H^+ + Cl^- \tag{3.3}$$

$$H_2O = H^+ + OH^- \tag{3.4}$$

The four equations based on the mass conservation, charge conservation, and the reaction constants can be written as follows.

$$K_d = \frac{m_{H^+} m_{Cl^-} \gamma_\pm^2}{m_{HCl} \gamma_{HCl}} \tag{3.5}$$

$$K_w = m_{H^+} m_{OH^-} \gamma_\pm^2 \tag{3.6}$$

$$m_{HCl}^0 = m_{Cl^-} + m_{HCl} \tag{3.7}$$

$$m_{H^+} - m_{Cl^-} - m_{OH^-} = 0 \tag{3.8}$$

where $\gamma_\pm$ is the mean molar activity coefficient and m_{HCl}^0 is the stoichiometric molar concentration of HCl in solution. By combining Eq. 3.5 - Eq. 3.8 and assuming γ_{HCl}=1, we can obtain the following equation to estimate the molal concentration of hydrogen ions m_{H^+} in HCl solution,

$$m_{H^+}^3 + m_{H^+}^2 \frac{K_d}{\gamma_\pm^2} - m_{H^+} \left[\frac{K_w}{\gamma_\pm^2} + \frac{m^0 K_d}{\gamma_\pm^2} \right] - \frac{K_d K_w}{\gamma_\pm^4} = 0 \tag{3.9}$$

Providing that the ionic strength, I, is not too high (I < 0.1 mol/lit), the activity coefficients can be determined using Debye-Hückel theory for sufficient diluted solutions such as [7],

$$\log(\gamma_{\pm}) = -z_i^2 A\sqrt{I}/(1 + aB\sqrt{I}) \qquad (3.10)$$

where ionic strength I is defined as $I = 0.5\sum C_i z_i^2$, a is the 'distance of closest approach', and A (the Debye-Hückel limiting slope) and B are the constants depending on the density and dielectric constant of the medium. The molal dissociation constant of HCl, K_d, can be obtained from the data of Frantz and Marshall [8]. The temperature dependence of density, dielectric constant, viscosity, and ion product of K_w can be estimated from Ref. 9 and 10. The temperature dependence of molal concentration of the hydrogen ions m_{H^+} is obtained by solving Eq. 3.9 numerically. A similar model has also been developed for NaOH solutions [11].

3.3.2 Temperature and pressure dependence of pH of HCl solutions

pH is a measure of the acidity of a solution in terms of activity of hydrogen ions ($a(H^+)$) and it is defined thermodynamically as the negative logarithm of the activity of H^+. The activity at the ambient temperatures is usually based on the molar (mol/l) concentration scale. For example, for diluted solutions, the activity of the hydrogen ions can be substituted by the molarity (mol/l) of the solutions. However, this volumetric scale (mol/l) is very inconvenient for high temperature aqueous systems due to the temperature/pressure dependence of the density (volume) of the systems. Therefore, the molal (mol/kg H_2O) concentration scale has been proposed by Macdonald for using in high temperature aqueous systems [11]. pH in molar (mol/l) and in molal (mol/kg H_2O) scales are defined as following,

$$\text{pH(molar scale)} = -\log(y_{\pm} c_{H^+}) \tag{3.11}$$

$$\text{pH(molal scale)} = -\log(\gamma_{\pm} m_{H^+}) \tag{3.12}$$

where c_{H^+} and m_{H^+} are the molar and molal concentrations of hydrogen ions, $y_{\pm}$ and $\gamma_{\pm}$ are the corresponding mean activity coefficients. The two scales can be related approximately by Eq. 3.13 for diluted solutions based on $c \cong \rho m$ for concentrations up to 1 to 2 m [7],

$$\text{pH(molar scale)} \approx \text{pH(molal scale)} - \log(\rho) \tag{3.13}$$

It is important to note that the degree of dissociation of HCl decreases with increasing temperature due to the decreasing of dielectric constant. Therefore, the change of the stoichiometric HCl concentration does not correspond to the change of pH in a proportionate manner.

Analysis of the thermodynamics of aqueous electrolyte solutions shows that the pH at high subcritical and supercritical temperatures is dominated by incomplete dissociation of even the strongest acids and bases. Figure 3.1 shows the calculated pH of a dilute HCl solution (0.01 m) as a function of temperature (25 ^{o}C to 600 ^{o}C) at pressures ranging from 400 bar to 1000 bar. HCl is almost completely dissociated at temperatures below 350 ^{o}C and it becomes less soluble at higher temperatures. As illustrated by the figure, the pH increase precipitously with increasing temperature and becomes highly pressure dependent when temperatures are above 350 ^{o}C. The pressure dependence of pH at supercritical temperatures is such that the pH decreases with increasing pressure and dielectric constant. At the highest temperature (600 ^{o}C) and lowest pressure (400 bar), the pH approaches to the neutral value, illustrating the extremely low degree of dissociation of HCl.

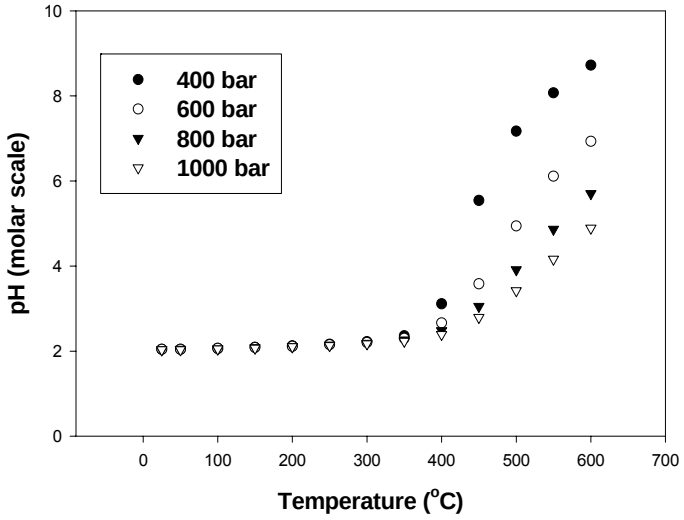

Figure 3.1: Calculated pH (molar scale) for 0.01 m HCl as a function of temperature and pressure

It is important to note that even though the HCl is strongly associated and pH is approximately as high as 8.72 (molar scale) and 7.81 (molal scale) at 600 ^{o}C and 400 bar, the solution is still acidic solution. Note that, the neural pH is pK_w/2 = 9.98 (molar scale) and pK_w/2 = 9.07 (molal scale) at 600 ^{o}C and 400 bar, therefore, a pH of 8.72 corresponds to an acidic solution under those conditions. Figure 3.2 shows the pH of pure water in both molar and molal scales as a function of temperature at 250 bar. In corresponding with the temperature dependence of ion product K_w, the neural pH of pure water decreases with increasing temperature before the temperatures reach to 250 ^{o}C. Then, the pH increases sharply with increasing temperature when the temperatures are above the critical temperature of 374.15 ^{o}C.

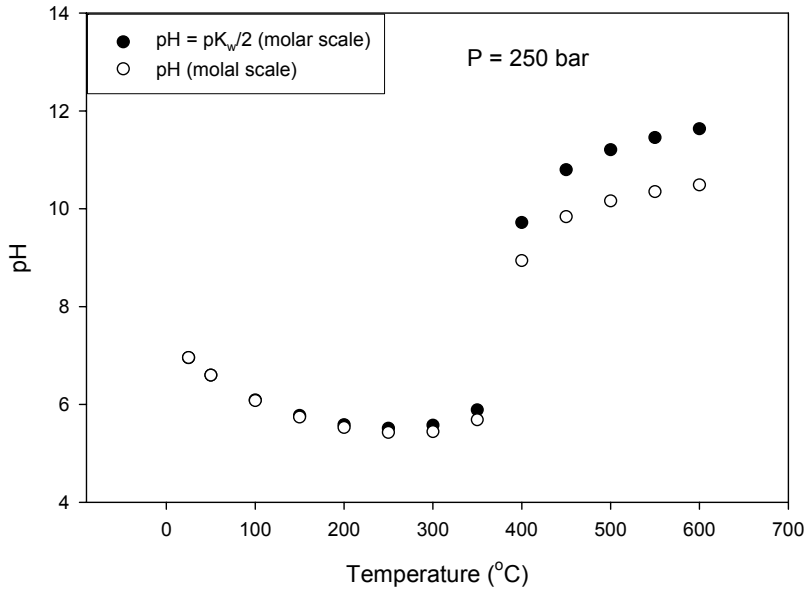

Figure 3.2: Calculated pH on the molal and molar scales of pure water as a function of temperature at 250 bar

Figure 3.3 presents calculated pH (molal scale) for stoichiometric concentrations of 0.1, 0.01, 0.001, and 0.0001 m HCl as a function of temperature at 250 bar. The figure shows the pH increases slightly with increasing temperature when temperatures are below 350 ^{o}C. After that, the pH increases significantly with increasing temperature. It can be explained by the temperature dependence of the dielectric constant of high temperature water. Figure 3.4 shows the density and dielectric constant of water as a function of temperature at 250 bar. As illustrated, the dielectric constant drops precipitously from 14.85 at 350 ^{o}C to 2.5 at 400 ^{o}C. Consequently, the degree of dissociation of HCl decreases significantly, illustrating that the chloride exists dominantly in the form of undissociated HCl in supercritical conditions. Therefore, the pH increases significantly with increasing temperature at supercritical conditions and it approaches to the neutral value at 600 ^{o}C.

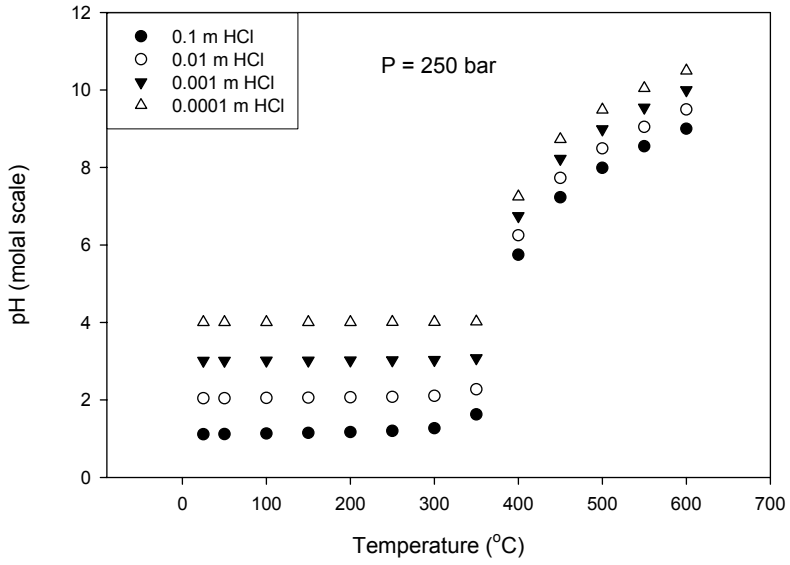

Figure 3.3: Calculated pH (molal scale) for stoichiometric concentrations of 0.1, 0.01, 0.001, and 0.0001 m HCl as a function of temperature at 250 bar

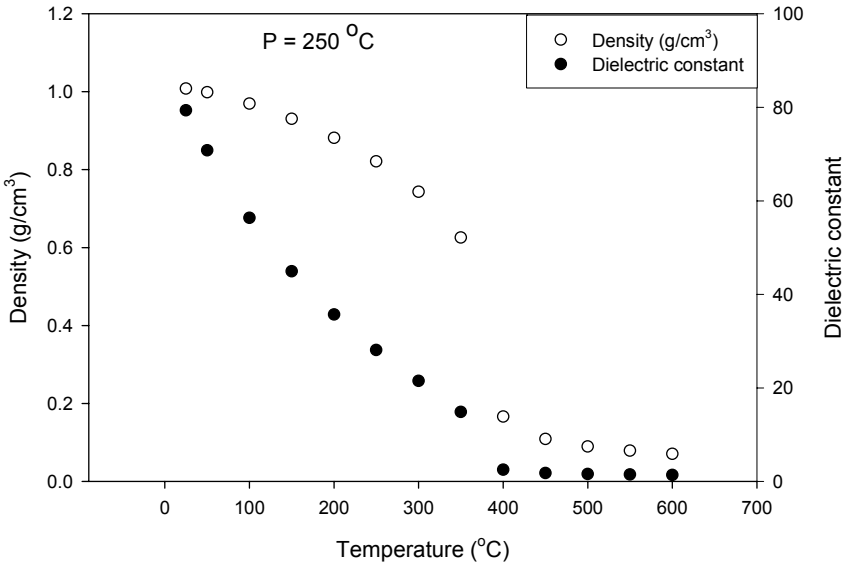

Figure 3.4: Density and dielectric constant of water as a function of temperature at 250 bar

Figure 3.5 shows calculated pH (molal scale) for stoichiometric concentrations of 0.1, 0.01, 0.001, and 0.0001 m HCl as a function of density at 250 bar. The figure shows the pH increases slightly with decreasing density when temperatures are below 350 ^{o}C (0.6255 g.cm^{-3}). Then, the pH increases significantly with increasing temperature at supercritical temperatures. It correlates with the temperature dependence of the dielectric constant in a way that the pH increases with increasing temperature and decreasing dielectric constant. Since the degree of dissociation of HCl drops with decreasing density/dielectric constant, the pH (negative logarithm of activity of hydrogen ions) increases with decreasing density.

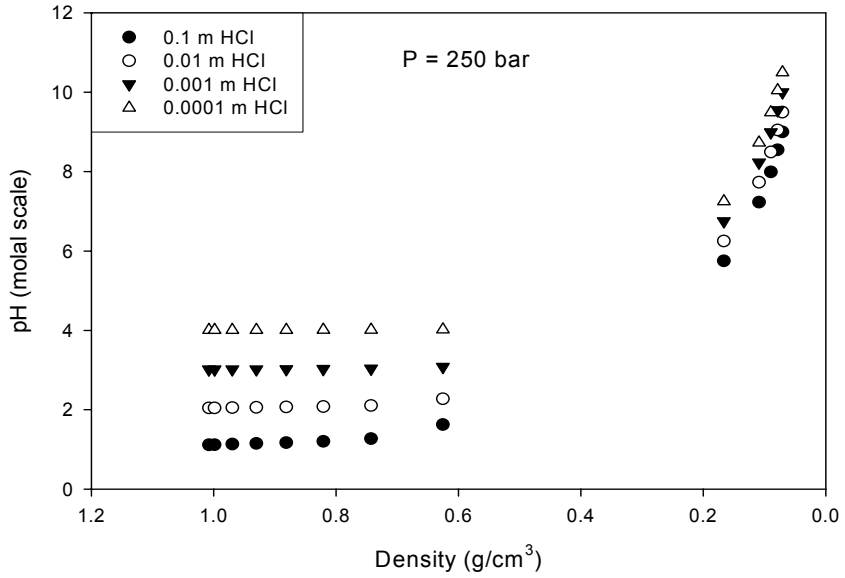

Figure 3.5: Calculated pH (molal scale) for stoichiometric concentrations of 0.1, 0.01, 0.001, and 0.0001 m HCl as a function of density at 250 bar

Figure 3.6 and Figure 3.7 present the calculated pH of 0.01 m HCl and dielectric constant of water as a function of pressure at 350 ^{o}C and 450 ^{o}C respectively. As demonstrated by the figures, the dielectric constant increases

with increasing pressure at high subcritical and supercritical temperatures, corresponding with the density increasing with increasing pressure. Since the degree of dissociation of HCl increases with increasing pressure, the pH (negative logarithm of the activity of H^+) decreases with increasing pressure. Figure 3.6 shows that the pH (molal scale) of stoichiometric 0.01 m HCl is in the range of 2.2 – 2.4 in the pressure range of 200 – 350 bar at 350 ^oC. On the other hand, the pH of stoichiometric 0.01 m HCl is in the range of 6 – 9 in the pressure range of 200 – 350 bar at 450 ^oC. Since the dielectric constant of supercritical water is approximately a "gas phase" value (dielectric constant = 1.721 at 450 ^oC and 240 bar), the degree of dissociation of HCl is extremely low at supercritical temperatures, illustrating that the chloride exists dominantly in the form of undissociated HCl in supercritical conditions. Consequently, a high pH value (close to the natural value) is expected at 450 ^oC.

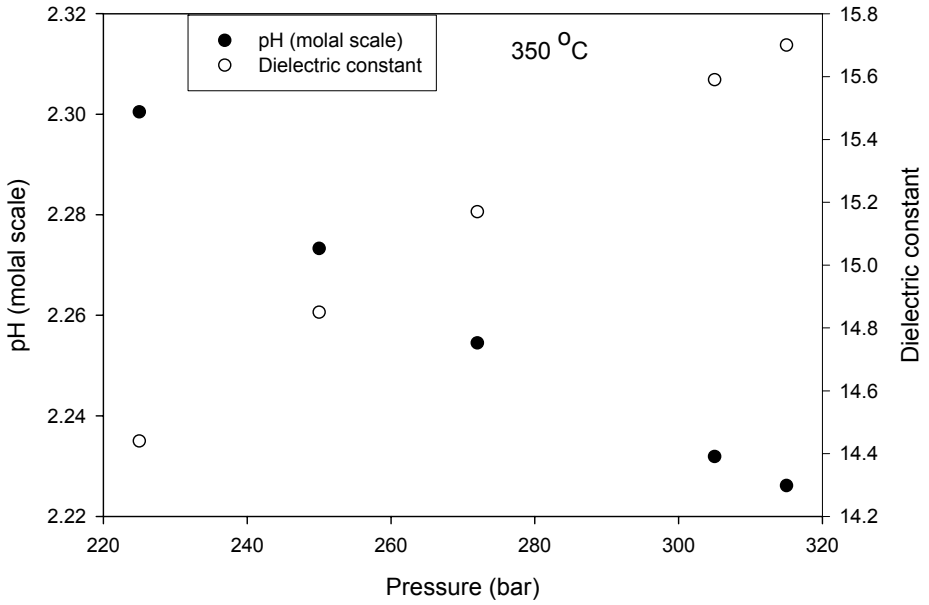

Figure 3.6: Calculated pH of 0.01 m HCl and dielectric constant of water as a function of pressure at 350 ^oC

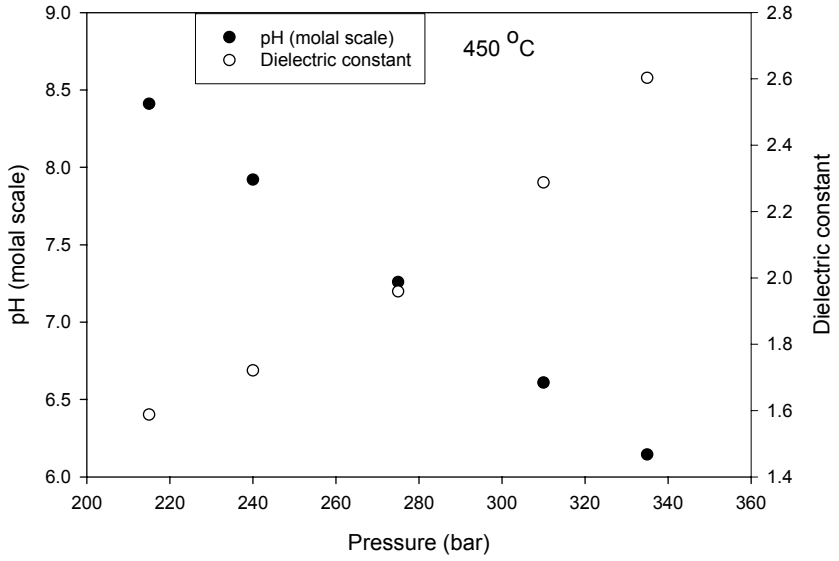

Figure 3.7: Calculated pH of 0.01 m HCl and dielectric constant of water as a function of pressure at 450 °C

3.3.3 Temperature dependence of m_{OH^-} of NaOH solutions

Figure 3.8 shows the calculated molal (mol/kg) concentration of OH^- for stoichiometric concentrations of 0.01, 0.001, and 0.0001 m NaOH as a function of temperature at 250 bar. As demonstrated by the figure, the molal concentration of OH^- decreases sharply with increasing temperature when temperatures are above 350 °C. It can be explained by the temperature dependence of dielectric constant of high temperature water in a way that the density and dielectric constant of water drops precipitously with increasing temperature at the supercritical conditions. Therefore, the degree of dissociation of NaOH drops significantly and m_{OH^-} drops sharply with increasing temperature at supercritical conditions.

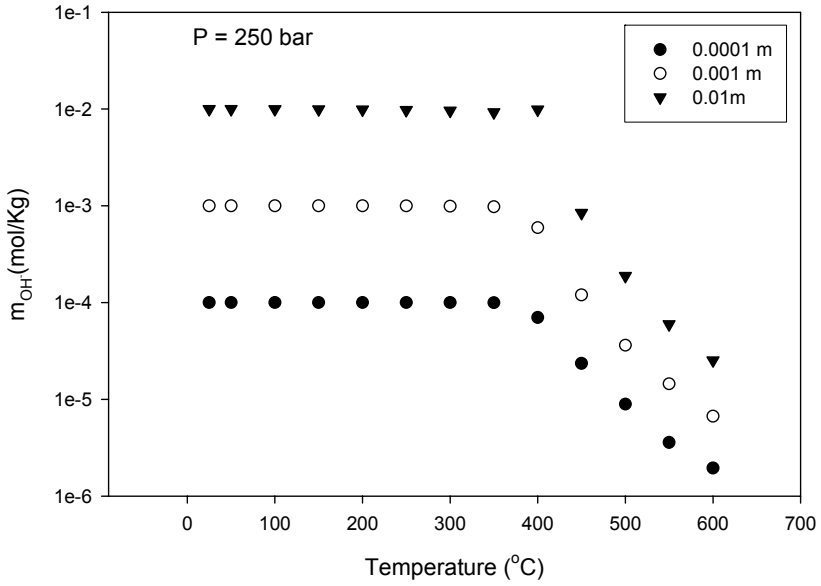

Figure 3.8: Calculated molal (mol/kg) concentration of OH^- for stoichiometric concentrations of 0.01, 0.001, and 0.0001 m NaOH as a function of temperature at 250 bar

Figure 3.9 shows calculated molal (mol/kg) concentration of OH^- for stoichiometric concentrations of 0.01, 0.001, and 0.0001 m NaOH as a function of density at 250 bar. As illustrated by the figure, the molal (mol/kg) concentration of OH^- decreases slightly with decreasing density when temperatures are below 350 ^oC (0.6255 $g.cm^{-3}$). After that, the m_{OH^-} decreases sharply with increasing temperature at supercritical conditions. It correlates with the temperature dependence of density and dielectric constant such as the density and dielectric constant decreases with increasing temperature. Consequently, the degree of dissociation of NaOH drops with decreasing density/dielectric constant, corresponding with decreasing molal concentration of OH^-.

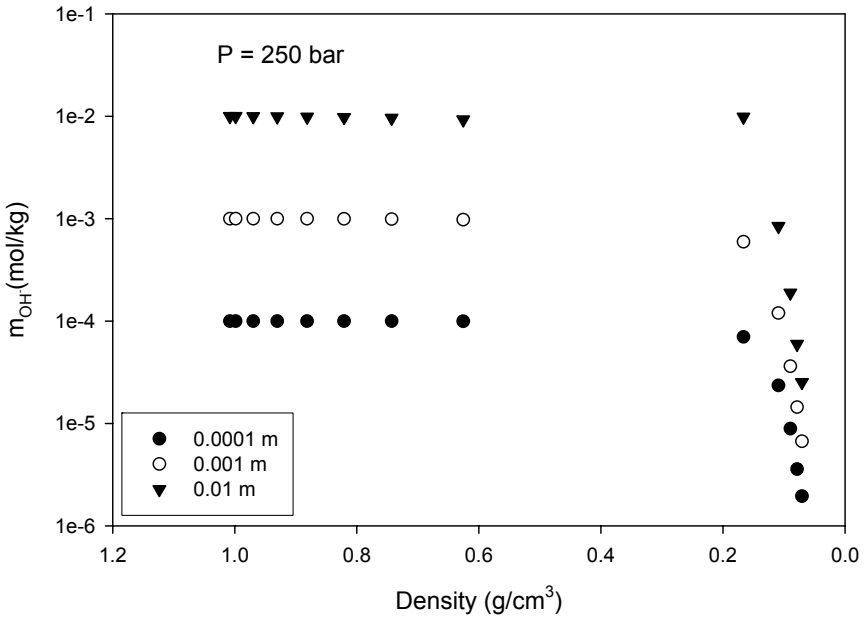

Figure 3.9: Calculated molal (mol/kg) concentration of OH^- for stoichiometric concentrations of 0.01, 0.001, and 0.0001 m NaOH as a function of density at 250 bar

3.4 Summary and Conclusions

Knowledge of pH of high temperature aqueous systems is very important for understanding corrosion processes and for estimating the susceptibility of structural materials to corrosion attacking because those corrosion processes may be related to acid attacking (H^+ and undissociated HCl). Incomplete dissociation of even strong acids/bases plays a dominant role in determination of pH of high subcritical and supercritical aqueous systems. For example, HCl is almost completely dissociated at temperatures below 350 ^oC and hence it is a strong acid. At supercritical temperatures, the degree of dissociation decreases significant and hence HCl becomes almost undissociable. Consequently, the pH

(negative logarithm of activity of H^+) increases precipitously. The pH of HCl has been calculated based on reaction constants, mass conservation, and charge conservation of HCl dissociation reaction in combination of water dissociation reaction. As expected, the pH increases slightly with increasing temperature when temperatures are below the critical temperature (374.15 ^oC). After that, the pH increases significantly with increase temperature at supercritical conditions. At the same time, it is important to note that the change of the pH does not correspond to the change of stoichiometric HCl concentrations in a proportionate manner because the degree of dissociation of HCl decreases with increasing temperature.

References

1. A. A. Chialvo, P. T. Cummings, J. M. Simonson, R. E. Mesmer "Thermodynamics and kinetics of ion speciation in supercritical aqueous solutions: a molecular-based study" Fluid Phase Equilibria **150-151**, 107 (1998)

2. M. Hodes, P.A. Marrone, G.T. Hong, K.A. Smith, J.W. Tester. "Salt precipitation and scale control in supercritical water oxidation-Part A: fundamentals and research" *J. Supercritical Fluids* **29**, 265 (2004)

3. Hermann Weingartner, Ernst Ulrich Franck, "Supercritical water as a Solvent" Angew. Chem. Int. Ed., **44**, 2672 (2005)

4. K. P. Johnson, J. B. Chlistunoff, "Neutralization of acids and bases in subcritical and supercritical water: acetic acid and HCL" *J. Supercritical Fluids* **12**, 155 (1998)

5. A. A. Chialvo, P. T. Cummings, J. M. Simonson, R. E. Mesmer "Solvation in high-temperature electrolyte solutions. 1. Hydration shell behavior from molecular simulation" Journal of Chemical Physics,**110**, 1064 (1999)

6. Patience C. Ho, Donald A. Palmer "Ion association of dilute aqueous potassium chloride and potassium hydroxide solutions to 600 ^{o}C and 300 MPa determined by electrical conductance measurements" Geochimica et Cosmochimica Acta, **61**, 3027, (1997)

7. L. B. Kriksunov, D. D. Macdonald; "Corrosion in Supercritical Water Oxidation Systems: A Phenomenological Analysis", *J. Electrochem. Soc***. 142**, 4069 (1995)

8. J. D. Frantz, W. L. Marshall, Amer. J. Sci., **284**, 651 (1984)

9. NIST Properties of water software, National Institute of Science and Technology, Gaithersburg, MD, 1997

10. J. W. Johnson, E. Ho. Oelkers, H. C. Helgeson, *Computers and Geosciences*, **18**, 899 (1992)

11. D. D. Macdonald, L.B. Kriksunov, “Probing the chemical and electrochemical properties of SCWO systems” *Electrochimica Acta*, **47**, 775 (2001)

Chapter 4

CORROSION MECHANISMS AND KINETICS OF CORROSION IN HIGH TEMPERATURE AQUEOUS SYSTEMS

4.1 Introduction

High temperature water has been widely used as a reaction/transportation medium for chemical synthesis, materials synthesis, waste destruction, and biomass processing due to its unique properties such as nontoxic, polarity, low cost, and easy separation from many products [1,2]. However, those high subcritical and supercritical aqueous systems (SCAS) can be very aggressive to many metals and alloys that have been used as reactor fabrication materials due to the severe working environments of high temperatures and high pressures. Those harsh working conditions in SCAS reactors lead to mass corrosion that few materials can withstand [3,4].

Because SCAS have properties that range from those that are characteristic of a gas phase at low pressure (low dielectric constant) to those that are characteristic of a condensed liquid phase (moderate density and higher viscosity) at high pressure, two competing corrosion mechanisms can be envisioned: “chemical oxidation” (CO) and “electrochemical oxidation” (EO) mechanisms. CO mechanism is defined as the direct chemical reactions happened on metal surfaces and EO mechanism has properties such as electrons transferring among the different cathodic/anodic sites. Discriminating between the two corrosion mechanisms is the key to developing appropriate techniques for corrosion protection of metallic reactors. In those cases where the

electrochemical mechanism dominates, various cathodic protection strategies might be effective as corrosion control techniques. On the other hand, if the chemical mechanism dominates, the most effective methods of corrosion control would be to lower the maximum operating temperature and the oxygen fugacity.

In this chapter, corrosion processes in SCAS is analyzed theoretically, with emphasis on identifying corrosion mechanisms and estimating energy of activations for electrochemical corrosion reactions in high temperature aqueous systems.

4.2 Corrosion Mechanisms and Corrosion Reaction Rate Model

The density (ρ) and dielectric constant (ε) of high temperature water depend on the temperature and pressure of the system. For instance, $\rho = 0.6255$ g·cm^{-3}, ε = 14.85 at T = 350 ^{o}C, P = 250 bar and $\rho =$ 0.1090 g·cm^{-3}, ε = 1.78 at T = 450 ^{o}C, P = 250 bar. The change of the dielectric constant of high temperature water corresponds to the change of the system density in a way that the dielectric constant decreases with increasing temperature and decreasing density. Solutes such as HCl and H_2SO_4 are fully dissociated in ambient conditions, in which the dielectric constant of water is relatively high at 78. On the other hand, strong electrolytes under ambient conditions may be very poorly ionized in low-density supercritical aqueous systems because of the low dielectric constant of the system. Consequently, the corrosion of metals in high temperature aqueous systems is significantly influenced by the temperature and pressure of the systems.

Due to the unique properties of high temperature water, the corrosion of metals and alloys in high subcritical and supercritical aqueous systems (SCAS) shows characteristics that can be attributed to either “electrochemical oxidation

(EO)" or "chemical oxidation (CO)" mechanisms, depending upon the density and dielectric constant of the media. A corrosion reaction involving partial interfacial charge transfer process, as envisioned by the Wagner-Traud hypothesis [5] in relatively high-density subcritical and supercritical solutions is called an "electrochemical oxidation" process, because the overall reaction can be decomposed into partial anodic and partial cathodic charge transfer reactions: $M \rightarrow M^{n+} + ne^-$ (partial anodic reaction) and $O_2 + 4H^+ + 4e^- \rightarrow 2H_2O$ (partial cathodic reaction). The overall reaction is: $M + (n/4)O_2 + nH^+ \rightarrow M^{n+} + (n/2)H_2O$. Because charge species are stabilized at higher dielectric constant, and because ions are more effectively hydrated at higher densities, the EO mechanism is favored in relatively high density solutions.

In general, low-density SCAS (which are often analogous to low pressure gas phases) have characteristics such as low dielectric constants, low degrees of dissociation for acids, bases, and salts, and low salt solubility. In addition, the hydrogen bonds in low-density SCAS are short. And it is much difficult for those short hydrogen bonds to accept free protons (H^+) existed in SCAS. Therefore those free protons are preferred to go back to their conjugate bases in low-density SCAS [6]. The attenuated dielectric screening of solvents enhances the tendency of ions pairing in low-density SCAS [7]. Consequently, corrosion processes occurring in low-density SCAS are dominated by direct molecular processes and are termed as "chemical oxidation" processes. Unlike the EO mechanism, in which corrosion typically involves two or more coupled redox reactions at different sites on the corroding metal surfaces, the CO mechanism is a result of the direct reaction of the metal with the corrodent (e.g., O_2 or HCl) at a single site, as indicated by the reaction $M + O_2 \rightarrow MO_2$ [8]. It is postulated that either a chemical or an electrochemical mechanism is the dominant corrosion mechanism under any given set of temperature/pressure conditions. In

"condensed aqueous systems" (defined arbitrarily here as having ρ > 0.3 gm.cm^{-3}) the EO mechanism is postulated to prevail, such that the electrochemical activity is detected in the form of noise in the coupling current between two identical specimens. The CO mechanism is the dominant corrosion process in "gaseous systems", where the density is very low (< 0.1 gm.cm^{-3}). A distinctive characteristic of the CO mechanism is that there are no electrons transferring from anodic sites to cathodic sites in corroding metals and no ions moving through the aqueous phase between the same sites. In general, the chemical oxidation mechanism becomes important when: 1) aggressive, nonionic components are present; and 2) the reaction medium has a low dielectric constant. As expected, those conditions inhibit the EO corrosion processes.

The electrochemical oxidation (EO) corrosion reaction in a deaerated acidic solution can be expressed by a chemical reaction form such as $M + 2H^+ \rightarrow M^{2+} + H_2$, which is indistinguishable from a chemical oxidation (CO) corrosion reaction such as $M + 2HCl \rightarrow MCl_2 + H_2$. The activity (concentration) of H^+ has been widely used to indicate the corrosion susceptibility in condensed liquid solutions (Pourbaix diagram). On the other hand, undissociated aggressive species such as HCl and H_2S become important in low-density supercritical aqueous systems, corresponding to the CO dominant corrosion processes. Consequently, the reaction rate of an electrochemical/chemical corrosion process in a deaerated, acidic high subcritical and supercritical solution can be expressed by the chemical reaction rate law as Eq. 4.1 [8],

$$R = k\left[C_{H^+}\right]^a \tag{4.1}$$

where k is the heterogeneous rate constant. Based on the transition state theory, the rate constant can be expressed as $k = k^0 \exp(-\Delta G^{\neq} / R_g T)$, in which superscript "^{0}" designates the reference temperature, $\Delta G^{\neq}$ is the energy of

activation and is defined as the difference in Gibb's free energy between the reactants and the transition state, and R_g is the universal gas constant. C_{H^+} in Eq. 4.1 is the volumetric concentrations of hydrogen ions and a is the corresponding reaction order. The dominant form of corrosion in high temperature acidic solutions is acid attack. Therefore, the Y^- ion is not treated as an aggressive ion and the Y^- ion induced corrosion, such as pitting, is not included in Eq. 4.1.

The volumetric concentration (mol/l of the solution) of C_{H^+} in Eq. 4.1 is density dependent and it can be expressed by molal (mol/kg of solvent) concentration by,

$$C = \frac{1000 m \rho}{1000 + m M_s} \tag{4.2}$$

where M_s is the molecular weight of dissolved species (g/mol), m the molal concentration (mol/kg), ρ the density of the solution (g/cm^3). For dilute solutions, we can approximate $C \approx m\rho$ as $mM_s << 1000$. Therefore, $C_{H^+} = m_{H^+}\rho$. A relative corrosion rate in deareated acidic solutions can be written as follows [8],

$$\frac{R}{R^0} = \left[\frac{m_{H^+}}{m^0_{H^+}}\right]^a \left[\frac{\rho}{\rho^0}\right]^a \exp\left(\frac{-\Delta G^{\neq}}{RT} + \frac{\Delta G^{\neq}}{RT^0}\right) \tag{4.3}$$

where "^{0}" designates the reference state such as ambient temperature of 25 ^{o}C, m is the molal concentration, and ρ is the density of the solution. Eq. 4.3 can be expressed in logarithmic form such as,

$$\ln\left(\frac{R}{R^0}\right) = a \ln\left[\frac{m_{H^+}}{m^0_{H^+}}\right] + a \ln\left[\frac{\rho}{\rho^0}\right] + \left(\frac{-\Delta G^{\neq}}{RT} + \frac{\Delta G^{\neq}}{RT^0}\right) \tag{4.4}$$

The first term in the right hand side of Eq. 4.4 is the temperature dependent degree of dissociation of H^+; the second term represents the effect of temperature on the volumetric concentration of attacking species; and the last term corresponds to the temperature dependence of the reaction rate constant. The model shows that the temperature dependence of the corrosion rate can be attributed to two competing effects: (1) the corrosion rate increases with increasing temperature due to the exponential (Arrhenius) dependence of the rate constant on temperature; (2) the corrosion rate decreases with increasing temperature corresponding with the decreasing dissociation constant of attacking species and decreasing density due to the temperature increasing.

4.3 Electrochemical Noise Analysis

The corrosion of reactor structural materials in high temperature, high pressure working conditions is typically evaluated by surface observation or gravimetric test. Those methods seldom provide detailed information about corrosion processes such as differential corrosion mechanisms (electrochemical vs. chemical), corrosion kinetics, and the activation parameters. Electrochemical methods, such as the linear polarization method (LPM), electrochemical impedance spectroscopy (EIS), and electrochemical emission spectroscopy (EES) [also known as electrochemical noise analysis (ENA)], can be used to study and monitor corrosion processes *in situ*. A reference electrode is required for the LPM and EIS methods, but may not be required for EES, depending upon the version of the technique adopted. In a recent review of the subject, Macdonald et al. [9] concluded that no generally applicable, accurate, reference electrode technology for measuring potentials in high subcritical and supercritical aqueous solutions exists at the present time. Additionally, EES is a non-perturbative method as no external electrical perturbation is needed to excite the system and the corrosion is measured under freely corroding conditions [10].

Electrochemical noise (EN) measurements for corrosion studies were first introduced by Iverson [11] and have become, over the last two decades, one of the most promising methods for monitoring and studying corrosion processes in high temperature aqueous solutions. The EN can be described as a series of naturally-occurring transient events and is measured as fluctuations of current noise and potential noise. Since the electrochemical noise is produced by the fluctuation in corrosion rates across the electrode surfaces, it has been proposed that the shape and size of the noise transients, among other characteristics of the EN data, are directly dependent on the type and severity of corrosion in the system [12]. Typically, electrochemical noise data are analyzed either in the time domain or in the frequency domain (and hence its designation as being a "spectroscopy"). Time domain parameters are time-varying quantities, such as the mean and the standard deviation. The analysis in the frequency domain is also called spectral estimation and the objective is to present the power as a function of frequency. The characteristic features of a specific corrosion can be analyzed in the time domain such as nucleation, propagation, and death in pitting processes should be observed as independent transient events in the time domain [12]. The spectral analysis method is used to transform the noise signals into power spectral density (PSD) plots in the frequency domain. One of the advantages of operating in the frequency domain is the fact that data can be deconvolved much more easily in the frequency domain than in the time domain.

Mansfeld et al. [13] applied the electrochemical noise analysis (ENA) to study the corrosion process of iron in different NaCl solutions and they observed that the root mean square (RMS) of electrochemical current noise is largest for iron in aerated NaCl solution where significant corrosion occurs. By applying ENA to monitor corrosion processes of carbon steel and stainless steel in high temperature (including supercritical) aqueous systems, Macdonald et al. [14,15] suggested that the RMS of the electrochemical noise is related to the corrosion rate, with a high current noise being associated with a high corrosion rate.

Experiments showed that the noise characteristic of Type 304 SS is significantly smaller than 1013 carbon steel (about 2 order of magnitude) at low temperatures (<200 ^{o}C) in oxygen-saturated water. At high temperatures (>250 ^{o}C), the amplitude of the corrosion noise from Type 304 SS increases sharply [14]. They also concluded that corrosion was the dominant source of electrochemical noise based on the correlation between the measured noise and the extent of corrosion, thus EES can be used to monitor corrosion activity in elevated temperature systems [14,15].

4.4 Experimental Setup

The experimental apparatus consists of a closed, circulating loop system as shown in Figure 4.1, within which the test solution was heated to the operating temperatures (up to 550 ^{o}C) and then was pumped into the reaction cell. The internal pressure (up to 400 bar) was generated by a mini-pump and regulated by a check valve with a precision of ±15 bar. Heating of the cell was provided for by an OMEGA heating-band and the temperature was controlled by a temperature controller with a precision of ±1^{o}C. Temperature and pressure were controlled by a K-type thermal couple and analog pressure gauge, respectively.

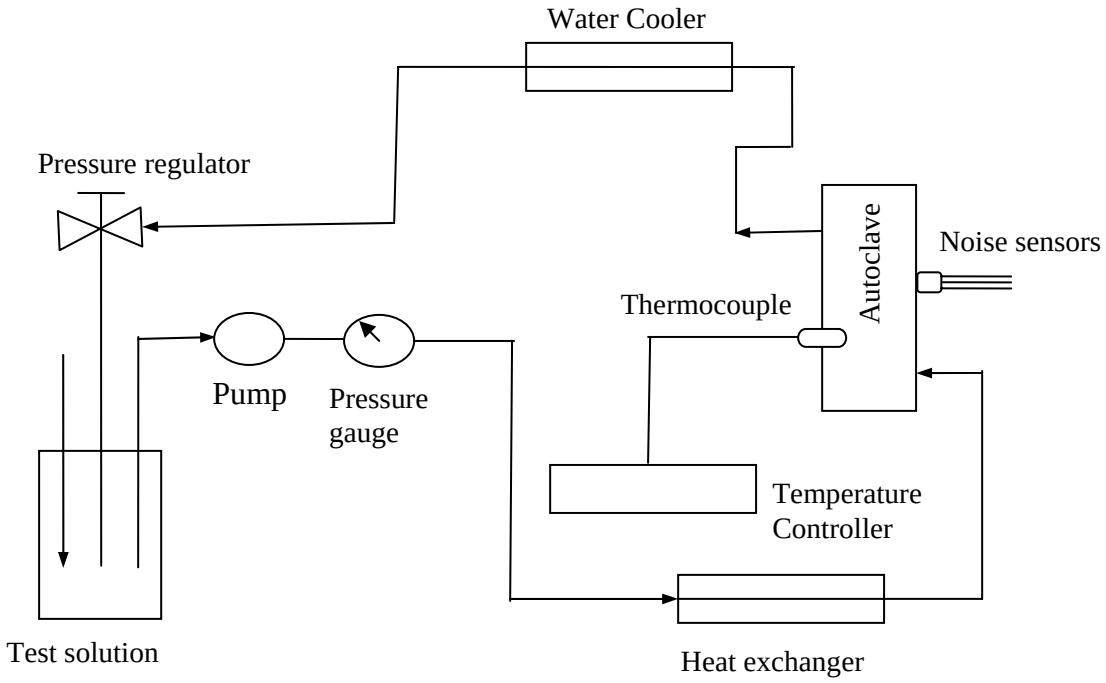

Figure 4.1:Experimental setup of high temperature, high pressure circulating loop system

Typically, electrochemical noise sensors (ENS) comprise three electrodes. Two of these are nominally identical working electrodes and the third one is used as a reference electrode. A zero-resistance ammeter (ZRA), which maintains the two identical working electrodes at the same potential level, is used to measure the coupling current noise between the identical working electrodes. The potential fluctuation between the coupled working electrodes and the reference electrode is measured as the electrochemical noise potential (ENP). If the working conditions permit, a true reference electrode, such as a saturated calomel reference electrode (SCE), is generally used as a reference electrode in ENS. In our case, a third identical working electrode is used as a pseudo reference electrode and the potential noise is measured between the paired working electrodes and the pseudo reference electrode.

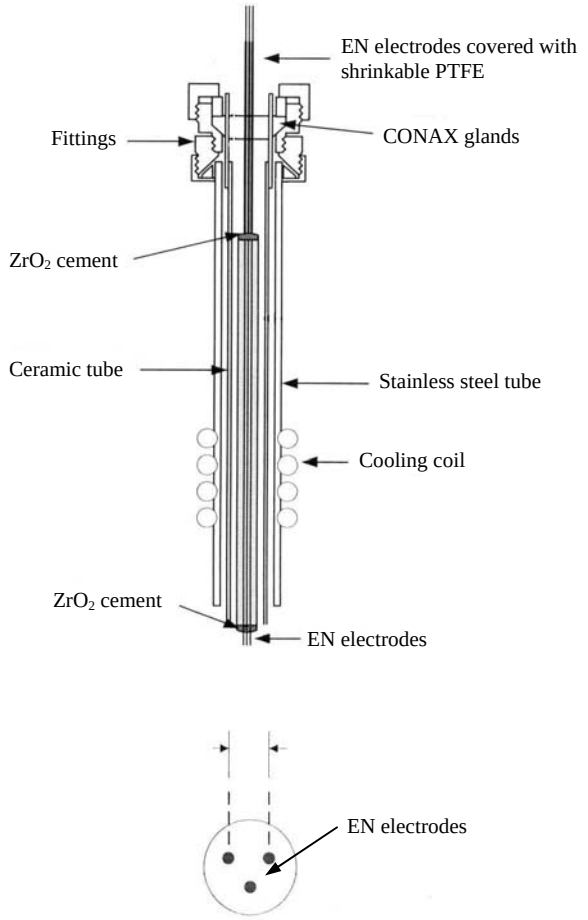

Figure 4.2: Prototype of the electrochemical noise sensor

The electrochemical noise (EN) sensors used in this study consist of three identical 0.5 mm diameter Type 304 stainless steel wires (annealed 99.99% titanium wires later) as shown by Figure 4.2. Two of the electrodes were used as the counter and working electrodes and the third was employed as the pseudo reference electrode. The three 0.5 mm diameter, identical wire electrodes were inserted into separate 1.0 mm diameter quartz tubes. The remaining space in the quartz tubes was filled with Zirconia (ZrO_2) cement to electrically insulate

electrodes from each other. The three quartz tubes were then inserted into a ceramic tube before inserting the ceramic tube into a stainless steel outer tube, which served as the pressure boundary. The ceramic and stainless steel outer tubes were sealed by Zirconia cement. The cement was dried for up to 24 hours under ambient conditions (25 ^{o}C, 1 atm) before placing the whole assembly into a furnace at 70 ^{o}C and 150 ^{o}C for 24 hours each. The length of each wire was trimmed to 15 mm at one end, which was exposed to the high temperature test solution. The electrodes were separated from each other by a distance of 3-4 mm. The exposed wire was lightly polished and washed with acetone/de-ionized water before use. The other ends of the wires were inserted into a three-hole ceramic tube. A CONAX gland with Lava sealant was used to seal the EN sensors.

Two major challenges exist in developing sensors that can be used under SCW environmental conditions. They are: (1) Electrode sealing and; (2) working solution contamination, due to dissolution of the metallic components in the high temperature, high pressure loop. A number of techniques have been employed to solve these problems. However, it is not a trivial task, primarily because a non-reactive, elastomer that can operate under supercritical water conditions is not currently available. Zirconia cements are used to insulate the electrode wires, but, as noted above, their utility is questionable, unless they are sintered at temperatures well above the melting temperatures of the metal electrodes (which cannot be done *in situ*), in order to achieve near-theoretical density. Clearly, it would be difficult to ensure electrode integrity.

The corrosion current noise between the two identical working electrodes and the potential noise between the coupled working electrodes and the pseudo reference electrode were measured simultaneously using a Gamry PC400 electrochemical system. The data were collected at an acquisition rate of 2Hz as most noise transient events are in the low frequencies range of 10^{-3}Hz to 1Hz

[12]. A high-frequency filter was used in this studying to prevent aliasing. The instrument was used as a Zero Resistance Ammeter (ZRA, to maintain the two identical working electrodes at same potential level), in order to measure the coupling current noise, and as an electrometer to measure the potential noise, with both measurements being made simultaneously. A platinum/hydrogen internal electrode was used as a reference electrode for polarization study. All of the experiments were performed in diluted HCl solution (0.01 m).

4.5 Results and Discussion

4.5.1 Corrosion mechanisms

One of the two corrosion mechanisms (chemical oxidation and electrochemical oxidation) should prevail under any given set of working conditions. Electrochemical noise (spontaneous potential and current emissions) should be observed only in the case of the electrochemical oxidation (EO) mechanism and not in the case of the chemical oxidation (CO) mechanism. This is postulated, because only in the EO case is the partial anodic and partial cathodic reactions spatially and temporally separated, resulting in current transients being induced in the wire coupling identical specimens. Thus, the noise in the coupling current between a pair of identical working electrodes in high pressure, high temperature aqueous environments has been measured as a function of pressure (up to 300 bar) and temperature (up to 500 ^{o}C). It is assumed that the amplitude of the current noise (standard deviation of current noise) is proportional to the electrochemical corrosion rate, when the electrochemical mechanism is operative [14, 15].

Figure 4.3 shows the relationship between the standard deviation of the current noise (proportional to electrochemical corrosion rate) and temperature for Type 304 stainless steel in deaerated 0.01 M HCl. The working pressure was 250 bar and the HCl solution was deaerated by nitrogen gas sparging. The current noise is observed to increase to a maximum as the temperature rises to approximately 350 ^{o}C. Then, the current noise decreases sharply after the temperature passes the critical point (374.15 ^{o}C). This can be explained by the chemical/electrochemical corrosion mechanisms theory, as outlined earlier in this paper. Below the critical temperature, the increased corrosion activity, due to increasing temperature (exponential dependence of the rate constant on temperature), dominates over the effects of changing density and dielectric constant, resulting in the electrochemical corrosion rate increasing as the temperature increases. Beyond the critical temperature, the test solution changes from a condensed, liquid aqueous phase to a gas-like phase and the density decreases sharply. Consequently, the molal concentration of H^{+} decreases sharply with increasing temperature at high subcritical and supercritical temperatures. Under those conditions, the electrochemical oxidation (EO) corrosion mechanism is less prevalent and the corrosion current noise decreases sharply due to the dominant effects of increasing temperature on the concentration of the aggressive species and on the dielectric constant of the solution. This result corresponds to experimental observations that severe corrosion damage occurs in those regions of a reactors that operate at temperatures just below the critical temperature, whereas less damage is observed at higher or lower temperatures [3,4,16].

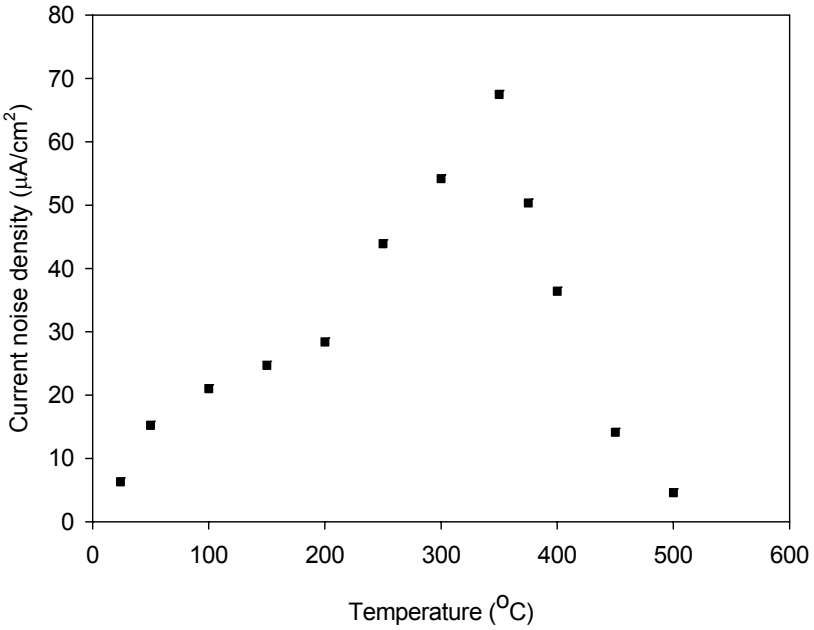

Figure 4.3: Electrochemical corrosion rate (standard deviation of the current noise) of Type 304 SS as a function of temperature at 250 bar in deaerated 0.01 M HCl

Figure 4.4 shows the effect of the presence of oxygen on the electrochemical corrosion rate of Type 304 SS in 0.01 M HCl. The solid points in the figure represent the electrochemical current noise of Type 304 SS in deaerated 0.01 M HCl (N_2 sparged) and the open points represent the electrochemical current noise of the steel in 0.01 M HCl purged by oxygen gas. The working pressures for both experiments were 250 bar. Similar as the corrosion process of Type 304 SS in deareated 0.01 M HCl (Figure 4.3), the current noise (proportional to electrochemical corrosion rate) of Type 304 SS in oxygenated 0.01 M HCl increases with increasing temperature before the temperature reaches to the critical region, and then the current noise decreases as the temperature passes the critical temperature of water (374.15 ^{o}C). The

electrochemical corrosion rate at the maximum at 350 ^{o}C in the oxygenated environment (115 ppm or 0.0063 mol/kg O_2) is only marginally greater than that in the deaerated environment. These data indicate that, by itself, oxygen is not a particularly aggressive solute, as indicated by the relative corrosion rates observed in the deaerated vs. the oxygenated environments. The graph shows that the presence of oxygen increases the corrosion rate within the temperature range of 150 ^{o}C to 400 ^{o}C. At the peak, the increase is ~50%. It is important to note that the drop-off of the current noise becomes less steep as temperature ascends above 400 ^{o}C in both experiments. This indicates that, under constant pressure conditions in a high supercritical environment, the effect of temperature on reaction rate constant becomes important and the effect of temperature on system density is decreased at temperatures above 400 ^{o}C.

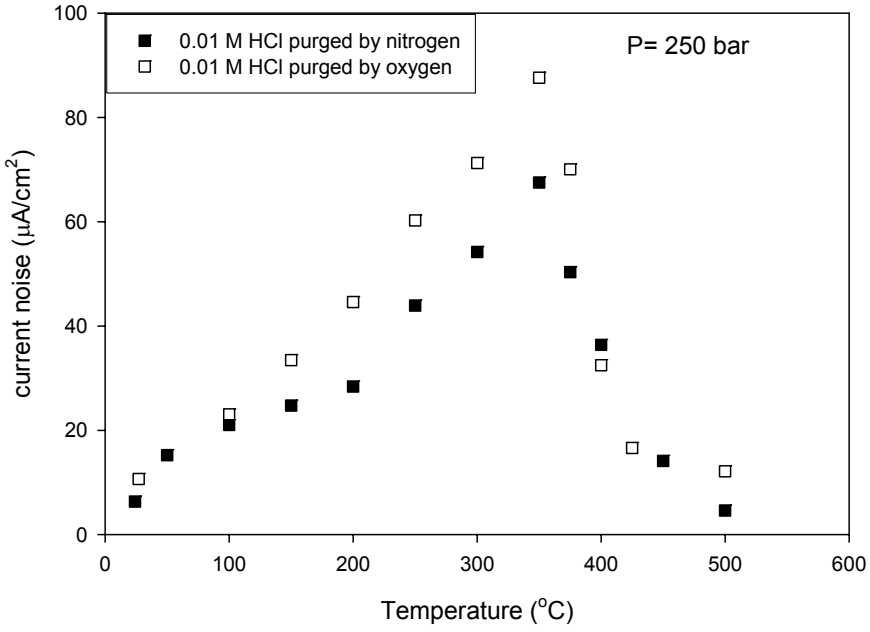

Figure 4.4: Comparison of electrochemical corrosion rates (standard deviations of current noise) of Type 304 SS in deaerated 0.01 M HCl and in 0.01 M HCl purged with oxygen gas as a function of temperature at 250 bar

Figure 4.5 compares electrochemical current noise (proportional to electrochemical corrosion rates) of Type 304 SS and of titanium in deaerated 0.01 M HCl as a function of temperature at 250 bar. The solid squares are the current noise of Type 304 SS and open squares are the current noise of titanium respectively. As shown by the figure, the current noise of titanium increases with increasing temperature before the temperature reaches the critical area, then the current noise decreases with increasing temperature. The phenomenon can be explained by the electrochemical/chemical corrosion mechanisms. The electrochemical corrosion rate increases with increasing temperature before it reaches a maximum value at 350 ^{o}C because the corrosion process is dominated by increasing corrosion activity with increasing temperature. Then the electrochemical corrosion rate decreases sharply in the high subcritical and supercritical region, because of the low degree of dissociation of aggressive species and low dielectric constant of the systems. The graph shows that the titanium is more corrosion resistant than Type 304 SS in 0.01 M HCl as the current noise of Type 304 SS is around 20-50% higher than the current noise of titanium. Botella et al. [17] reported that the titanium and its alloys have relatively high corrosion resistance when they were exposed to high subcritical and supercritical HCl solutions, which can be attributed to the formation of the protective passive film on the titanium surface. They also reported that the titanium corrosion rate increases with increasing temperature in subcritical temperature range and decreases with increasing temperature in supercritical temperature range. It is consistent with the results observed from Figure 4.5**.**

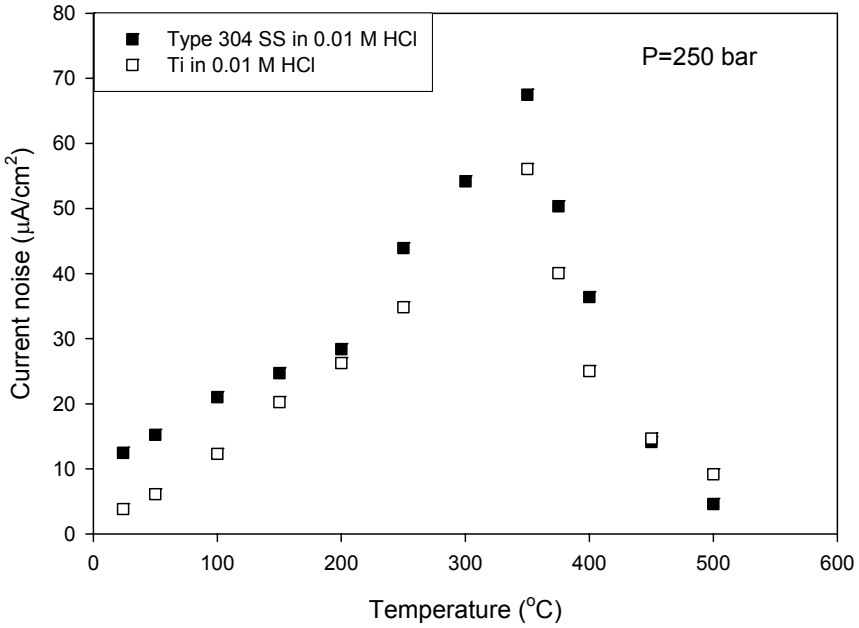

Figure 4.5: Comparison of electrochemical corrosion rates (standard deviations of current noise) of Type 304 SS and Ti in deaerated 0.01 M HCl as a function of temperature at 250 bar

Figure 4.6 shows the current noise of Type 304 SS as a function of temperature in 0.01 M HCl and in 0.01 M H_2SO_4 respectively. The working pressures for both experiments were 250 bar. Both HCl and H_2SO_4 solutions in the figure were purged by oxygen. Similar as in 0.01 M HCl, the electrochemical corrosion rate of Type 304 SS in 0.01 M H_2SO_4 increases with increasing temperature before reaching a maximum value at approximate 350 ^oC. Then the electrochemical current noise decreases sharply in the supercritical temperature region (T > 375 ^oC) because of the low dielectric constant and low-density of the high temperature medium. As demonstrated by the figure, a relatively large current noise was obtained in 0.01 M HCl than in 0.01 M H_2SO_4, which may be due to the presence of pitting corrosion in HCl solution.

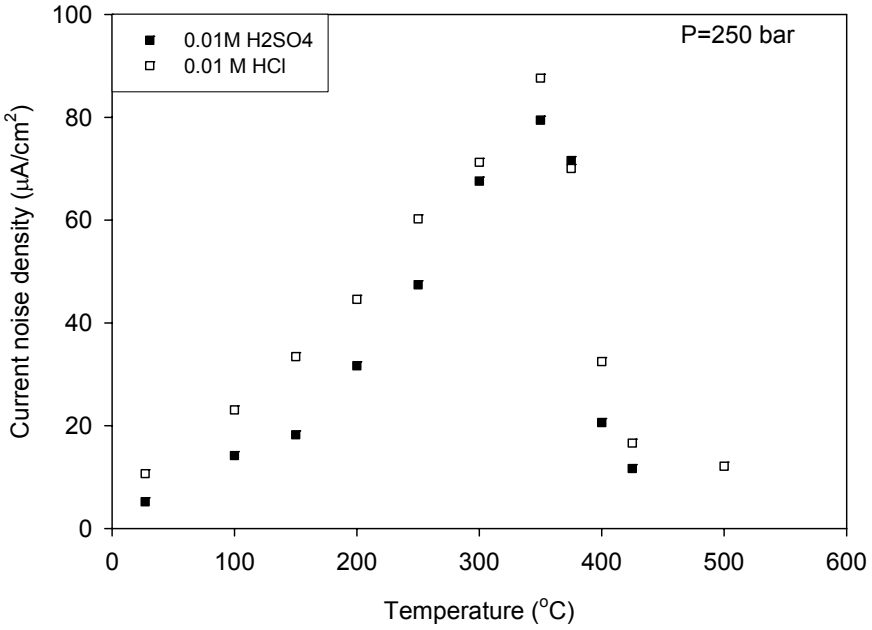

Figure 4.6: Comparison of electrochemical corrosion rates (standard deviations of the current noise) of Type 304 SS in 0.01 M H_2SO_4 purged by oxygen and in 0.01 M HCl purged by oxygen as a function of temperature at 250 bar

Figure 4.7 shows the response of standard deviation of current noise of Type 304 SS in deaerated 0.01 M NaOH as a function of temperature. The working pressure was 250 bar. The current noise is observed to increase to a maximum value as the temperature rises to 300 ^{o}C. Then, the current noise decreases sharply. This can be explained by the chemical/electrochemical corrosion mechanisms theory, as outlined previously in this paper. Again, the corrosion process is dominated by exponentially (Arrhenius) dependence of the rate constant on increasing temperature when temperature is less than 300 ^{o}C. At temperatures higher than that at which the maximum corrosion rate occurs, the standard deviation of the current noise decreases sharply with increasing

temperature, following the same behavior observed in other systems for the same reasons.

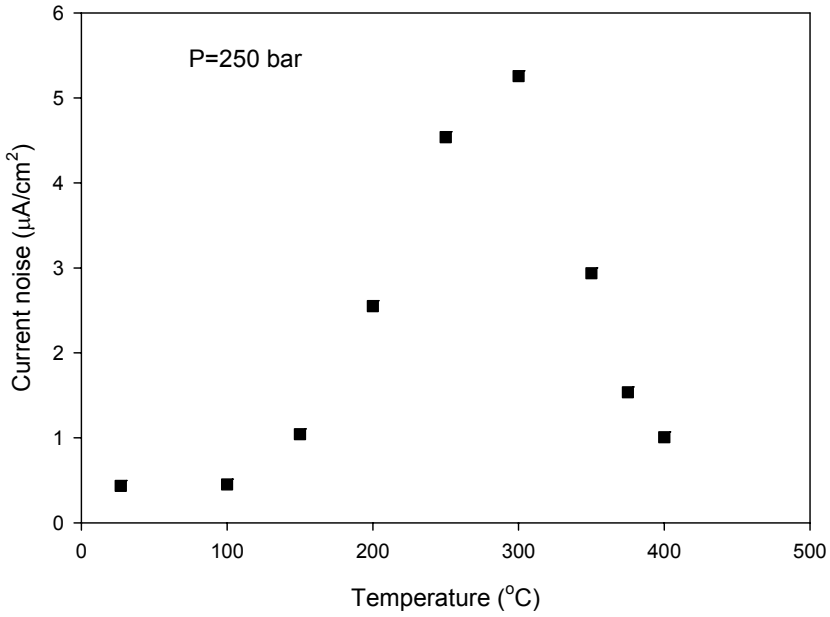

Figure 4.7: Electrochemical corrosion rate (standard deviation of the current noise) of Type 304 SS as a function of temperature at 250 bar in 0.01 M NaOH purged with nitrogen

Figure 4.8 compares electrochemical corrosion rates (standard deviation of current noise) of Type 304 SS in water, 0.01 M NaOH, and in 0.01 M HCl. The media in all three experiments were purged by N_2 and the working pressures were identical at 250 bar. The electrochemical current noise of Type 304 SS in 0.01 M NaOH is around 5 times higher than that in water at 350 ^{o}C. The current noise of Type 304 SS in 0.01 M HCl is much higher than those in 0.01 M NaOH and water as demonstrated by the figure. The standard deviation of the current

noise from Type 304 SS in 0.01 M HCl is 20 times higher than that from the same alloy in 0.01 M NaOH at 350 ^{o}C.

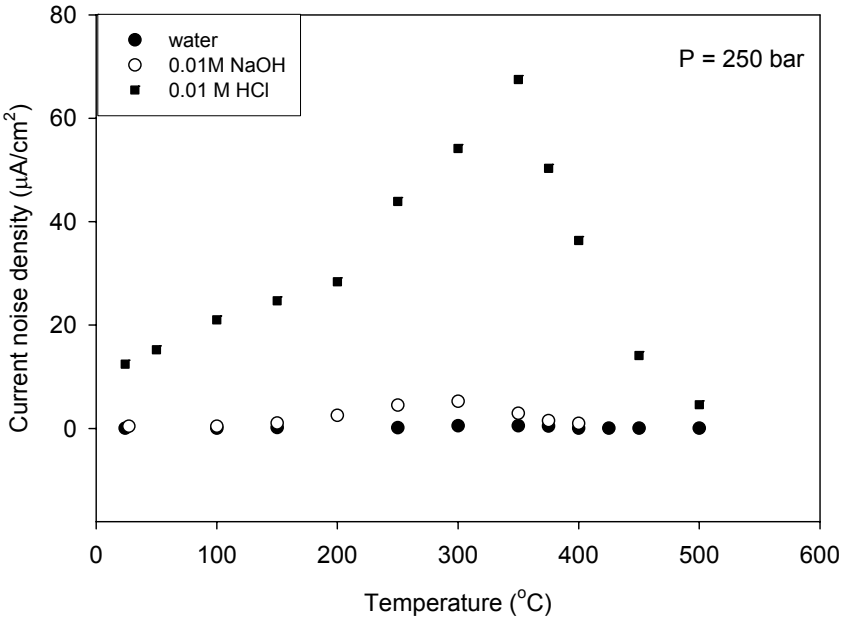

Figure 4.8: Comparison of electrochemical corrosion rates (standard deviations of the current noise) of Type 304 SS in deaerated water, in deaerated 0.01 M NaOH and in deaerated 0.01 M HCl at 250 bar as a function of temperature

Figure 4.9 compares electrochemical corrosion rates (standard deviation of current noise) of Type 304 SS in 0.01 M HCl and in 0.05 M HCl as a function of temperature. The solid circles in the figure represent the electrochemical current noise of Type 304 SS in deaerated 0.01 M HCl (N_2 sparged) and the open circles represent the electrochemical current noise of the steel in deaerated 0.05 M HCl. The working pressures for both experiments were 250 bar. Similar as the corrosion process of Type 304 SS in deareated 0.01 M HCl, the current noise (proportional to electrochemical corrosion rate) of Type 304 SS in

deaerated 0.05 M HCl increases with increasing temperature before the temperature reaches to the critical region, and then the current noise decreases as the temperature passes the critical temperature of water (374.15 ^{o}C). This can be explained by the chemical/electrochemical corrosion mechanisms theory, as outlined previously in this chapter. As expected, the electrochemical corrosion rate in 0.05 M HCl is higher than the electrochemical corrosion rate in 0.01 M HCl due to the high concentration of aggressive species H^{+} in 0.05 M HCl.

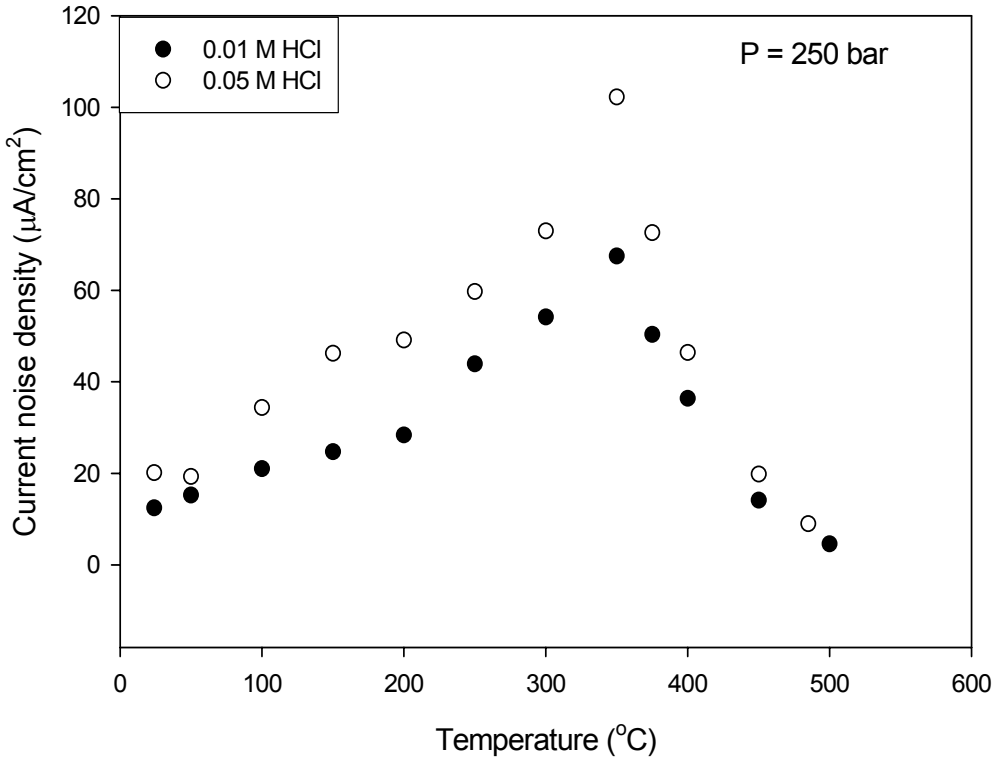

Figure 4.9: Comparison of electrochemical corrosion rates (standard deviations of the current noise) of Type 304 SS in deaerated 0.01 M HCl and in deaerated 0.05 M HCl at 250 bar as a function of temperature

4.5.2 Energy of activation of corrosion in high temperature aqueous systems

The electrochemical corrosion reaction rate of metals in deaerated acidic solutions can be expressed as follows,

$$R = k\left[C_{H^+}\right]^a = k\left[m_{H^+}\right]^a\left[\rho\ \right]^a \qquad (4.5)$$

where a is the reaction order with respect to H^+. As there is no data available for the reaction order (with respect to H^+) of electrochemical corrosion reactions of metals in high temperature acidic solutions, it is assumed that the reaction is a half order reaction and $a = 1/2$ in the study. The energy of activation ($\Delta G^{\neq}$), which may be determined by diffusion or charge transfer of corrosion processes, is defined as the difference in Gibb's free energy between the reactants and the transition state based on the transition state theory. The extent of kinetics of corrosion processes can be analyzed by estimating the energy of activation of the corrosion processes. In this study, the energy of activation of corrosion processes in high temperature aqueous systems has been obtained by solving Eq. 4.4. The density in the equation was taken as that for pure water and it can be obtained from the NIST steam data as the work solutions were diluted solutions [18]; the relative corrosion rate R/R^0 was measured experimentally by electrochemical noise analysis (ENA); and the molal concentration of hydrogen ions (m_{H^+}) was calculated by solving the dissociation reaction of HCl in combination with the dissociation reaction of water based on mass balance, charge balance, and reaction constants [8].

Figure 4.10 shows the energy of activation of electrochemical corrosion processes of Type 304 SS and titanium in deaerated 0.01 M HCl at the temperature range of 50 - 250 ^oC. The solid squares in the figure are the energy of activation of Type 304 SS and the open squares are the energy of activation of

titanium. As shown by the figure, the energy of activation of corrosion process of Type 304 SS in HCl is lower than the energy of activation of corrosion process of titanium. This means that titanium is more corrosion resistant than Type 304 SS in 0.01 M HCl. This observation is consistent with the results obtained before as demonstrated by Figure 4.5, in which the magnitude of electrochemical current noise of titanium is lower than the magnitude of electrochemical current noise of Type 304 SS in 0.01 M HCl. The high corrosion resistance of titanium can be attributed to the formation of a protective passive film on its surface. It is important to note that the above calculation of the energy of activation is based on the assumptions such as the electrochemical corrosion rate is proportional to the current noise and the corrosion reaction is a half order reaction. At the current time, there is no theoretical and experimental support for those assumptions.

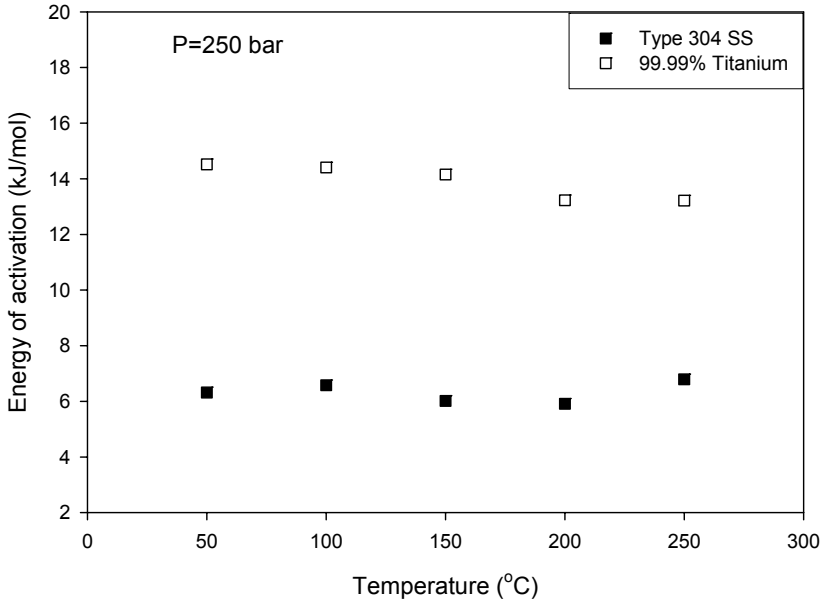

Figure 4.10: Comparison of energy of activation of electrochemical corrosion processes of Type 304 SS and Ti in deaerated 0.01 M HCl solution at 250 bar as a function of temperature

4.6 Summary and Conclusion

Two corrosion mechanisms, i.e. “electrochemical oxidation” and “chemical oxidation”, have been proposed to describe corrosion processes in high temperature aqueous systems. A corrosion reaction model has been applied for describing the corrosion reactions in high subcritical and supercritical acidic solutions with emphasis on the temperature effect on corrosion rates. The model shows that the temperature dependence of corrosion rates can be attributed to the temperature effects on the concentration of the aggressive species, on the dielectric constant of the solution, and on the reaction activation energy. The model has been evaluated by monitoring corrosion processes of Type 304 SS in HCl solutions as a function of temperature. At the same time, the energy of activation of corrosion processes of different alloys has been estimated. The principle findings of this study are as follows.

1. Analysis of corrosion reactions by electrochemical emission spectroscopy (EES) demonstrates that two corrosion mechanisms, i.e. “chemical oxidation” (CO) and “electrochemical oxidation” (EO), can be used to explain the corrosion processes in high subcritical and supercritical aqueous systems. The electrochemical mechanism prevails in “aqueous systems” (ρ > 0.3 g.cm^{-3}), such that the electrochemical activity is detected in the form of noise in the coupling current between two identical specimens. When the temperature exceeds the critical temperature (374.15 ^{o}C), the test solution changes from the condensed liquid phase to the “gaseous” phase and the corrosion current noise decreases, corresponding to the dominance of the chemical mechanism. The maximum in the corrosion rate is found to occur at temperatures between 310 ^{o}C and 360 ^{o}C.

2. The energy of activation of Type 304 SS and titanium in 0.01 M HCl at the temperature range of 50 – 250 ^{o}C was estimated. As expected, the energy of

activation of electrochemical corrosion processes of Type 304 SS in HCl solutions is lower than that of titanium, which can be explained by the high corrosion resistance of titanium in high temperature HCl solutions due to the formation of the strong protective passive film on the surface of titanium.

References

1. P. Savage, S. Gopalan, T. Mizan, C. Martino, E. Brock, “Reactions at Supercritical Conditions: Applications and Fundamentals”, *AIChE Journal*, **41**, 1723 (1995)

2. H. Weingartner, E. Franck, “Supercritical Water as a Solvent” *Angew.Chem.Int. Ed*. **44**, 2672 (2005)

3. P. Kritzer, N. Boukis, E. Dinjus, “Corrosion of Alloy 625 in Aqueous Solutions Containing Chloride and Oxygen”, *Corrosion,* **54**, 824 (1998)

4. R. M. Latanision, R. W. Shaw, “Corrosion in supercritical water oxidation systems, Workshop Summary”, MIT The Energy Laboratory, Workshop Summary, Massachusetts Institute of Technology, Boston, MA. 1993

5. K. Wagner, W. Traud, Z. *Elektrochem* **44**, 391 (1938)

6. A. A. Chialvo, P. T. Cummings, J. M. Simonson, “H_3O^+/Cl^- ion-pair formation in high-temperature aqueous solutions” *J. Chem. Phys*. **113**, 8093 (2000)

7. N. Akiya, P. E. Savage, *Chem. Rev*. **102**, 2725 (2002)

8. L. B. Kriksunov, D. D. Macdonald; “Corrosion in Supercritical Water Oxidation Systems: A Phenomenological Analysis”, *J. Electrochem. Soc***. 142**, 4069 (1995)

9. Macdonald, D. D., T. Zhu, and X. Guan, “Current State-of-the-Art in Reference Electrode Technology for Use in High Subcritical and Super Critical Aqueous Systems”, *Corrosion*, submitted (2006)

10. J. L. Dawson, “Electrochemical Noise Measurement for Corrosion Applications”, p.3-35 ASTM Publication Code Number (PCN) 04-012770-27

11. W. P. Iverson, *J. Electrochem. Soc*. **115**, 617 (1968)

12. R. A. Cottis, “Interpretation of Electrochemical Noise Data”, *Corrosion*, **57**, 265 (2001)

13. F. Mansfeld and H. Xiao, “Electrochemical Noise Analysis of Iron Exposed to NaCl Solutions of Different Corrosivity”, *J. Electrochem. Soc*. **140**, 2205 (1993)

14. C. Liu, D. D. Macdonald, E., Medina, J. J. Villa, and J. M. Bueno; “Probing Corrosion Activity in High Subcritical and Supercritical Water Through Electrochemical Noise Analysis”, *Corrosion,* **50**, 687 (1994)

15. X. Y. Zhou, S. N. Lvov, X. J. Wei, L. G. Benning, D. D. Macdonald, “Quantitative Evaluation of General Corrosion of Type 304 Stainless Steel in Subcritical and Supercritical Aqueous Solutions via Electrochemical Noise Analysis”, *Corrosion Science,* **44**, 841 (2002)

16. D. A. Hazlebeck, K. W. Downey, D. D. Jensen, and M. H. Spritzer, *in Physical Chemistry of Aqueous Proc. 12 th International Conference on the Properties o Water and Steam*, H. J. White, et al., Editors, p. 632, Begell House, New York (1995)

17. Ph. Botella, C. Frayret, Th. Jaszay, M. H. Delville; “Experimental study, via current-potential curves, of the anodic behavior of Alloy C-276 and T60 titanium in chlorinated and oxygenated aqueous media under sub- to supercritical conditions” *J. of Supercritical Fluids*, **25**, 269 (2003)

18. NIST Steam Algorithm, National Institute of Science and Technology, Gaithersburg, MD, 1994

19. D. D. Macdonald, L.B. Kriksunov, “Probing the chemical and electrochemical properties of SCWO systems” *Electrochimica Acta*, **47**, 775 (2001)

20. Y. Y. Chen, U. T. Hong, H. C. Shih, J. W. Yeh, and T. Duval “Electrochemical kinetics of the high entropy alloys in aqueous environment-a comparison with type 304 stainless steel” *Corrosion Science*, **47**, 2679 (2005)

Chapter 5

POLARIZATION STUDY AND MONITORING INSTANTANEOUS CORROSION RATE

5.1 Polarization Study

5.1.1 Introduction

Electrochemical analysis of corrosion processes, such as polarization study and impedance spectroscopy technology, plays an important role in selecting proper materials for using in many industrial environments, including high temperature and high pressure working conditions. Unlike *ex situ* corrosion analysis methods (i.e. surface observation and gravimetric test), the electrochemical corrosion analysis methods can monitor corrosion processes *in situ*. Therefore, detailed information about corrosion processes such as corrosion mechanisms and corrosion kinetics can be obtained. Even though extensive polarization studies of metals and alloys have been performed in the ambient and low subcritical temperature conditions, electrochemical polarization studies in high subcritical and supercritical aqueous systems (SCAS) are rarely reported due to the harsh thermodynamic conditions and experimental difficulties [1,2]. Huang et al. evaluated corrosion processes of Type 304 SS at 400 ^{o}C and 24 MPa in both deionized water and a 0.005 M Na_2SO_4 solution by polarization method [3]. They observed an abnormal high corrosion current, which may be caused by improper experimental procedures such as the application of extremely high polarization rate of 8.33 mV/s and the low reliability of the proposed reference electrode. Macdonald et al. reported that polarization curves

can be observed for nickel in 0.01 m NaOH up to the temperature of 430 ^{o}C [2]. They applied an external silver/silver chloride external pressure balanced electrode (EPBRE) as the reference electrode in the experiments. In which, thermal liquid junction potential was expected.

In this study, experimental techniques for performing dynamic electrochemical polarization in high temperature aqueous systems have been developed (up to the temperature of 500 ^{o}C). The polarization experiments were carried out for Type 304 SS and titanium in 0.01 m HCl solution.

5.1.2 Experimental setup

Electrochemical measurement of corrosion in high subcritical and supercritical aqueous systems (SCAS) faces many experimental difficulties such as susceptibility of the reaction cell to corrosion, electrodes electrical insulation, water tightness, and lack of reliable reference electrodes at supercritical conditions. In this study, experimental techniques for performing dynamic electrochemical polarization study in SCAS have been developed, in which the measurements were taken in a high temperature/high pressure stainless steel reaction cell. The experimental apparatus consists of a closed, circulating loop system as shown by Figure 5.1, within which the test solution was heated to the operating temperatures (up to 550 ^{o}C) and then was pumped into the reaction cell. The internal pressure (up to 400 bar) was generated by a mini-pump and regulated by a check valve with a precision of ±15 bar. Heating of the cell was provided for by an OMEGA heating-band and the temperature was controlled by a temperature controller with a precision of ±1^{o}C. Temperature and pressure were controlled by a K-type thermal couple and analog pressure gauge, respectively.

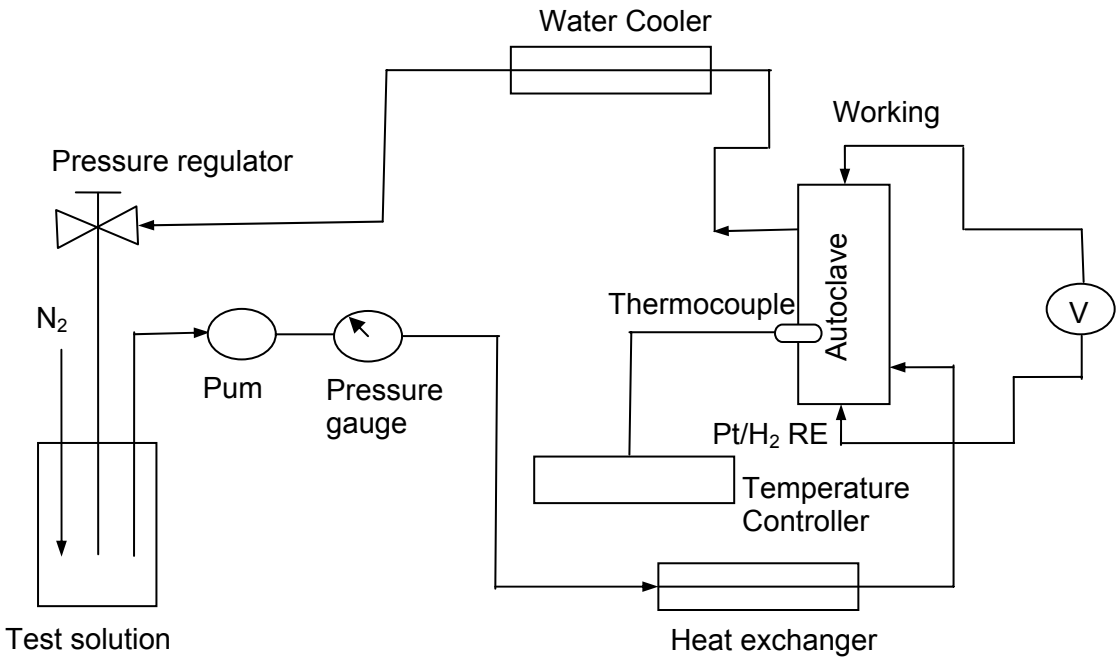

Figure 5.1: Experimental setup of high temperature, high pressure circulating loop system

The three-electrode reaction cell consists a 0.5 mm diameter Type 304 SS (titanium wire later) working electrode, a 0.5 mm diameter platinum counter electrode, and a platinum/hydrogen internal reference electrode. The 0.5 mm diameter working electrode was inserted into a 1.0 mm diameter quartz tube. The remaining space in the quartz tube was filled with Zirconia (ZrO_2) cement to water-tight the electrode. The quartz tube was then inserted into a ceramic tube before inserting the ceramic tube into a stainless steel outer tube, which served as the pressure boundary. The ceramic and stainless steel outer tubes were sealed by Zirconia cement. The length of the working electrode was trimmed to 20 mm at one end, which was exposed to the high temperature test solution, and it was lightly polished and washed with acetone/de-ionized water before use. A CONAX gland with Lava sealant was used to seal the working electrode. The platinum/hydrogen reference electrode employed in experiments is a 0.5mm

diameter platinum wire (99.99% pure from Alfa Aesar). The platinum wire was coiled and then lightly platinized by cathodic polarization in a solution of platonic chloride. The manufacture procedure for the platinum/hydrogen reference electrodes is similar as the manufacture procedure for the working electrode. The polarization potential between the working electrode and the reference electrode and the corrosion current density between the working electrode and the counter electrode were measured simultaneous by Gamry PC400 electrochemical system.

Potential dynamic polarization has been performed to obtain the polarization curves. In order to achieve the psedo-steady state condition, a relatively low potential sweep rate (0.15 mV/s) was applied. Deaerated 0.01 M HCl was used as the working solution to mimic the working environments.

5.1.3 Potential Normalization

By applying the Nernst equation, the potential measured with respect to platinum/hydrogen reference electrode can be normalized to the standard hydrogen electrode (SHE) scale, such as

$$E_{H^+/H_2(vs.SHE)} = -\frac{RT}{2F}\ln f_{H_2} + \frac{RT}{F}\ln[H_2] \qquad (5.1)$$

where f_{H_2} is the fugacity of hydrogen and F is Faraday constant. The equilibrium vapor pressure of diluted solutions can be expressed by Henry's law as follows,

$$P_A = k_A X_A \qquad (5.2)$$

where k is the Henry's constant and X_A is mole fraction of element A. We assume that the mole concentration of H^+ is constant at temperatures below the critical temperature (374.15 ^oC), therefore we have

$$f_{H_2}^T / k_{H_2}^T = f_{H_2}^0 / k_{H_2}^0 \tag{5.3}$$

in which $k_{H_2}^T$ is Henry's constant at temperature T and "0"is the reference point such as at the ambient temperature. Henry's constant for $H_2 - H_2O$ system at temperatures below 365 ^oC can be written as a function of temperature such as [4],

$$\ln k = \frac{B_0}{T}(T_{cr} - T)\ln(\frac{T_{cr} - T}{T_{cr}}) + \sum_{i=0}^{N} \frac{B_{i+1}}{T^i}(1000)^i \tag{5.4}$$

in which B_i are constant values.

At temperatures > 374.15 ^oC, the fugacity of hydrogen can be estimated by the mole fraction of hydrogen in the "gaseous" solution, such as,

$$P_{H_2(>T_{cr})} = X_{H_2} P_{total} \tag{5.5}$$

and the mole fraction of hydrogen at the reference state can be calculated based Henry's law. A software developed by Macdonald and his colleagues has been used to estimate the concentration of H^+ in HCl solution at different temperatures [6].

5.1.4 Results and Discussion

Polarization study of corrosion processes of Type 304 SS and titanium in 0.01 M HCl was performed at various temperatures (up to 500 ^oC). The working pressure was constant at 250 bar for all experiments. The polarization potential

was applied between the working electrode and the internal Pt/H_2 reference electrode at a relatively low potential sweep rate of 0.15 mV/s. The current density was measured between the working electrode and the counter electrode by Gamry PC400.

Figure 5.2 shows the polarization curves obtained for Type 304 SS in deaerated 0.01 M HCl over the temperature range of 50 - 500 ^{o}C. The passivity is observed at temperatures up to 300 ^{o}C, with the secondary passivation potential being observed over the temperature range of 50 - 200 ^{o}C. The secondary passivation potential divided the passivation range into the two sub-domains, which may be caused by the transition of the passive film from $Cr(OH)_2$ to $Cr(OH)_3$ [5]. As illustrated by the figure, the range of passivity shrinks considerably and passive current density increases sharply with increasing temperature over the temperature range of 50 - 300 ^{o}C. The shrinkage of the passive film with increasing temperature may be caused by the shifting of the transpassive potential (the upper boundary of the passive region) to lower values. The increasing passive current density with increasing temperature can be attributed to the temperature related kinetics of ion transport through the passive film [6]. As shown by the figure, at temperatures $\geq$ 400 ^{o}C, the corrosion current density increases monotonically with increasing anodic overpotentials and no passivity can be observed. The absence of passivity can be explained by weakening/destruction of passive film in those extremely high temperature working environments. In any event, the weakening/destruction of the passive film imply the increased susceptibility to corrosion. In addition, the figure also shows that the corrosion potential, E_{corr}, of Type 304 SS becomes more active (negative) with increasing temperature. It implies that Type 304 SS tends to corrode more easily with increasing temperature.

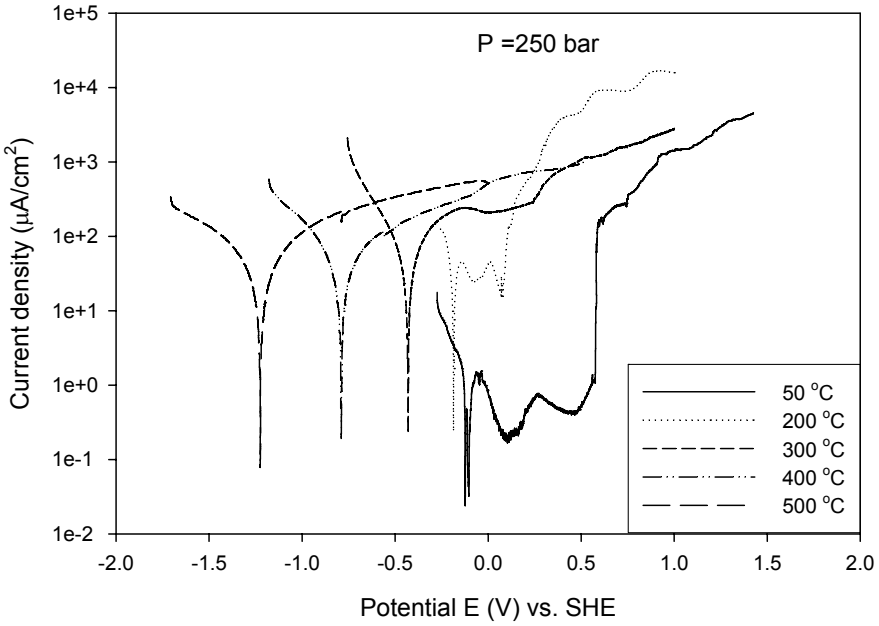

Figure 5.2:polarization curves for Type 304 SS in 0.01 M HCl (purged by hydrogen) at various temperatures

The polarization curves of titanium in 0.01 M HCl over the temperature range of 100 - 500 ^{o}C are presented in Figure 5.3. As illustrated by the figure, the passivity can be observed at the temperatures range of 100 - 400 ^{o}C. The polarization graphs at 300 ^{o}C and 400 ^{o}C are characterized by the existence of plateaus over the anodic range, which corresponds to the passivity processes [7]. Similar as the polarization graphs of Type 304 SS in Figure 5.2, the passive current density of titanium in 0.01 M HCl increases with increasing temperature, which can be attributed to the temperature related kinetics of ion transport through the passive film. At 500 ^{o}C, no passivity can be observed as the current density increases monotonically with increasing anodic overpotentials.

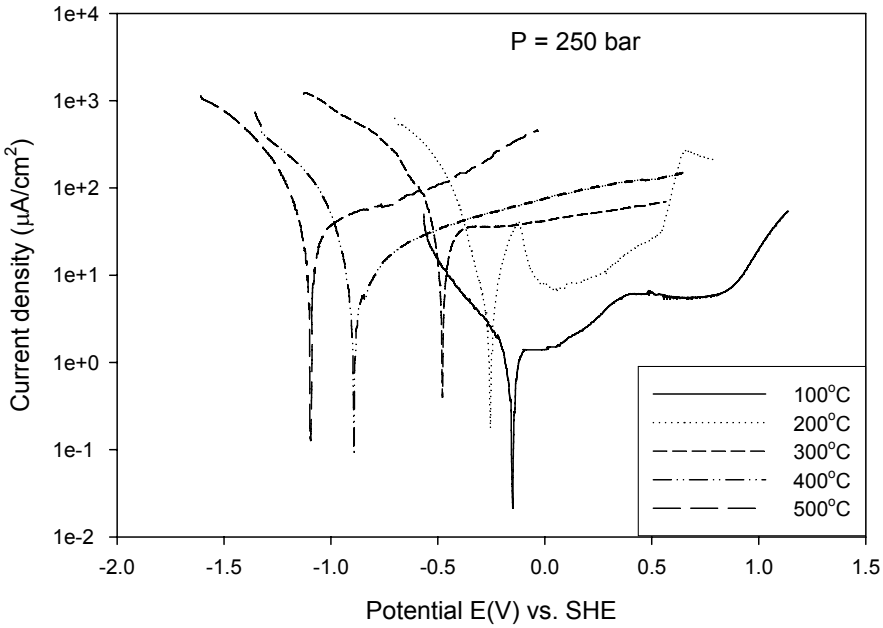

Figure 5.3: polarization curves for Ti in 0.01 M HCl (purged by hydrogen) at various temperatures

Figure 5.4 presents the comparison of dynamic polarization curves of Type 304 SS and titanium in deaerated 0.01 M HCl at 200 ^{o}C. The solid line is the polarization curve of Type 304 SS and the dash line is the polarization curve of titanium. The classic behavior of passivity can be observed for both Type 304 SS and titanium at 200 ^{o}C in 0.01 M HCl. As shown by the figure, the amplitude of passive current density of Type 304 SS is much higher than the amplitude of passive current density of titanium and the passivity range of Type 304 SS is shorter than the passivity range of titanium, which can be explained by the weakening of passive film of Type 304 SS in high temperature working environment.

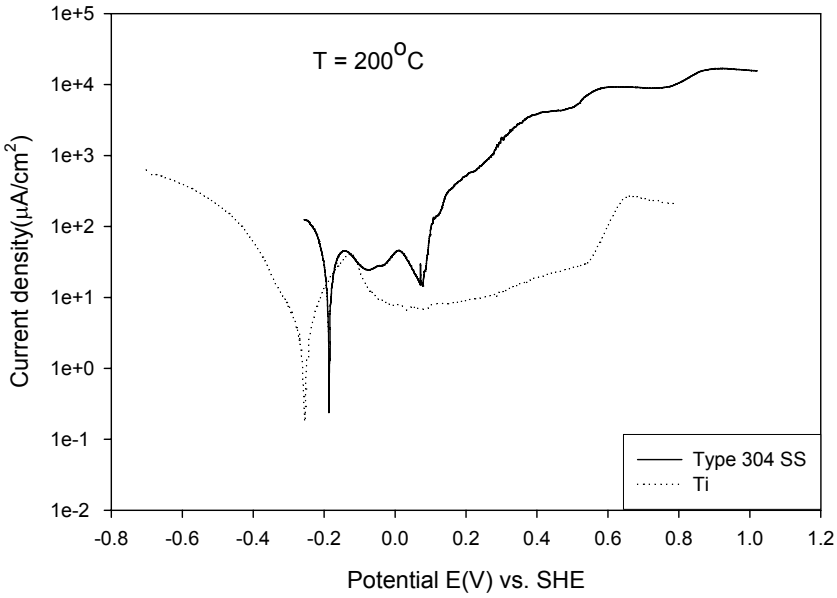

Figure 5.4: Comparison of dynamic polarization curves of Type 304 SS and Ti in deaerated 0.01 M HCl solution at 200 ^{o}C and 250 bar

Figure 5.5 compares the polarization curves of Type 304 SS and titanium in deaerated 0.01 M HCl at 400 ^{o}C. As shown by the figure, the current density of Type 304 SS increases monotonically with increasing anodic overpotential, which can be explained by the weakening of the passive film in the supercritical conditions. On the other hand, a relative flat of current density (plateau) can be observed for titanium, which corresponds with the passivity of titanium. In addition, the amplitude of the current density of titanium is much lower than the amplitude of current density of Type 304 SS at 400 ^{o}C. The above results further imply that titanium is more corrosion resistant than Type 304 SS in high temperature 0.01 M HCl solution.

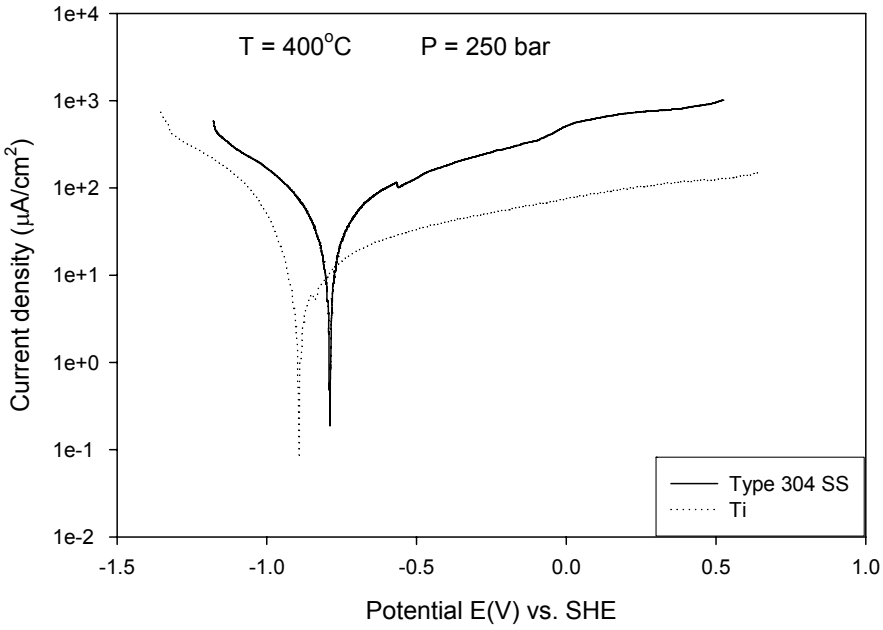

Figure 5.5: Comparison of dynamic polarization curves of Type 304 SS and Ti in deaerated 0.01 M HCl solution at 400°C and 250 bar

5.1.5 Summary and Conclusions

The experimental techniques have been developed to provide electrochemical polarization characterizations of metals/alloys in high temperature aqueous systems. The results demonstrate the possibility of conducting electrochemical polarization experiments in supercritical conditions. As illustrated, no passivity can be observed for Type 304 SS in 0.01 M HCl at temperatures > 300 °C. The shrinkage of passive range for both Type 304 SS and titanium with increasing temperature can be attributed to the increasing of aggressiveness of working solutions with increasing temperature. Comparing with the passive current density of Type 304 SS at the same temperature condition, the relatively low amplitude of passive current density of titanium

further proves that the titanium is more corrosion resistance in high temperature HCl solutions than Type 304 SS.

5.2 Monitor Instantaneous Corrosion Rates

5.2.1 Theoretical background

In-situ electrochemical corrosion rate measurement would provide very important information about the accumulation of corrosion damage in high temperature and high pressure working conditions and might allow strategies to be developed “on the fly” to minimize the corrosion damage, while maintaining an acceptable throughput of the reactor. Two electrochemical methods are commonly used for monitoring instantaneous corrosion rates: Tafel extrapolation method and polarization resistance method.

According to the activation energy model (Butler-Volmer Equation), the Tafel type relationship can be observed for a charge-transfer controlled reaction in which relatively large values of overpotential were applied [8].

$$\eta = \beta \ln(i / i_0) \tag{5.6}$$

where overpotential η is defined as $\eta = E - E_{eq}$ (E is the applied potential and E_{eq} is the equilibrium potential), i is the current density, i_0 is the exchange current density, β is the Tafel slope. Mixed potential theory suggests that the sum of anodic oxidation currents must equal to the sum of cathodic reduction current [9]. Therefore, the electrochemical corrosion current density and corrosion potential can be estimated by the intersection of the cathodic and anodic Tafel curves.

Experiments have shown that the electrochemical corrosion current density (i_{corr}) is in a linear relationship with $\Delta\varepsilon$ ($\Delta\varepsilon = E - E_{corr}$) when applied potentials (E) are within ± 5 mV to ± 20 mV range of the corrosion potential (E_{corr}). The slope of this linear relationship is defined as the polarization resistance $R_p = (d\varepsilon / di)_{\varepsilon \to 0}$. Based on the Stern-Gary relationship, the polarization resistance R_p can be used to predict instantaneous corrosion rate as [10]

$$i_{corr} = \frac{1}{(2.3R_p)}\left(\frac{b_a b_c}{b_a + b_c}\right) = \frac{B}{R_p} \tag{5.7}$$

where B is the Stern-Geary constant, b_a is the anodic Tafel slope and b_c is the cathodic Tafel slope. A reference electrode is required in both Tafel extrapolation and polarization resistance methods. However, no universally accepted reference electrode has emerged for potential monitoring in supercritical aqueous systems [11].

The concept of electrochemical noise resistance (R_n) was first introduced by Eden and his coworkers in order to obtain more corrosion process information such as the corrosion rate [12]. R_n is defined as the ratio of the standard deviation of potential noise (σ_E) over the standard deviation of current noise (σ_i).

$$R_n = \sigma_E / \sigma_i \tag{5.8}$$

Bertocci et al. reported that the noise resistance (R_n) and the polarization resistance (R_p) can be related as: $R_n = R_{sn}(f \to 0) = |Z(f = 0)| = R_p$ at very low frequencies range, in which R_{sn} is the spectral noise impedance [13]. Therefore, the electrochemical corrosion rates can be estimated by monitoring

electrochemical noise through the Stern-Geary relationship if the electrochemical mechanism is operative.

5.2.2 Results and discussion

It is suggested that the amplitude of electrochemical current noise is related to the electrochemical corrosion rate, with a high amplitude of the current noise being associated with a high corrosion rate [14]. However, there has no direct evidence to support the above assumption and it has proven to be very difficult to develop a quantitative relationship between the electrochemical corrosion rate and the electrochemical current noise because the theoretical background of electrochemical noise analysis has not yet been fully established.

The Tafel extrapolation test was performed to measure the instantaneous corrosion rate of Type 304 SS in 0.01 M HCl solution as a function of temperature. The reaction cell consists a 0.5 mm diameter Type 304 SS working electrode and a hydrogen/platinum internal reference electrode. The potential scan rate was selected at 0.17mV/s in order to maintain the pseudo steady-state conditions. The measured potentials were normalized to standard hydrogen electrode (SHE) scale [4].

Figure 5.6 displays the electrochemical corrosion current density (by Tafel extrapolation method) of Type 304 stainless steel in 0.01 M HCl as a function of temperature at 250 bar. The corrosion current density is observed to increase to a maximum as the temperature rises to approximately 350 ^{o}C. Then, the corrosion current decreases sharply after the temperature passes the critical point (374.15 ^{o}C). This can be explained by the theory of chemical/electrochemical corrosion mechanisms, as outlined earlier in this thesis. The corrosion process is dominated by increasing corrosion activity, due to

increasing temperature when the temperatures are below the critical point. Then the corrosion rate decreases sharply in the supercritical regions, because of the low dielectric constant and low density as the test solution changes from a condensed, liquid aqueous phase to a gas-like phase. Under those conditions, the electrochemical oxidation (EO) corrosion mechanism is less prevalent, and as a result, the electrochemical corrosion current decreases sharply.

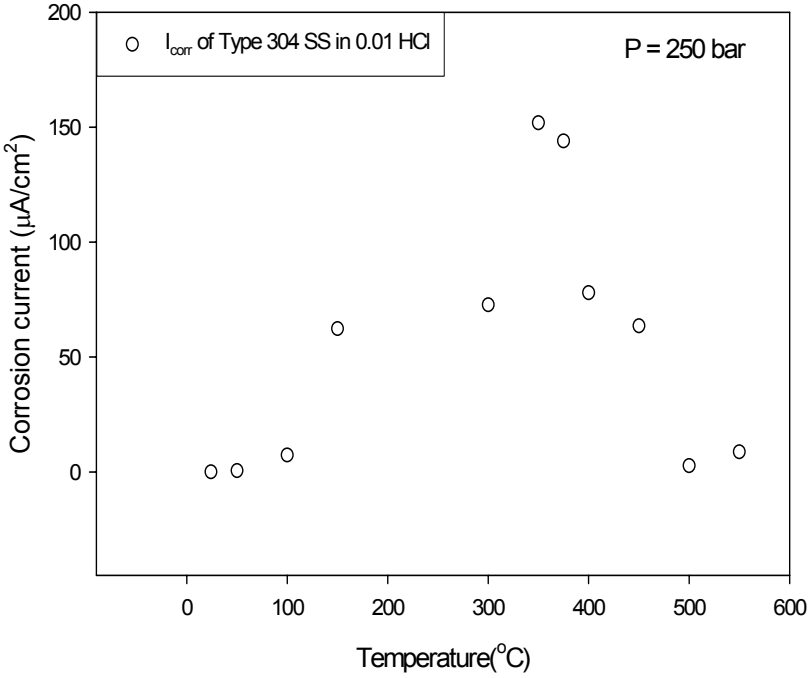

Figure 5.6: Electrochemical corrosion current (Tafel extrapolation method) of Type 304 SS in 0.01 M HCl solution purged with hydrogen as a function of temperature at 250 bar

Figure 5.7 compares the electrochemical current noise density (by electrochemical noise analysis) and corrosion current density (by Tafel extrapolation method) of Type 304 SS in 0.01 M HCl as a function of temperature. The solid circles in the graph represent the current noise density of

Type 304 SS in 0.01 M HCl solution purged by nitrogen and the open circles are the electrochemical corrosion current density of Type 304 SS in 0.01 M HCl solution purged by hydrogen. The working pressures for both experiments were identical at 250 bar. As demonstrated by the figure that both electrochemical current noise and corrosion current of Type 304 SS in 0.01 M HCl increases with increasing temperature before reaching a maximum value at approximate 350 ^{o}C. Thereafter, both electrochemical current noise density and corrosion current density decrease with increasing temperatures. However, the figure shows the amplitudes of the electrochemical current noise density and corrosion current density are quite different in the temperature range of 150 ^{o}C – 450 ^{o}C, with higher amplitude of corrosion current density is observed. The results demonstrate the existence of a correlation between the amplitude of electrochemical current noise density and the electrochemical corrosion rate. On the other hand, the magnitude of current noise is not equal to the magnitudes of corrosion current. It is important to note that the extrapolation experiments were performed in HCl solution sparged by hydrogen gas due to the application of Pt/H2 internal reference electrode. On the other hand, the electrochemical noise experiments were carried out in HCl solution sparged by nitrogen gas. In addition, the interpretation of extrapolation experimental data should be further verified by more experimental data in future studies.

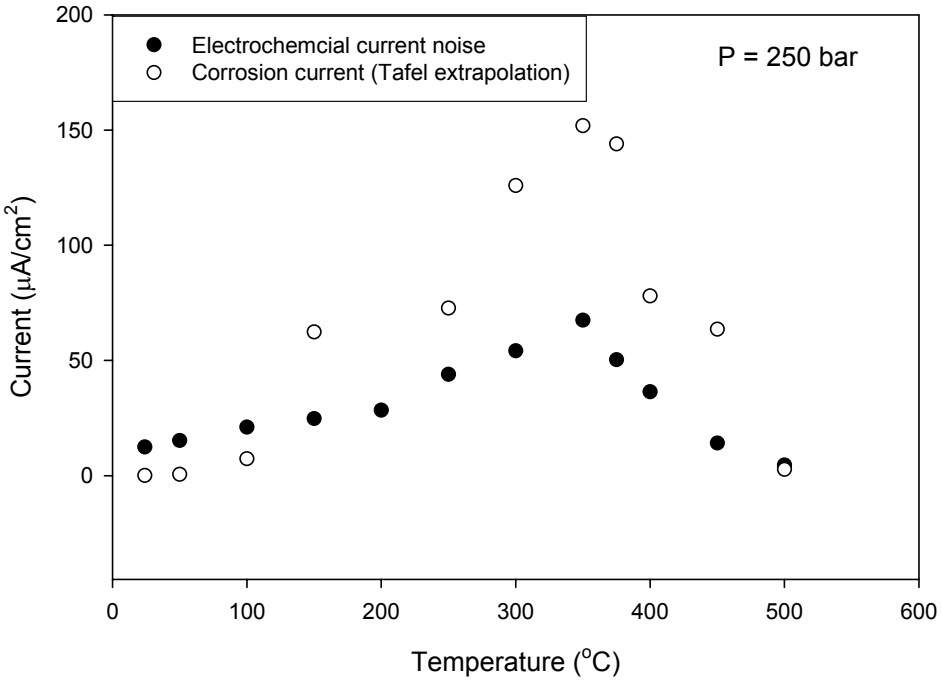

Figure 5.7: Comparison of electrochemical current noise of Type 304 SS in 0.01 M HCl purged by N_2 and electrochemical corrosion current of Type 304 SS in 0.01 M HCl solution purged by hydrogen at 250 bar as a function of temperature

Electrochemical noise resistance method has been applied to monitor instantaneous corrosion rate in high temperature aqueous systems, with emphasis on exploring the relationship between the noise resistance (R_n) and the polarization resistance (R_p). The electrochemical noise resistance is defined as the ratio of the standard deviation of potential noise over the standard deviation of current noise. The potential noise and current noise were measured by the electrochemical noise sensor (method) as described in chapter 4. The polarization resistance measurement was performed in a two-electrodes cell consists of a 0.5 mm diameter Type 304 SS working electrode and a hydrogen/platinum internal reference electrode. The potential was swept on the

working electrode in the range of ± 30 mV vs. corrosion potential at a scan rate of 0.15 mV/s in order to obtain the pseudo-steady state condition.

Figure 5.8 qualitatively demonstrates the relationship between the electrochemical current noise (proportional to the electrochemical corrosion rate) and the reciprocal of electrochemical noise resistance of Type 304 SS in 0.01 M HCl solution (purged by nitrogen) as a function of temperature over the temperature range of 100 ^{o}C through 500 ^{o}C at the pressure of 250 bar. The solid triangles in the graph represent the reciprocal of noise resistance and the solid squares are the current noise. As illustrated by the figure, the reciprocal of the noise resistance ($1/R_n$) and the current noise (electrochemical corrosion rate) have similar trend as the function of temperatures. Both of them increase with increasing temperature before reaching maximum values at around 350 ^{o}C, then decrease sharply in the supercritical temperature region (T > 374.15 ^{o}C). Therefore, a reciprocal relationship exists between the noise resistance and electrochemical corrosion rate. Figure 5.9 shows the correlation between the electrochemical corrosion current density (by Tafel extrapolation method) and the reciprocal of polarization resistance (by polarization resistance method) of Type 304 SS in 0.01 M HCl solution (purged by hydrogen) as a function of temperature over the temperature range from 100 ^{o}C to 550 ^{o}C. As predicted by the Stern-Gary relationship, a reciprocal relationship exists between the polarization resistance (R_p) and corrosion current density as demonstrated by the figure. Since the value of electrochemical current noise density corresponds with the value of electrochemical corrosion current density, a correlation is expected between the polarization resistance and noise resistance.

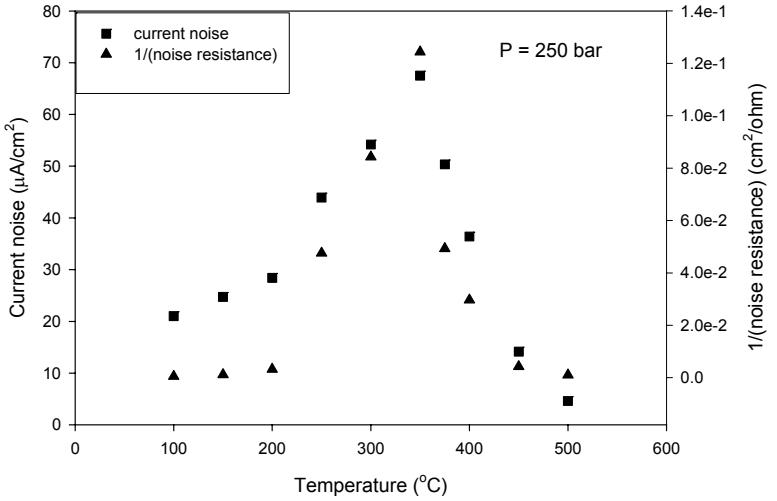

Figure 5.8: Comparison of 1/(noise resistance) and electrochemical current noise of Type 304 SS in 0.01 M HCl (purged by nitrogen) as a function of temperature at 250 bar

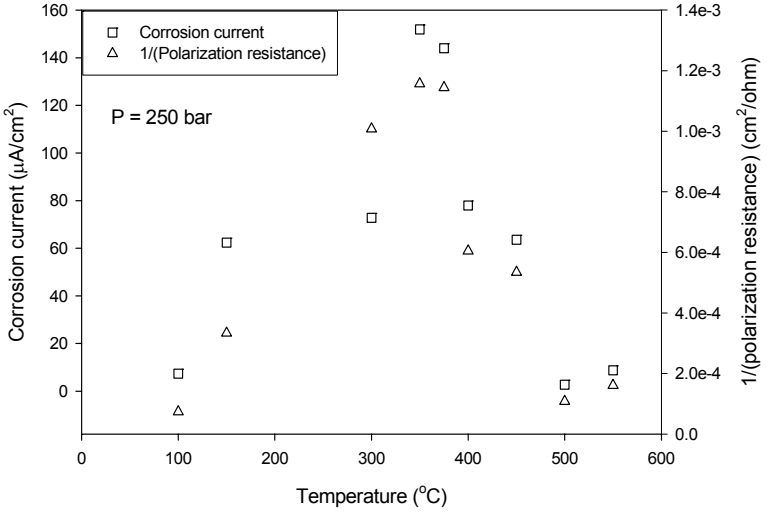

Figure 5.9: Comparison of 1/(polarization resistance) and electrochemical corrosion current of Type 304 SS in 0.01 M HCl (purged by hydrogen) as a function of temperature at 250 bar

Figure 5.10 compares the noise resistance (R_n) of Type 304 SS electrodes in 0.01 M HCl (sparged by nitrogen) and the polarization resistance (R_P) of Type 304 SS electrodes in 0.01 M HCl (sparged by hydrogen). It shown from the figure that R_n and R_P are not in the same order of magnitude with a much higher R_P has been observed, even though the dependence of both parameters on the temperature are quite similar. Both R_n and R_P decrease with increasing temperature before the temperature reaches to the critical value. Thereafter, both R_n and R_P increase with increasing temperature. Recognizing that both R_n and R_P have reciprocal relationships with the electrochemical corrosion rate, it is evident that a correlation exists between the noise resistance and the polarization resistance, but they are not equivalent.

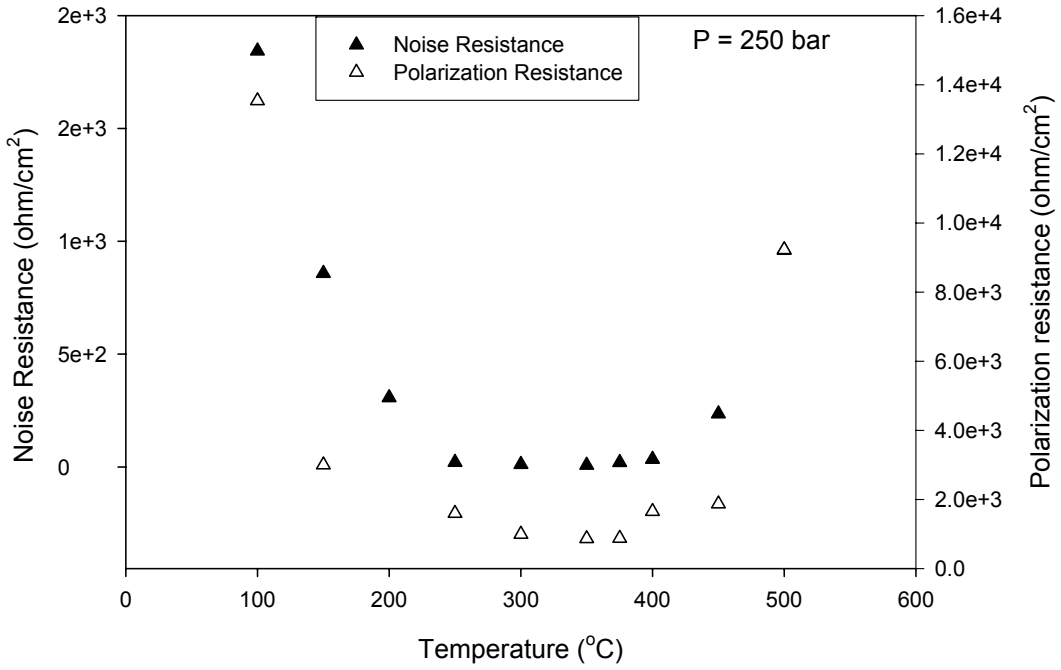

Figure 5.10: Comparison of noise resistance of Type 304 SS in 0.01 HCl (purged by nitrogen) and polarization resistance of Type 304 SS in 0.01 HCl (purged by hydrogen) as a function of temperature at 250 bar

5.2.3 Summary and Conclusions

This work has proven the existence of a correlation between the electrochemical current noise density and the corrosion current density in high temperature aqueous systems. A reciprocal relationship between the noise resistance and the electrochemical corrosion rate in high temperature working environments has also been observed. Therefore, a correlation between the noise resistance (R_n) and the polarization resistance (R_p) in high temperature aqueous systems is expected. Base on Stern-Gary relationship: $i_{corr} = B / R_p$, the corrosion rate can be estimated by measuring the noise resistance provided that the correlation between R_n and R_p is known.

References

1. Ph. Botella, C. Frayret, Th. Jaszay, M. H. Delville; “Experimental study, via current-potential curves, of the anodic behavior of Alloy C-276 and T60 titanium in chlorinated and oxygenated aqueous media under sub- to supercritical conditions” *J. of Supercritical Fluids*, **25**, 269 (2003)

2. D. D. Macdonald, L.B. Kriksunov, “Probing the chemical and electrochemical properties of SCWO systems” *Electrochimica Acta*, **47**, 775 (2001)

3. S. Huang, K. Daehling, T. E. Carleson, M. Abdel-Latif, P. Taylor, C. Wai, “A prop, Electrochemical measurements of corrosion of iron alloys in supercritical water” *Supercrit. Fluid Sci. Tehnol*. 287 (1989)

4. R. F. Prini, R. Crovetto, “Evaluation of data on solubility of simple apolar gases in light and heavy water at high temperature” *J. Phys. Chem. Ref. Data* **18** 1231 (1989)

5. Y. Y. Chen, U. T. Hong, H. C. Shih, J. W. Yeh, and T. Duval “Electrochemical kinetics of the high entropy alloys in aqueous environment-a comparison with type 304 stainless steel” *Corrosion Science*, **47**, 2679 (2005)

6. D. D. Macdonald, L.B. Kriksunov, “Probing the chemical and electrochemical properties of SCWO systems” *Electrochimica Acta*, **47**, 775 (2001)

7. Ph. Botella, C. Frayret, Th. Jaszay, M. H. Delville; “Experimental study, via current-potential curves, of the anodic behavior of Alloy C-276 and T60 titanium in chlorinated and oxygenated aqueous media under sub- to supercritical conditions” *J. of Supercritical Fluids*, **25**, 269 (2003)

8. A. Bard, L. Faulkner, *Electrochemical Methods Fundamentals and Applications*, Second Edition, John Wiley & Sons, INC.

9. D. Jones Principles and Prevention of Corrosion, Second Edition, Prentice-Hall. Inc 1996

10. J. Scully “Polarization resistance method for determination of instantaneous corrosion rates” Corrosion **56**, 199 (2000)

11. D.D. Macdonald, T. Zhu, and X. Guan, “Current State-of-the-Art in Reference Electrode Technology for Use in High Subcritical and Super Critical Aqueous Systems”, *Corrosion*, submitted (2006)

12. D. A. Eden, K. Hladky, D. G. John, and J. L. Dawson, Corrosion’86, Paper No. 274 NACE International, 1986

13. U. Bertocci, C.Gabrielli, F. Huet, and M. Keddam, “Noise resistance applied to corrosion measurements I. Theoretical analysis.” J. Electrochem. Soc, **144** 31 (1997)

14. C. Liu, D. D. Macdonald, E., Medina, J. J. Villa, and J. M. Bueno; “Probing Corrosion Activity in High Subcritical and Supercritical Water Through Electrochemical Noise Analysis”, *Corrosion* **50**, 687 (1994)

Chapter 6

EFFECT OF PRESSURE ON KINETICS OF CORROSION OF METALS IN HIGH TEMPERATURE AQUEOUS SYSTEMS

6.1 Introduction

High temperature water (HTW) has been widely used in many chemical and engineering applications as a reaction medium for chemical synthesis, materials synthesis, biomass processing, and waste destruction. High subcritical and supercritical aqueous media have properties that range from those that are characteristic of a gas phase at low pressure to that are characteristic of a condensed ionically conductive liquid phase at high pressure. The corrosion of metals and alloys in those high temperature aqueous systems shows characteristics that can be attributed to either “electrochemical oxidation” (EO) or “chemical oxidation” (CO) corrosion processes [1]. EO corrosion processes are featured by partial charge transfer processes in relatively high-density subcritical and supercritical systems. On the other hand, corrosion in low-density supercritical aqueous solutions is dominated by molecular processes (CO corrosion processes), such as the direct reaction of metals with corrodents. A modest change in conditions (including pressure) of the high temperature aqueous systems can strongly affect the corrosion reaction rates due to the changing of the characteristic of the systems such as the solubility of reacting species, dielectric constant, and the reaction rate constants.

Pressure has a significant influence on the density (ρ) of a supercritical solution and on density-related properties, such as the dielectric constant (ε)

and the concentration of aggressive species. For instance, $\rho = 0.1090$ g·cm^{-3}, ε=1.78 at T=450 °C, P=250 bar and $\rho = 0.2017$ g·cm^{-3}, ε=2.836 at T=450 °C, P=350 bar. The dielectric constant of high temperature water increases with increasing density and hence with increasing pressure. Solutes, such as HCl and H_2SO_4, may be very poorly ionized in low-density supercritical aqueous systems due to the low dielectric constant of the solvents. Consequently, metals corrosion in a high temperature aqueous system is highly correlated with the system pressure. Macdonald [2] applied activated complex theory to develop a relationship between the corrosion reaction rate constant and pressure. Based on this analysis, increasing pressure enhances solute heterolytic dissociation (e.g., ionization of an acid) and increases volumetric concentrations, which, in turn, leads to an enhanced collisional frequency and hence to higher reaction rate.

In this chapter, a phenomenological model is applied to outline the effect of pressure on corrosion reaction rates of metals in high subcritical and supercritical aqueous systems (SCAS), with emphasis on illustrating the contributions that are made by the activation processes, system compressibility, and degree of dissociation of aggressive species. One principal goal of this chapter is to understanding pressure effect on corrosion rate constants by estimating the volume of activation for corrosion processes in SCAS.

6.2 Pressure Effect on the Metals Corrosion Reaction Rate

Due to the unique properties of high subcritical and supercritical aqueous systems (SCAS), two corrosion mechanisms, i.e. “electrochemical oxidation (EO)” and “chemical oxidation (CO)”, were proposed to describe the corrosion of metals and alloys in high temperature media. EO usually involves two or more coupled redox reactions at different sites on the corroding metal surfaces in

relatively high-density SCAS. On the other hand, CO occurs through direct reaction of aggressive species with the metal in one act (or in several elemental steps) on one site in low-density supercritical aqueous solutions due to the low degree of dissociation and low dielectric constants. Since the overall reaction form of a EO process (such as $M + 2H_2O \rightarrow MO_2 + 4H^+ + 4e^-$ + $O_2 + 4H^+ + 4e^- \rightarrow 2H_2O$ to give the overall reaction $M + O_2 \rightarrow MO_2$) is indistinguishable from that of a CO process ($M + O_2 \rightarrow MO_2$), the reaction rate of an electrochemical/chemical corrosion process in a deaerated, acidic, high subcritical and supercritical solution can be expressed as follows,

$$R = k\left[C_{H^+}\right]^a \tag{6.1}$$

where k is the heterogeneous rate constant with $k = \kappa(k_B T / h)\exp(-\Delta G^{0,\neq} / RT)$, k_B is Boltzmann's constant, *h* is Planck's constant, *T* is the Kelvin temperature, $\Delta G^{0,\neq}$ is the standard Gibbs energy of activation, C_{H^+} is the volumetric concentration of hydrogen ion, and a is the corresponding reaction orders with respect to H^+. It is postulated that either a chemical or an electrochemical mechanism is the dominant corrosion mechanism under any given set of temperature/pressure conditions. The activity of H^+ has been widely used to indicate the corrosion susceptibility in condensed liquid solutions (Pourbaix diagram). The dominant form of corrosion in high temperature acidic solution is acid attack. Consequently, corrosion in those solutions is an electrochemical oxidation (EO) dominant process in which the cathodic partial reaction is hydrogen evolution. Other species, such as Cl^-, may be aggressive and induce particular forms of corrosion, such as pitting. These species are not included in Eq. 6.1. By taking the natural logarithm of Eq. 6.1 and differentiating with respect to pressure, the pressure dependence of the corrosion reaction rate in high temperature aqueous systems can be expressed as,

$$\left(\frac{\partial \ln R}{\partial P}\right)_T = \left(\frac{\partial \ln k}{\partial P}\right)_T + a\left(\frac{\partial \ln C_{H^+}}{\partial P}\right)_T \tag{6.2}$$

As illustrated by Eq. 6.2, the pressure effects on corrosion reaction rate can be attributed to pressure effects on activation processes and on volume concentration of aggressive species [2]. The volumetric concentrations (mol/l of the solution) of aggressive species C_{H^+} in Eq. 6.2 is density dependent and can be expressed by molal (mol/kg of solvent) concentration by

$$C = \frac{1000m\rho}{1000 + mM_s} \tag{6.3}$$

where m is the molal concentration (mol/kg), M_s the molecular weight of dissolved species (g/mol), ρ the density of the solution (g/cm^3). For dilute solutions, we can approximate that $C \approx m\rho$ as $mM_s << 1000$. Consequently, the relationship of $C_{H^+} \approx m_{H^+}\rho$ can be obtained for the dilute solutions. The pressure dependence of the molar concentration becomes

$$\left[\frac{\partial \ln(C)}{\partial P}\right]_T = \left[\frac{\partial \ln(m)}{\partial P}\right]_T + \left[\frac{\partial \ln(\rho)}{\partial P}\right]_T = \left[\frac{\partial \ln(m)}{\partial P}\right]_T + \kappa_T \tag{6.4}$$

where $[\partial \ln(\rho)/\partial P]$ is defined as the isothermal compressibility (κ_T) of the system and $\kappa_T = \partial \ln(\rho)/\partial P = -(\partial V/\partial P)_T/V$. Since solutes, such as acids and bases, are partially dissolved in low-density high temperature water, the degree of dissociation of $\alpha = m/m^0$ is introduced to demonstrate the pressure effect on solubility of aggressive species, where m is the molal concentration of the dissociated species such as Cl^- from HCl and m^0 is the stoichiometric concentration of the solutes. Eq. 6.4 becomes,

$$\left[\frac{\partial \ln(C)}{\partial P}\right]_T = \left[\frac{\partial \ln(\alpha)}{\partial P}\right]_T + \kappa_T \tag{6.5}$$

The pressure dependence of corrosion reaction rate can be further modified by applying Eq. 6.5 to Eq. 6.2, such as

$$\left(\frac{\partial \ln R}{\partial P}\right)_T = \left(\frac{\partial \ln k}{\partial P}\right)_T + a\left(\frac{\partial \ln \alpha_{H^+}}{\partial P}\right)_T + a(\kappa_T) \qquad (6.6)$$

As illustrated in Eq. 6.6, the effect of pressure on the rate of corrosion of metals in high temperature aqueous systems can be attributed to the activation process, to changes in the degree of dissociation of aggressive species, and to the system isothermal compressibility.

6.3 Volume of Activation

The effect of pressure on reaction rate constant k can be explained by the activated complex theory. The theory claims that the elementary chemical reactions occur via a transition state, such as $A + B \leftrightarrow M^{\neq} \rightarrow products$, in which the reactants and transition state are assumed to be in equilibrium. The transition state (activated complex) $M^{\neq}$ is defined as the state of the maximum energy along the reaction path ("reaction coordinate"). The rate constant can be expressed as follows based on the activated complex theory [3],

$$k = \kappa \frac{k_B T}{h} \exp\left(\frac{-\Delta G^{\neq}}{R_g T}\right) \qquad (6.7)$$

where κ is the transmission coefficient, $\Delta G^{\neq}$ is the difference in Gibb's free energy between the reactants and the transition state, R_g is the universal gas constant. Based on activated complex theory, the standard volume of activation ($\Delta V^{\neq}$) of a reaction is related to the pressure dependence of the reaction rate constant as expressed by [3],

$$\Delta V^{0,\neq} = -RT(\partial \ln k / \partial P)_T = \overline{V}^{0,\neq} - \overline{V}_M^0 - \overline{V}_{H^+}^0 \qquad (6.8)$$

where k is the rate constant, $\overline{V}^{0,\neq}$ is the standard partial molar volume of the transition state, and $\overline{V}_M^0$ and $\overline{V}_{H^+}^0$ are the standard partial molar volumes of the reactants; metal *M* and H^+. It is recognized that the volume of activation includes volume changes due to solvent-solute electrostatic interaction as the reaction proceeds along the reaction coordinate toward the transition state [4]. The volume of activation for chemical reactions in liquid aqueous solutions is generally ± 50 cm^3/mol. On the other hand, a much larger volume of activation has been observed for chemical reactions in the highly compressible supercritical fluids [4,5]. For instance, the volume of activation for the uni-molecular decomposition of chlorobenzyl methyl ether in supercritical 1,1-difluoroethane is -6,000 cm^3/mol at 130 ^oC and 50 bar and volume of activation for uncatalyzed reaction of butyronitrile in high temperature water is around -362 cm^3/mol at 330 ^oC and 128.5 bar [4,5]. This large volume of activation may reflect the large magnitudes of partial molar volumes of species in highly compressible supercritical fluids. Beside the electrostatic and compressibility effects, Wu et al [6] suggested that the phase-behavior and diffusional limitations effects also can affect the volumes of activation.

Based on the partial charge method, Macdonald [2] suggested that the reaction coordinate of corrosion processes of metals in deaerated acidic solutions can be expressed as follows:

$$M + 2H^+ \rightarrow [\delta M^{2+} + (1-\delta)M + \delta H_2 + 2(1-\delta)H^+]^{\neq} \rightarrow M^{2+} + H_2 \qquad (6.9)$$

where M is the metal, the entity in square brackets is the transition state, and δ is the extent of charge development at the knoll in the reaction coordinate between the initial state and the final state and is restricted to values between 0 and 1. The volume of activation of this corrosion processes can be expressed as:

$$\Delta V^{0,\neq} = \overline{V}^{0,\neq} - \overline{V}_M^0 - 2\overline{V}_{H^+}^0 \tag{6.10}$$

where $\overline{V}^{0,\neq}$, $\overline{V}_M^0$, and $\overline{V}_{H^+}^0$ are the standard partial molar volumes of the transition state, the metal, and the hydrogen ion, respectively. If the volume of activation and the partial molar volumes of the reactants are known, the standard partial molar volume of the transition state $\overline{V}^{0,\neq}$ can be determined and the extent of the charge development in the transition state may be estimated by comparison with the partial molar volumes of model compounds, as has been done with solvolysis reactions at ambient or near ambient temperatures [2]. . It is important to note that the corrosion reaction is being treated as elementary process in Eq. 6.9 even though the corrosion processes are typical complex, multi-step processes. However, this simplification does not compromise the present application of the partial charge method since it is equally valid for multi-step reactions [2].

As described before, the corrosion reaction rates can be expressed by the chemical reaction rate law for both chemical and electrochemical corrosion processes and the volume of activation can be expressed by Eq. 6.8. Applying Eq. 6.8 to Eq. 6.6 and integrating it, Eq. 6.6 becomes,

$$\int_{P^0}^{P} \ln R dP = \left(-\frac{1}{RT}\right)\int_{P^0}^{P} \Delta V^* dP + a\int_{P^0}^{P} \ln[\alpha_{H^+}(P)]dP + a\int_{P^0}^{P} \kappa_T(P)dP \tag{6.11}$$

where P^0 is the reference pressure. It is important to note that the isothermal compressibility of high temperature aqueous systems is pressure dependent. The relative corrosion reaction rate at pressure P and P^0 is expressed as,

$$\ln\left(\frac{R_P}{R_{P^0}}\right) = \left(-\frac{1}{RT}\right)\int_{P^0}^{P} \Delta V^* dP + a\ln\left(\frac{\alpha_{H^+}(P)}{\alpha_{H^+}(P^0)}\right) + a\int_{P^0}^{P} \kappa_T(P)dP \tag{6.12}$$

where R_p / R_{p^0} is the relative corrosion reaction rate. The first term in the right hand side of Eq. 6.12 is related to the activation process; the second term is the contribution from the dissociation of aggressive species; and the third term corresponds to the pressure dependence of the volumetric concentration of aggressive species.

6.4 Experimental Setup and Electrochemical Noise Analysis

The experimental setup used in this study consists of a closed, circulating loop system as illustrated by Figure 4.1, within which the test solution was heated to the desired temperatures (up to 500 ^{o}C) and then was pumped into the reaction cell. The internal pressure (up to 400 bar) was generated by a mini-pump and regulated by a check valve with a precision of ±15 bar. Heating of the cell was provided for by an OMEGA heating-band and the temperature was controlled by a temperature controller with a precision of ±1^{o}C. The working solution was 0.01 M HCl.

Electrochemical noise analysis (ENA) also known as electrochemical emission spectroscopy (EES) was first introduced by Iverson for corrosion studies around 40 years ago and it has become one of very promising corrosion monitoring methods due to its unique advantages, such as non-perturbative, *in-situ* application, and simplicity [7,8]. Electrochemical noise (EN) is a series of naturally-occurring transient events and is measured as fluctuations of current noise and potential noise between the working electrodes. Since the electrochemical noise is produced by the fluctuation in corrosion rates across the electrode surfaces, it has been proposed that the shape and amplitude of the noise transients, among other characteristics of the EN data, are directly related to the electrochemical corrosion rates in the system [8,9]. By applying ENA to monitor corrosion processes of carbon steel and stainless steel in high

temperature (including supercritical) aqueous systems, Macdonald et al. [11,12] suggested that the RMS of the electrochemical noise is related to the corrosion rate, with a high current noise being associated with a high corrosion rate. They also concluded that corrosion was the dominant source of electrochemical noise based on the correlation between the measured noise and the extent of corrosion. Recently, ENA has been successfully applied in monitoring and differentiating corrosion mechanisms in high subcritcal and supercritical aqueous systems [13].

The electrochemical noise sensors (ENS) used in this study consist three identical 0.5 mm diameter Type 304 SS wires (annealed 99.98% nickel wires later). Two of the electrodes were used as the counter and working electrodes and the third one was employed as the pseudo reference electrode. The manufacture procedure is identical with the manufacture procedure introduced in chapter 3. The length of each wire was trimmed to 15 mm at one end, which was exposed to the high temperature test solution. The electrodes were separated from each other by a distance of 3-4 mm. The exposed wire was lightly polished and washed with acetone/de-ionized water before use. A CONAX gland with Lava sealant was used to seal the ENS. The corrosion current noise between the two identical working electrodes and the potential noise between the coupled working electrodes and the pseudo reference electrode were measured simultaneously using a Gamry PC 400 electrochemical system. The data were collected at an acquisition rate of 2Hz and a high-frequency filter was used in this studying to prevent aliasing. This instrument was used as a Zero Resistance Ammeter (to maintain the two identical working electrodes at same potential level), in order to measure the coupling current noise, and as an electrometer to measure the potential noise, with both measurements being made simultaneously.

6.5 Results and Discussion

The purpose of this study is to understand the effect of pressure on the rate of corrosion of a metal in high subcritical and supercritical aqueous systems (SCAS), with emphasis on the contributions from activation, system compressibility, and degree of dissociation of aggressive species. Since the amplitude of the electrochemical noise is postulated to be proportional to the electrochemical corrosion rate, the electrochemical corrosion rate can be estimated using electrochemical noise analysis (ENA). Note that, because the CO mechanism does not involve partial charge transfer processes, it is not expected to produce electrochemical noise. Accordingly, measurement of the current noise and the weight loss over a period of time and knowledge of the relationship between the current noise amplitude and the instantaneous corrosion rate provides a means of delineating the EO and CO mechanisms. This was partially achieved by Liu et al [11] who measured the RMS of the noise in the coupling current between identical carbon steel electrodes in water at 450 ^{o}C as a function of density and found that the noise disappeared at densities below 0.06 g/cm^3. Accordingly, we may conclude that at lower densities the dominant corrosion process in CO and at higher densities EO prevails.

As described above, the corrosion reaction rate in deaerated acidic solutions can be expressed by Eq. 6.1, in which the corrosion mechanism is electrochemical oxidation (EO) with H^+ being the principal corrodent. As there are no data available for the reaction order of the electrochemical corrosion of stainless steel in high temperature acidic solutions, it is assumed that the reaction is a half order reaction and that $a = 1/2$. The relative corrosion reaction rate at pressure P with respect to that at pressure P^0 is expressed as:

$$\ln\left(\frac{R_P}{R_{P^0}}\right) = \left(-\frac{1}{RT}\right)\int_{P^0}^{P} \Delta V^{\neq} dP + \frac{1}{2}\ln\left(\frac{\alpha_{H^+}(P)}{\alpha_{H^+}(P^0)}\right) + \frac{1}{2}\int_{P^0}^{P} \kappa_T(P) dP \qquad (6.13)$$

where P^0 is the reference pressure, and R_p / R_{P^0} is the relative corrosion reaction rate. The first term in the right hand side of Eq. 6.13 is due to activation; the second term corresponds to the change in the degree of dissociation of the aggressive species; and the third term describes the pressure dependence of the volumetric concentration of aggressive species. The degree of dissociation of aggressive species (α_{H^+}) in SCAS is defined as $\alpha_{H^+} = m_{H^+} / m^0$, in which m_{H^+} is the molal concentration of the dissociated species of H^+ from *HCl*, and m^0 is the stoichiometric concentration of the solute *HCl*. The value of m_{H^+} can be determined by solving HCl dissociation reaction combining with water dissociation reaction based on mass balance, charge balance, and the reaction rate law [1]. In this study, the compressibility of working solutions was estimated from steam data obtained from the NIST steam algorithm recognizing that 0.01 M HCl is a dilute solution [14]. The relative reaction rate of R_p / R_{P^0} was measured by ENA. Consequently, the volume of activation can be estimated. Macdonald suggested that the volume of activation is essentially independent of pressure in liquid phases over relatively narrow pressure ranges [3]. However, the volume of activation is expected to change dramatically as the system transitions the critical temperature and is expected to display strong pressure dependence in super critical systems for the reasons discussed above. Johnson et al. [4] reported that the volume of activation of uni-molecular decomposition of chlorobenzyl methyl ether in supercritical 1,1-difluoroethane ranges from a negative few thousand cm^3/mol in the highly compressible, near-critical region to a negative few dozen cm^3/mol in the liquid state. As the compressibility of SCAS is high and hence the density of SCAS is highly pressure dependent, the volume of activation of corrosion processes in SCAS may also be highly pressure dependent. In order to solve Eq. 6.13, we assumed that the volume of activation of a corrosion process in SCAS is constant between the two neighboring measured pressures as there are no data available for the differential relationship between the volume of activation of an electrochemical corrosion processes and pressure.

Figure 6.1 shows the standard deviation of the electrochemical current noise (postulated to be proportional to the electrochemical corrosion rate) of Type 304 stainless steel in deaerated 0.01 M HCl as a function of pressure at a high subcritical temperature (T = 350 ^{o}C). As demonstrated by the data, the electrochemical corrosion rate increases with increasing pressure, corresponding to negative value for the volume of activation. The figure illustrates that the current noise increases from 50.5μA/cm^2 at 224 bar to 74.7μA/cm^2 at 272 bar, and then to 85.8 μA/cm^2 at 317 bar. The increasing corrosion rates may be attributed to the pressure effects on the solvent-solute interactions and on the degree of dissociation of aggressive species.

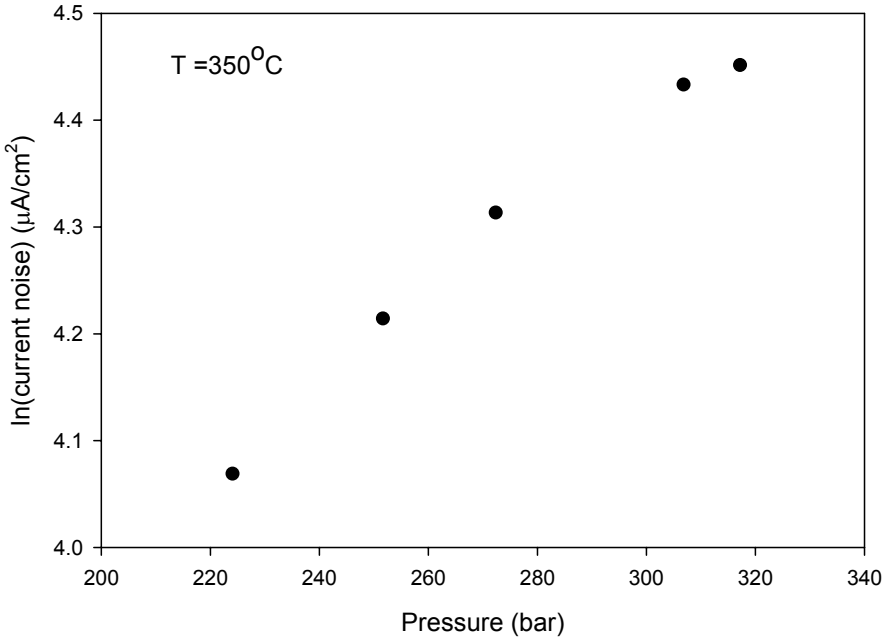

Figure 6.1:Electrochemical corrosion rate (standard deviation of the current noise) of Type 304 SS as a function of pressure at 350 ^{o}C in deaerated 0.01 M

Figure 6.2 presents the volume of activation of the electrochemical corrosion of Type 304 SS in 0.01 M HCl at 350 ^{o}C as a function of pressure. In this study, the relative electrochemical corrosion rate is estimated as the ratio of the two neighboring measured standard deviations in the current noise, such as

the current noise of 67.6μA/cm^2 at 252 bar divided by the current noise of 50.5μA/cm^2 at 224 bar. In addition, we also assumed that the volume of activation is constant between the two neighboring measured pressures, such that the volume of activation is taken to be -210.8 cm^3/mol over the pressure range of 224 to 252 bar, -183.3 cm^3/mol over the pressure range of 252 to 272 bar, and -120.3 cm^3/mol over the pressure range of 272 to 306 bar, as explained above. As demonstrated by the data in the figure, a large, negative volume of activation (-210.8 cm^3/mol) is observed at the lowest pressure range of 224 – 252 bar and a relatively smaller, but still negative volume of activation (-63 cm^3/mol) is obtained at the highest pressure range of 306 – 317 bar. The negative value of the volume of activation can be attributed to electrostriction of the solvent as charge is developed and/or redistributed in the transition state. Because electrostriction is expected to result in a smaller negative volume change as the density increases, the volume of activation should become smaller as the pressure is increased, as observed.

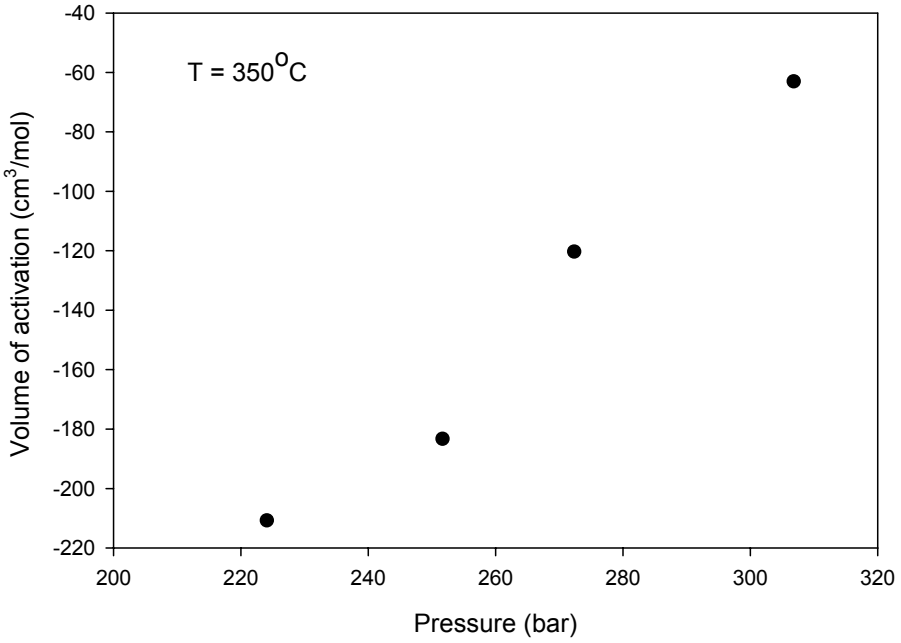

Figure 6.2: Volume of activation of corrosion reactions of Type 304 SS in deaerated 0.01 M HCl as a function of pressure at 350 °C

The larger volume of activation at lower pressures may be due to the large pressure effect on the compressibility of solvent and on the degree of dissociation of aggressive species. So far, there are no other studies of the volume of activation of corrosion processes that could confirm or deny above position. Theoretically speaking, the postulate is reasonable, as the corrosion process presumably passes through a transition state of the type indicated by the Eq. 6.9. In forming the transition state, the charge is dispersed over a larger sphere than in the initial state, with the result that solvent electrostriction is greater and hence the activation volume should be negative as the water is drawn into the transition state by ion-dipole interaction [2]. Clearly, this issue needs to be explored in future work, possibly by molecular dynamics simulation.

The relative importance of the activation, compressibility, and degree of dissociation of HCl to the relative corrosion rate of Type 304 SS in deaerated 0.01 M HCl at of 350 ^{o}C is illustrated in Figure 6.3. As indicated by the figure, the contribution from the compressibility is much less important, compared with the contributions from the activation and HCl dissociation at high subcritical temperatures (350 ^{o}C). This can be explained by the relatively small compressibility of the condensed “liquid” system. The figure also shows that the contribution from the activation term to the relative reaction rate is more important than the contribution from the degree of dissociation at high subcritical temperatures.

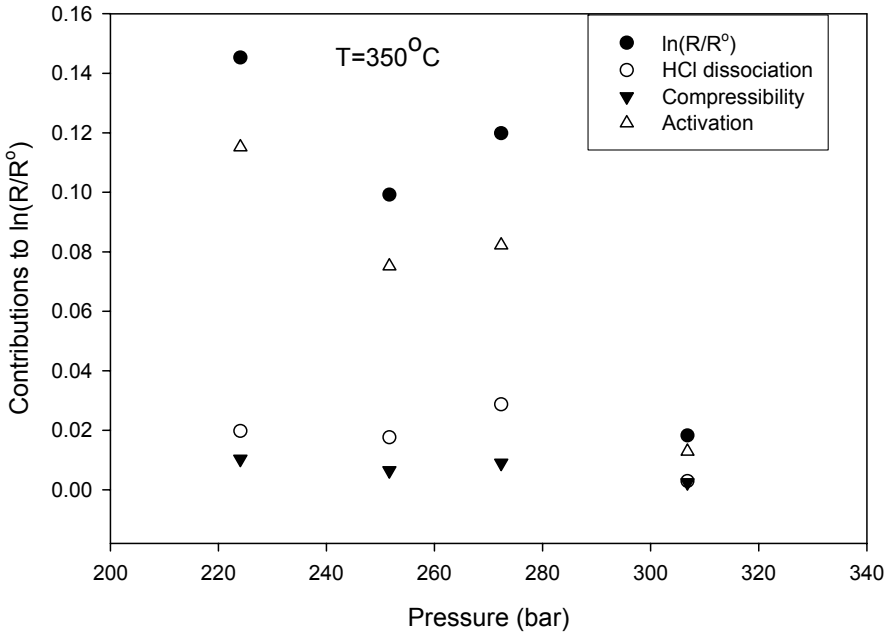

Figure 6.3: Contribution of activation, density, and HCl dissociation to corrosion rate of Type 304 SS as a function of pressure at 350 ^{o}C in deaerated 0.01 M HCl solution

Figure 6.4 compares the electrochemical current noise of Type 304 SS in deaerated water and in deaerated 0.01 M HCl at 350 ^{o}C as a function of pressure. The open squares in the graph represent the corrosion rate of the steel in the 0.01 HCl solution as a function of pressure, and the solid squares represent the corrosion rate in water under the identical condition of temperature and pressure. Both solutions were deaerated by nitrogen gas. As shown by the figure, pressure has a more significant influence on the corrosion rate of Type 304 SS in 0.01 M HCl solution than it does in water. This may be attributed to the impact of pressure on the degree of dissociation of HCl, compared with that of H_2O, resulting in a much higher concentration of H^+ from HCl than from water.

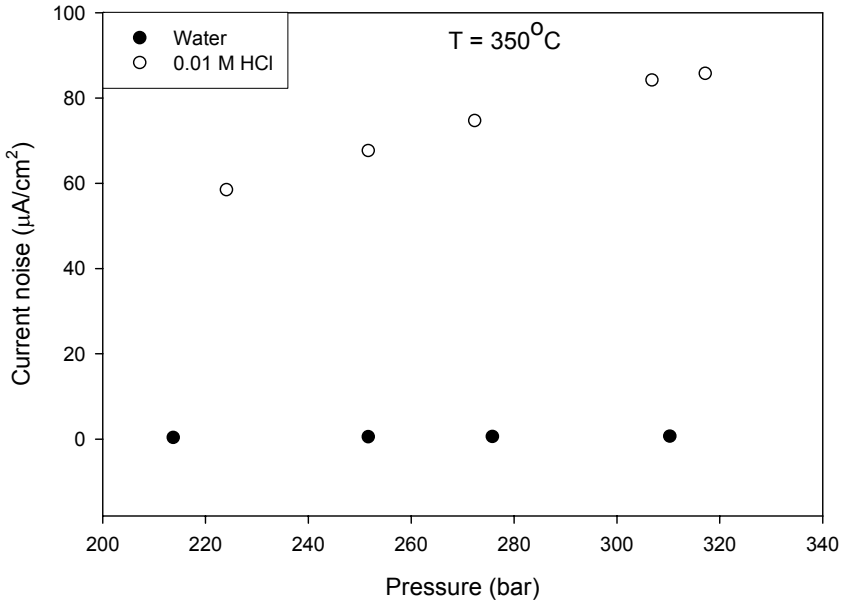

Figure 6.4: Comparison of electrochemical corrosion rates of Type 304 SS as a function of pressure in deaerated water in deaerated 0. 01 M HCl

Figure 6.5 displays the electrochemical current noise of Type 304 SS in deaerated 0.01 M HCl as a function of pressure at a supercritical temperature of 450 ^{o}C. Similar to the pressure dependence of corrosion processes at subcritical temperatures (Figure 6.1), the corrosion rate increases with increasing pressure yielding an apparently negative value for the activation volume. The current noise rises from 8.7μA/cm^2 at 197 bar to 14.1μA/cm^2 at 255 bar and to 20.1μA/cm^2 at 327 bar. However, in this case, the system is characterized by a very high compressibility so that the effects of pressure on the activation process must be delineated from the other contributions before a rational discussion of the data can be undertaken.

Solutes, such as acids and bases, may not be fully ionized under supercritical conditions, due to the low density and low dielectric constant of the

solvent. For example, the density and dielectric constant of water at 450 ^{o}C and 327 bar are 0.1757g/cm^3 and 2.5, respectively, compared with that of 1 g/cm^3 and 80 under ambient conditions. Additionally, a modest change in pressure of a supercritical aqueous system can strongly affect the degree of dissociation, due to the high compressibility of those systems. For instance, the degree of dissociation of 0.01 M HCl is 1.62E-7 at T=450 ^{o}C, P=197 bar, but is 5.29E-5 at T=450 ^{o}C, P=327 bar.

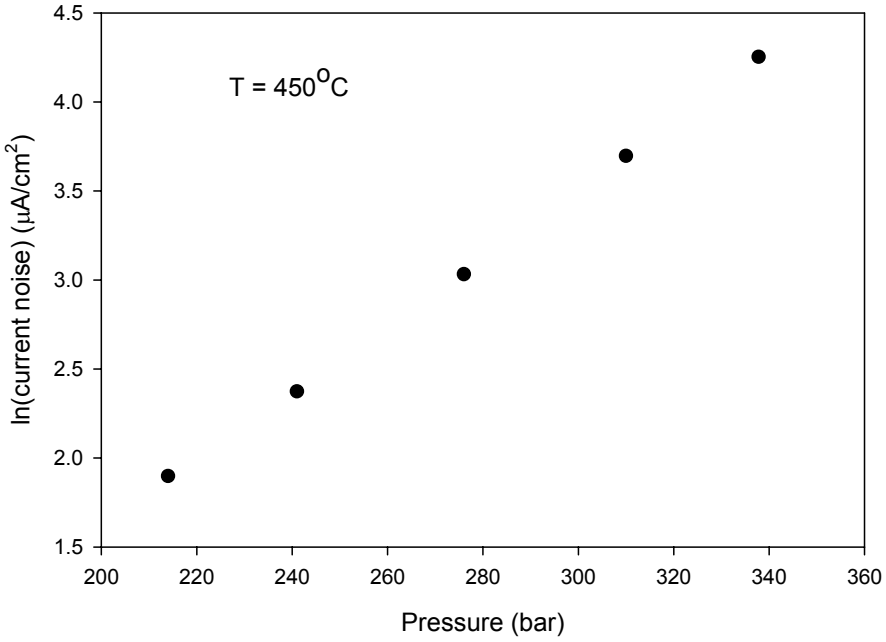

Figure 6.5: Electrochemical corrosion rate (standard deviation of the current noise) of Type 304 SS as a function of pressure at 450 ^{o}C in deaerated 0.01 M HCl

Figure 6.6 shows the volume of activation of Type 304 SS in 0.01 M HCl at 450 ^{o}C as a function of pressure after correction for the change in the volumetric concentration and the dissociation of HCl. In this case, the volume of activation is positive, rather than being negative as indicated by the raw data

(Figure 6.4). Similar to the corrosion processes at 350 ^{o}C (Figure 6.2), the magnitude of the volume of activation (but of opposite design) decreases with increasing pressure (density), corresponding with the decreasing compressibility of the solvent.

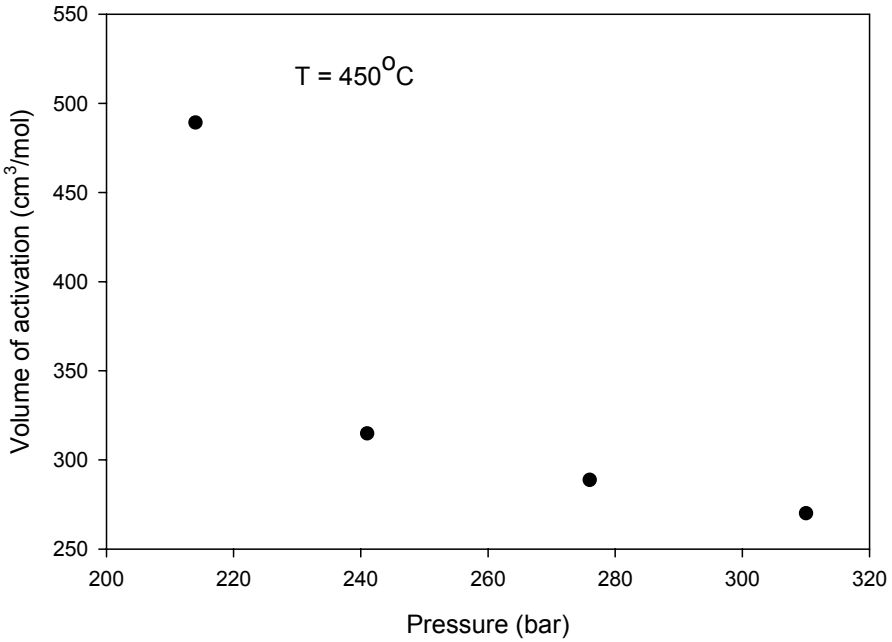

Figure 6.6: Volume of activation of corrosion reactions of Type 304 SS in deaerated 0.01 M HCl as a function of pressure at 450 ^{o}C

Figure 6.7 demonstrates the contributions of activation, the degree of dissociation, and density (isothermal compressibility) to the relative corrosion rate of Type 304 SS in deaerated 0.01 M HCl at temperature 450 ^{o}C. The figure shows that the contribution from the degree of dissociation dominates the pressure dependence of the relative reaction rate as the result of the significant pressure effect on the density and the degree of dissociation of systems. The contribution from compressibility is more significant for supercritical temperatures (450 ^{o}C) than it is for subcritical temperatures (350 ^{o}C), which is expected as the

compressibility of the supercritical systems (a gas phase) is much larger than the compressibility of a subcritical systems (a condensed liquid phase).

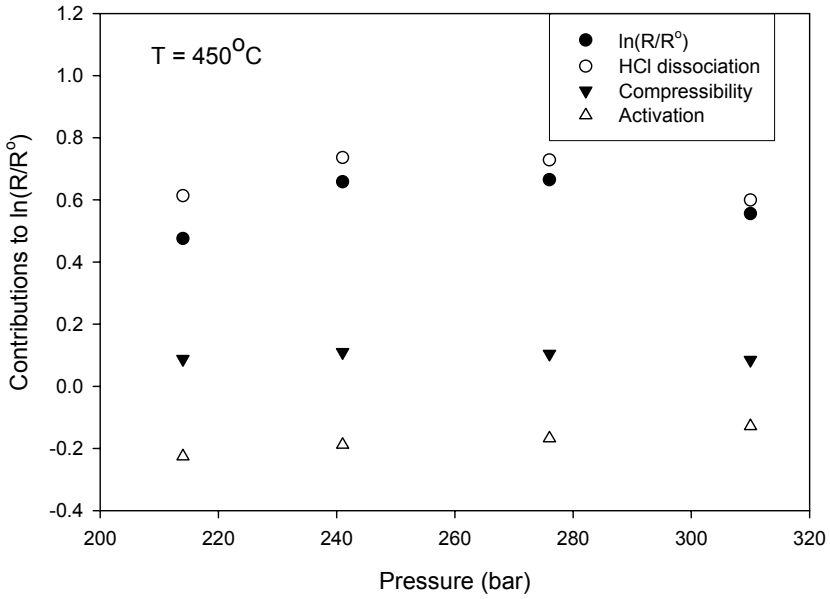

Figure 6.7: Contributions of activation, degree of dissociation, and compressibility to corrosion rate of Type 304 SS as a function of pressure at 450 °C in deaerated 0.01 M HCl

Figure 6.8 illustrates the electrochemical current noise of Type 304 SS in deaerated 0.01 M HCl as a function of pressure at a supercritical temperature of 500 °C. Similar to the pressure dependence of corrosion processes at 450 °C, the corrosion rate increases with increasing pressure due to the increasing of degree of dissociation of HCl with increasing pressure. Figure 6.9 displays the volume of activation of Type 304 SS in 0.01 M HCl at 500 °C as a function of pressure after correction for the change in the volumetric concentration and the dissociation of HCl. Similar to the pressure dependence of corrosion processes in 450 °C the volume of activation is positive and the magnitude of the volume of

activation decreases with increasing pressure (density), corresponding with the decreasing compressibility of the solvent.

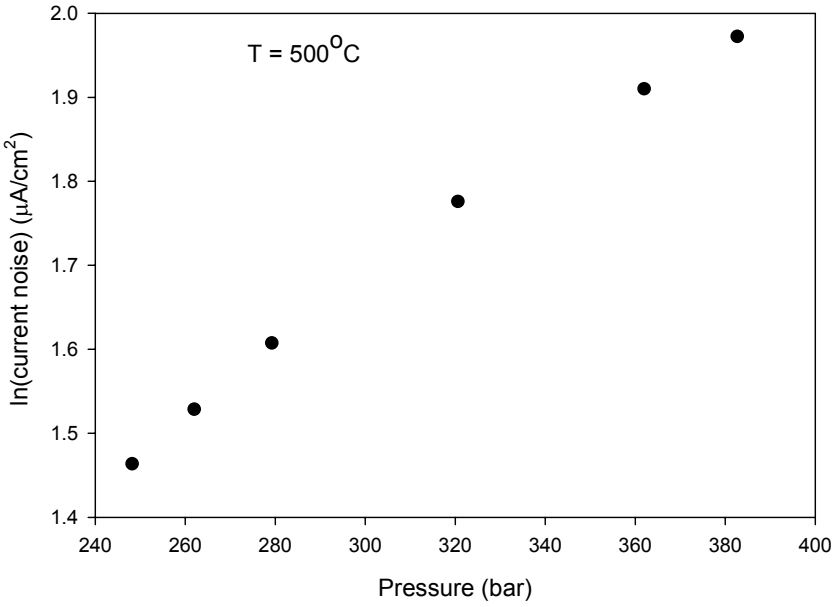

Figure 6.8: Electrochemical corrosion rate (standard deviation of the current noise) of Type 304 SS as a function of pressure at 500 ^{o}C in deaerated 0.01 M HCl

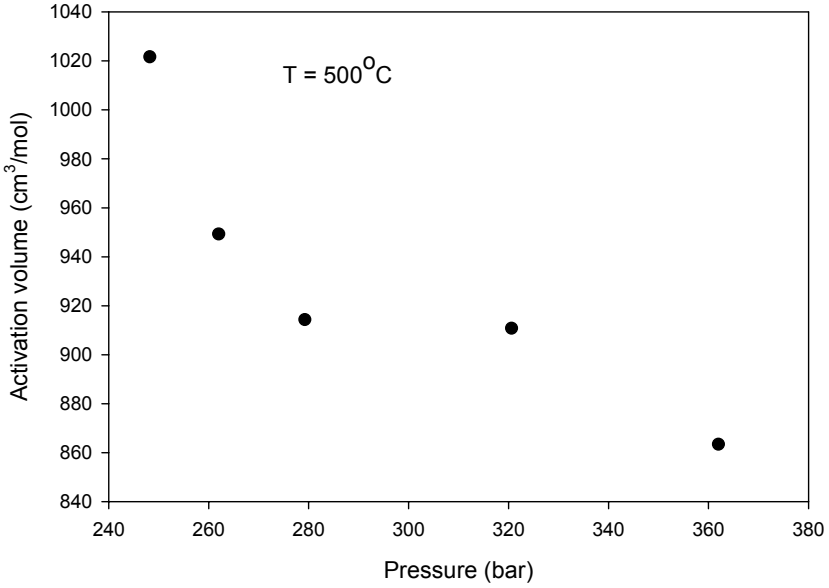

Figure 6.9: Volume of activation of corrosion reactions of Type 304 SS in deaerated 0.01 M HCl as a function of pressure at 500 ^{o}C.

Figure 6.10 demonstrates the contributions of activation, the degree of dissociation, and density (isothermal compressibility) to the relative corrosion rate of Type 304 SS in deaerated 0.01 M HCl at temperature 500 ^{o}C. The figure shows that the contribution from the degree of dissociation and activation volume term dominates the pressure dependence of the relative reaction rate as the result of the significant pressure effect on the density and the degree of dissociation of systems, which is expected as the activation volume is higher in low-density supercritical aqueous systems.

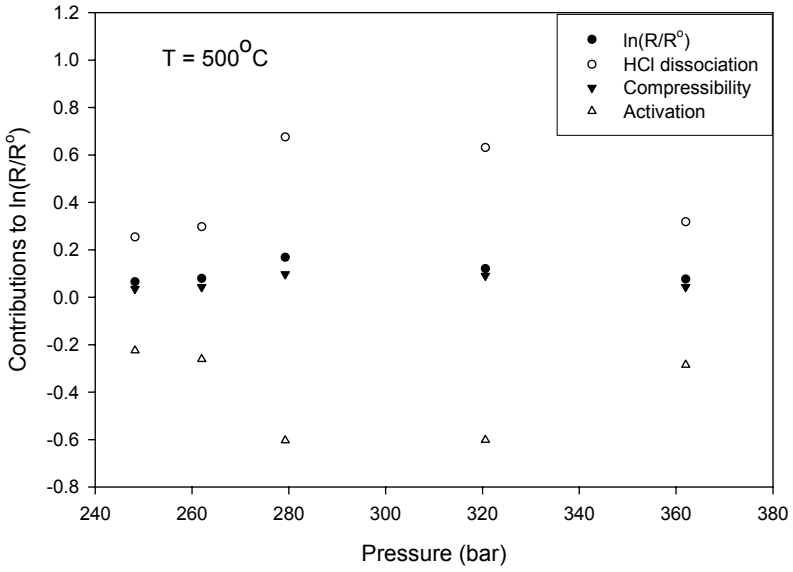

Figure 6.10: Contribution of activation term, degree of dissociation, and compressibility to corrosion rate of Type 304 SS as a function of pressure at 500 ^{o}C in deaerated 0.01 M HCl solution

Nickel is a very important component for many corrosion resistance alloys used in high temperature aqueous systems. Therefore, the effect of pressure on corrosion processes of nickel in high temperature acidic solutions has been analyzed. Similar as the manufacture procedure for Type 304 SS noise sensor, the nickel noise sensor consists three identical nickel electrodes (0.5 mm annealed 99.98% nickel wire) and electrochemical noise was measured in between. It is important to note that the corrosion reaction rate law (Eq. 6.1) is a generic reaction for corrosion of metals in high temperature acidic solutions, therefore the reaction rate law and the following relative reaction rate equations should be valid for nickel (and other metals or alloys) corrosion processes in high temperature aqueous systems.

Figure 6.11 shows the electrochemical current noise (proportional to the electrochemical corrosion rate) of nickel in deaerated 0.01 M HCl as a function of pressure at 350 ^{o}C. As illustrated by the figure, the corrosion rate increases with increasing pressure corresponding to the increasing density and dielectric constant of the solvent.

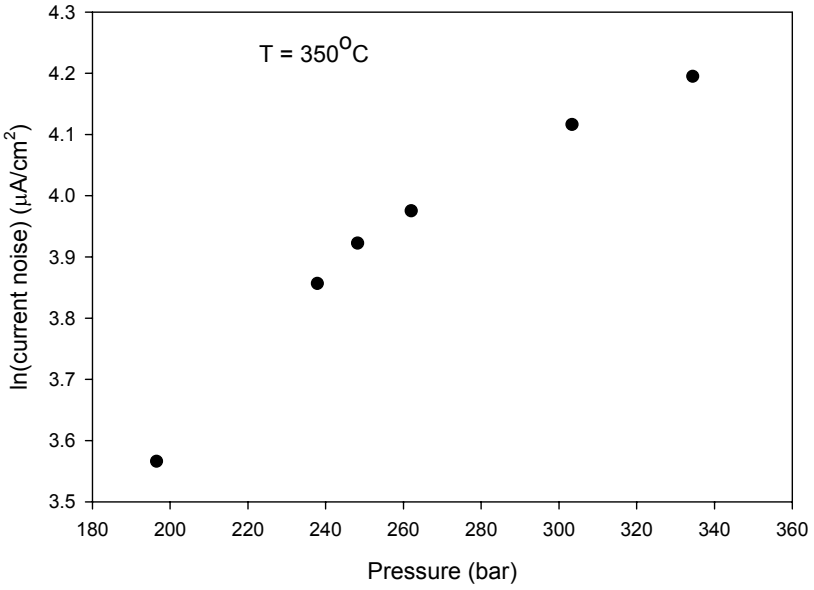

Figure 6.11: Electrochemical corrosion rate (standard deviation of the current noise) of Ni as a function of pressure at 350 ^{o}C in deaerated 0.01 M HCl.

Figure 6.12 displays the volume of activation of corrosion of nickel at 0.01 M HCl as a function of pressure at 350 ^{o}C. Similar as the volume of activation of SS 304 in 0.01 M HCl at 350 ^{o}C as a function of pressure, the magnitude of the volume of activation decreases with increasing pressure due to the pressure effect on the electrostriction of the solvent and on the solvent-solute interactions.

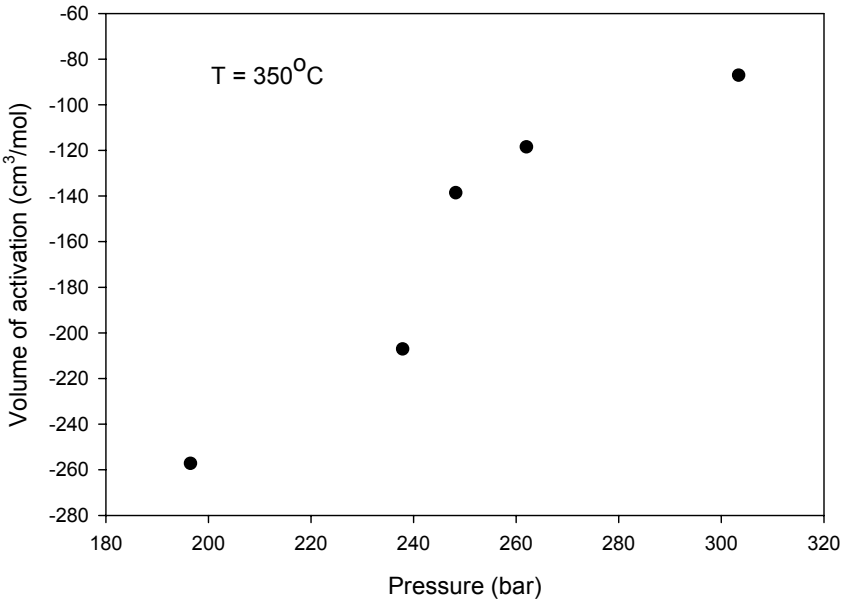

Figure 6.12: Volume of activation of corrosion reactions of Ni in deaerated 0.01 M HCl as a function of pressure at 350 ^{o}C

Figure 6.13 shows the contribution of the activation, system compressibility, and HCl dissociation to the relative corrosion rate of nickel in deaerated 0.01 M HCl at temperature of 350 ^{o}C. As demonstrated by the figure, the contribution from activation term plays a dominant role on the relative corrosion rate, compared with the contributions from the system compressibility and from HCl dissociation in high subcritical temperatures (350 ^{o}C). At the same time, the contribution from the system compressibility is less importance than the contribution from degree of dissociation as the solution is a condensed “liquid” phase and the compressibility of the system is small. The figure also shows that the contribution from the activation term to the relative reaction rate is more important than the contribution from the degree of dissociation at high subcritical temperatures.

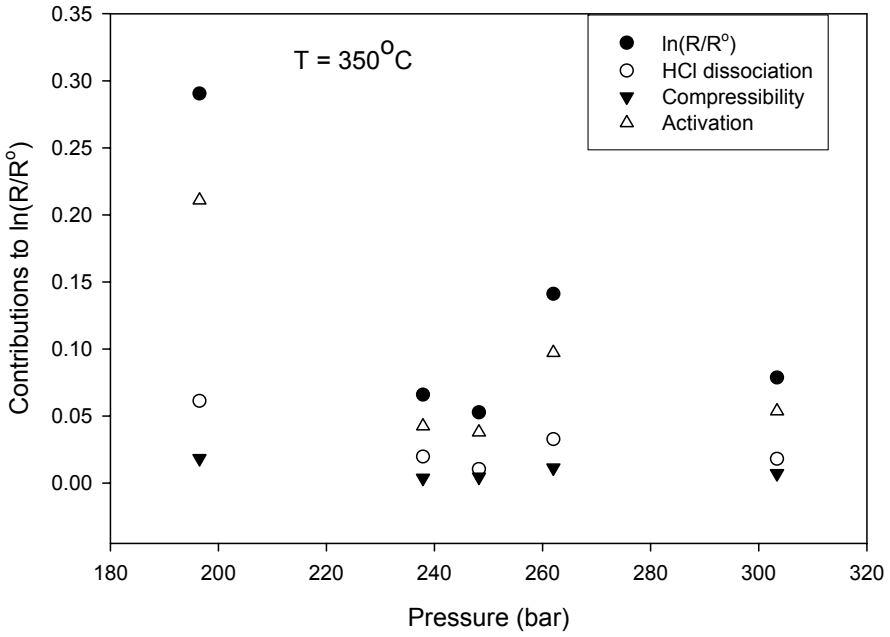

Figure 6.13: Contribution of activation, density, and HCl dissociation to corrosion rate of Ni as a function of pressure at 350 ^{o}C in deaerated 0.01 M HCl

6.6 Summary and Conclusions

A corrosion reaction rate model was applied for studying pressure effect on corrosion of metals in high temperature aqueous systems. The effect of pressure on the corrosion of metals in high temperature aqueous systems is analyzed in this work with emphasis on exploring contributions from the reaction activation process, in terms of the volume change, the system compressibility, degree of dissociation of aggressive species, and changes in the volumetric concentration. This is done by considering the electrochemical corrosion rate of Type 304 SS and Ni in 0.01 M HCl at 350 ^{o}C, 450 ^{o}C, and 500 ^{o}C. The principal findings of this study are as follows:

1. The volume of activation of the electrochemical corrosion of Type 304 SS in high subcritical and supercritical aqueous systems is pressure-dependent with the rate depending upon the effect of pressure on solvent-solute interactions and on the system compressibility.

2. At subcritical temperatures (T < 374.15 ^{o}C), the activation process for the dissolution of Type 304 SS dominates the effect of pressure on the reaction rate, with the effect of pressure on the volumetric concentration of reactants and the dissociation of acids to yield aggressive species (H^{+}) being of relatively lower importance. The volume of activation is found to be negative, reflecting more extensive electrostriction of the solvent in the transition state than in the initial state.

3. At supercritical temperatures (T > 374.15 ^{o}C), the apparent activation volume for the corrosion of Type 304 SS in 0.01 M HCl is also found to be negative, but upon correction for the impact of solvent compressibility on the volumetric concentration of the corrodent and upon the dissociation of HCl, the volume of activation of the activation process is found to be positive. This may reflect the relatively lower importance of electrostriction of the solvent in the reaction process in supercritical aqueous systems.

4. The effect of pressure on the volume of activation of the corrosion of Type 304 SS in 0.01 M HCl at both subcritical and supercritical temperatures can be explained by the decreasing electrostrictive volume loss as the density (pressure) increases.

References

1. L. B. Kriksunov, D. D. Macdonald; “Corrosion in Supercritical Water Oxidation Systems: A Phenomenological Analysis”, *J. Electrochem. Soc***. 142**, 4069 (1995)

2. D.D Macdonald, “Effect of Pressure on the Rate of Corrosion of Metals in High Subcritical and Supercritical Aqueous Systems” *J. Supercritical Fluids*, **30**, 375 (2004)

3. D. D. Macdonald, J. B. Hyne. “The Pressure Dependence of Benzyl Chloride Solvolysis in Aqueous Acetone and Aqueous DimethylSulfoxide”. Can. J. Chem., **48** 2494 (1970)

4. K. P. Johnston, C. Haynes “Extreme solvent effects on reaction rate constants at supercritical fluid conditions” *AIChE Journal*, **33,** 2017 (1987)

5. S. D. Iyer, M. T. Klein, “Effect of pressure on the rate of butyronitrile hydrolysis in high-temperature water” *J. Supercritical Fluids*, **10**, 191 (1997)

6. B. Wu, M. T. Klein, S. I. Sandler, “Solvent effects on reactions in supercritical fluids” *Ind. Eng. Chem. Res*. **30**, 822 (1991)

7. W. P. Iverson, *J. Electrochem. Soc*. **115**, 617 (1968)

8. J. L. Dawson, “Electrochemical Noise Measurement for Corrosion Applications”, p.3-35 ASTM Publication Code Number (PCN) 04-012770-27

9. R. A. Cottis, “Interpretation of Electrochemical Noise Data”, *Corrosion*, **57**, 265 (2001)

10. F. Mansfeld and H. Xiao, “Electrochemical Noise Analysis of Iron Exposed to NaCl Solutions of Different Corrosivity”, *J. Electrochem. Soc*. **140**, 2205 (1993)

11. C. Liu, D. D. Macdonald, E., Medina, J. J. Villa, and J. M. Bueno; “Probing Corrosion Activity in High Subcritical and Supercritical Water Through Electrochemical Noise Analysis”, *Corrosion,* **50**, 687 (1994)

12. X. Y. Zhou, S. N. Lvov, X. J. Wei, L. G. Benning, D. D. Macdonald, “Quantitative Evaluation of General Corrosion of Type 304 Stainless Steel in Subcritical and Supercritical Aqueous Solutions via Electrochemical Noise Analysis”, *Corrosion Science,* **44**, 841 (2002)

13. X. Y. Guan, T. Zhu, D. D. Macdonald, “Application of electrochemical noise analysis in high subcritical and supercritical aqueous systems”, NACE paper No. 06449, (2006)

14. NIST Steam Algorithm, National Institute of Science and Technology, Gaithersburg, MD, 1994

Chapter 7

GENERAL CONCLUSIONS AND FUTURE WORK

Corrosion processes of metals in high subcritical and supercritical aqueous systems have been investigated in this thesis. The major findings of this thesis are summarized as follows:

Two corrosion mechanisms, “chemical oxidation” (CO) and “electrochemical oxidation” (EO), have been proposed to describe the corrosion processes in high temperature aqueous systems, depending upon the density and dielectric constant of the systems. Electrochemical Emission Spectroscopy (EES) method is used to differentiate two corrosion mechanisms by postulating that only the electrochemical mechanism gives rise to spontaneous fluctuations in current and potential. The study shows that the electrochemical mechanism is the dominant corrosion mechanism when the temperatures are below 350 ^{o}C and that it becomes of progressively lower importance as the temperature increases above the critical temperature (T_c = 374.15 ^{o}C) and the test solution changes from the condensed-liquid phase to the “gaseous” phase. Experiments demonstrates that the electrochemical corrosion rate of Type 304 SS increases with increasing temperature before it reaches a maximum value at 350 ^{o}C because the corrosion process is dominated by increasing corrosion activity with increasing temperature. Thereafter, the corrosion rate decreases with increasing temperature, due to the impact of increasing temperature on the concentration of the aggressive species (the volumetric concentration decreases), on the dielectric constant of the solution (decreasing acid, base, and salt ionization), and on the reaction rate (increasing rate constant), with the impact on the concentration and extent of ionization dominating. The maximum in the corrosion rate is found to occur at temperatures between 310 ^{o}C and 360 ^{o}C.

Effect of pressure on corrosion rates of metals in high temperature aqueous systems has been analyzed in this thesis, with emphasis on exploring contributions from activation, the degree of dissociations of aggressive species, and the system isothermal compressibility. The volume of activation of the electrochemical corrosion of Type 304 SS in high subcritical and supercritical aqueous systems is pressure-dependent with the rate depending upon the effect of pressure on solvent-solute interactions and on the system compressibility. Experiments demonstrate that the activation process dominates the effect of pressure on the corrosion reaction rate of Type 304 SS in 0.01 M HCl at subcritical temperatures ($T < 374.15\ ^{o}C$) , with the effect of pressure on the volumetric concentration of reactants and the degree of dissociation of aggressive species being of relatively lower importance. At supercritical temperatures ($T > 374.15\ ^{o}C$), the degree of dissociation of HCl plays more dominant role. The effect of pressure on the volume of activation of the corrosion of Type 304 SS in 0.01 M HCl at both subcritical and supercritical temperatures can be explained by the decreasing electrostrictive volume loss as the density (pressure) increases.

The energy of activation of electrochemical corrosion of Type 304 SS and titanium in 0.01 M HCl has been estimated. Both estimated energy of activation and the polarization study suggested that titanium is more corrosion resistant in high temperature HCl solutions due to the formation of protective passive films on titanium surfaces.

Based on the results obtained, it is essential to continue to explore corrosion mechanisms of metals in high temperature aqueous systems. The theory of Electrochemical Oxidation/Chemical Oxidation corrosion mechanisms should be further verified by various reactor fabrication materials, including Ni based alloys and Ti based alloys, in different supercritical aqueous systems such

as in hydrochloric acid (HCl), nitric acid (HNO_3), phosphoric acid (H_3PO_4), and sodium hydroxide (NaOH). The effect of pressure on corrosion reaction rates of various metals in different high temperature aqueous systems should be further studied, with the emphasis on pressure dependence of volume of activation. The activation energy of corrosion processes of different metals/alloys in high temperature aqueous systems should be estimated to predict the corresponding corrosion resistance of metals/alloys in high temperature working environments.

As a non-perturbative corrosion measuring technique, electrochemical emission spectroscopy (EES) can be used to monitor corrosion rates on site. As proposed in this study, a proportional relationship exists between the electrochemical noise and corrosion rates. Weight method and EES should be applied simultaneous on different metals/alloys in various high temperature working solutions to further test the correlation between the electrochemical noise and corrosion rates. In addition, the relationship between the electrochemical noise resistance and polarization resistance should be studied, with the objective of quantitatively measuring the instantaneous corrosion rates in high temperature aqueous systems.

Metals and alloys in high temperature aqueous systems exhibit different types of corrosion. *In-situ* identification of different types of corrosion in supercritical aqueous systems is a precondition for applying a “correct” method to inhibit corrosion propagation and protect metal reactors in high temperature environments. One promising application of ENA is to identify the type of corrosion occurring in a specific system. The different types of corrosion are characterized by specific corrosion kinetics processes and thus produce specific forms of electrochemical noise. The shape of the electrochemical noise-time record can be used to differentiate between the general and localized corrosion, as distinct transient events can be observed in the latter. Additionally, electrochemical noise spectral analysis can be used to differentiate various

corrosion types because different corrosion processes yield different transient signatures in the frequency domain. For example, periodic signals clearly give rise to a peak in the power spectrum, and that characteristic can be related to crevice or pitting corrosion. Due to the complexities of corrosion processes and uncertainties of electrochemical noise data, it is certainly a very difficult task. However the payoff would be huge, if the corrosion types can be identified on site and it will be a great breakthrough in preventing corrosion propagation.

Appendix A

Program HCl_pH

```
C Program calculates the species concentrations in the HCl-H2O
C sysyem at subcritical and supercritical temperatures
C
C
C       m1 = molal concentration of H+
C       m2 =  "       "      "  Cl-
C       m3 =  "       "      "  OH-
C       m4 =  "       "      "  HCl(0)
C
C
      REAL
T,P,Tk,m0HCl,m1,m2,m3,m4,gam1,gam0,Ac,Bc,ST,STX,kappa,sig,xx1
      REAL ST_new,aw,Kw,K1,De,Vis,kappa0,pH,Den,aion,mu,yy1
      REAL VH2O,xka,zz1,zz2,zz3,Fx,dFx,m1_new
      INTEGER I,J,Ndec0,Ndec1
C Select method of data input
      Write(*,*)'Do you wish to input data from the screen?--If "yes" ty
     <pe "1"'
      READ(*,*)Ndec0
      IF(Ndec0.EQ.1) go to 30
C Input data via the program
      T=400.00
      P=340.00
      Call Props(T,den,vis,de)
      m0HCl=1.e-2
      go to 40
C Input parameters from the screen
   30 Write(*,*)' Temperature in degrees centigrade ='
      Read(*,*)T
      Write(*,*)' Pressure in bars ='
      Read(*,*)P
      Write(*,*)' Density in grams/cubic centimeter ='
      Read(*,*)Den
      Write(*,*)' Stoichiometric concentration of HCL(molal) ='
      Read(*,*)m0HCl
      Write(*,*)' Dielectric constant ='
      Read(*,*)De
      Write(*,*)' Viscosity in poise ='
```

```
      Read(*,*)Vis
   40 Continue
      Tk=T+273.15
C Calculate the dissociation product of water from Marshall & Franck
      Call KwCalc(T,den,Kw)
C Dissociation constant of HCl
c     K1=10.**(-5.405+3874.9/Tk+14.93*log10(den))  ! Marshall & Frantz
      K1=exp(-(12.45-8923.9/Tk-13.93*log(den)))    ! Simonson et al.
C Initiate the calculation
      gam0=1.
      gam1=1.
      aw=1.
      G1=1.
      Gw=1.
      z11=den/(de*Tk)
      kappa0=50.29e8*sqrt(z11)
      Ac=1.8246e6/((de*Tk)**1.5)
      Bc=50.29e8/sqrt(de*Tk)
      aion=4.5e-8
      mu=2.
      VH2O=18.016/den
C Initialize the H+ concentration
      m1=-K1/2.+0.5*sqrt(K1*K1+4.*K1*m0HCl)
      ST=2.*m1
C Begin iteration
      DO 100 I=1,100
        STX=sqrt(ST)
C       Calculate water activity (R & S p.235)
        kappa=kappa0*STX
        xka=kappa*aion
        sig=3.*(1.+xka-(1./(1.+xka))-4.606*log(1.+xka))/(xka**3.)
        xx1=55.51/(55.51+mu*2.*ST)
        yy1=VH2O*kappa*sig/4.5418e25
        aw=xx1*exp(yy1)
C       Calculate single ion activity coefficient (R & S p.229)
        zz1=Ac*sqrt(den*ST)/(1.+Bc*aion*sqrt(den*ST))
        zz2=log(1.+0.018016*mu*2.*ST)
        zz3=-zz1-zz2
        gam1=10.**zz3
C       Calculate activity coefficient of neutral species (R & S p.243)
        gam0=exp(0.018016*9.*2.*ST)
C       Calculate G values from activity coefficients and the activity of
water
        G1=gam1*gam1/gam0
        Gw=gam1*gam1/aw
```

```
C           Solve for species concentrations using Newton-Raphson
            DO 60 J=1,100
            Fx=m1-K1*m0HCL/(K1+m1*G1)-Kw/(Gw*m1)
            dFx=1.+K1*G1*m0HCl/((K1+m1*G1)**2.)+Kw/(Gw*m1*m1)
            m1_new=m1-Fx/dFx
            IF(abs((m1_new-m1)/m1_new).LT.1.e-6) go to 61
            m1=m1_new
   60 Continue
   61 Continue
C        Calculate species concentrations
         m2=K1*m0HCl/(K1+m1*G1)
         m3=Kw/(Gw*m1)
         m4=m1*m0HCl*G1/(K1+m1*G1)
         ST_new=0.5*(m1+m2+m3)
C        Test for convergence on ionic strength
         IF(abs((ST_new-ST)/ST_new).LT.1.e-6) go to 62
         ST=ST_new
  100 Continue
   62 Continue
      m1=m1_new
      ST=ST_new
C Calculate pH, note that pH is defined on the molar scale
      pH=-log10(m1*gam1*den)
C Write out the species concentrations
      Write(*,*)'*****************************************************
     <********** '
      Write(*,*)' '
      Write(*,*)'    COMPOSITION OF THE HCl-H2O SYSTEM '
      Write(*,*)' '
      Write(*,*)'*****************************************************
     <********** '
      Write(*,*)' '
      Write(*,*)' Temperature in degrees centigrade = ',T
      Write(*,*)' Pressure in bars                  = ',P
      Write(*,*)' Density in grams/cm^3             = ',Den
      Write(*,*)' Dielectric constant               = ',De
      Write(*,*)' Viscosity in poise                = ',Vis
      Write(*,*)' Stoich. conc. of HCl(mol/kg)      = ',m0HCl
      Write(*,*)' '
      Write(*,*)' '
      Write(*,*)'        Concentration of H+(mol/kg)    =     ',m1
      Write(*,*)'        Concentration of Cl-(mol/kg)   =     ',m2
      Write(*,*)'        Concentration of OH-(mol/kg)   =     ',m3
      Write(*,*)'        Concentration of HCL0(mol/kg)  =     ',m4
      Write(*,*)' '
```

```
      Write(*,*)' '
      Write(*,*)'                        pH(molar scale)   = ',pH
      Write(*,*)'                    Ionic strength(mol/kg) = ',ST
      Write(*,*)'     Activity coefficient for neutral species = ',gam0
      Write(*,*)'   Activity coefficient for uni-valent species = ',gam1
      Write(*,*)'                        Activity of water = ',aw
      Write(*,*)'              Dissociation constant of water = ',Kw
      Write(*,*)'                Dissociation constant of HCl = ',K1
      Write(*,*)' '
      Write(*,*)' '
      Write(*,*)'*********************************************************
     <***** '
C Ask if results should be printed out
      Write(*,*)' Do you wish to print the results?-- If "yes", type"1"'
      READ(*,*)Ndec1
      IF(Ndec1.NE.1) go to 300
C Print out results on a printer
      OPEN(6,file='HCl_pH.OUT',status='unknown')
      Write(6,500)
      Write(6,501)
      Write(6,502)
      Write(6,501)
      Write(6,500)
      Write(6,501)
      Write(6,501)
      Write(6,503)T
      Write(6,504)P
      Write(6,505)Den
      Write(6,506)De
      Write(6,507)Vis
      Write(6,521)m0HCl
      Write(6,501)
      Write(6,508)m1
      Write(6,509)m2
      Write(6,510)m3
      Write(6,511)m4
      Write(6,501)
      Write(6,514)pH
      Write(6,501)
      Write(6,515)ST
      Write(6,501)
      Write(6,516)gam0
      Write(6,501)
      Write(6,517)gam1
      Write(6,501)
```

```
      Write(6,518)aw
      Write(6,501)
      Write(6,519)Kw
      Write(6,501)
      Write(6,520)K1
      Write(6,501)
      Write(6,501)
      Write(6,500)
C Format statements
 500 Format('************************************************************
   <***** ')
 501 Format(' ')
 502 Format('              COMPOSITION OF THE HCl-H2O SYSTEM ')
 503 Format('    Temperature in degrees centigrade = ',F10.2)
 504 Format('    Pressure in bars                  = ',F10.2)
 505 Format('    Density in grams/cm^3             = ',F10.4)
 506 Format('    Dielectric constant               = ',F10.4)
 507 Format('    Viscosity in poise                = ',F10.5)
 508 Format('          Concentration of H+(mol/kg)       = ',E10.4)
 509 Format('          Concentration of Cl-(mol/kg)      = ',E10.4)
 510 Format('          Concentration of OH-(mol/kg)      = ',E10.4)
 511 Format('          Concentration of HCL0(mol/kg)     = ',E10.4)
 514 Format('                      pH(molar scale)   = ',F10.4)
 515 Format('                   Ionic strength(mol/kg) = ',F10.4)
 516 Format('     Activity coefficient for neutral species = ',F10.4)
 517 Format('   Activity coefficient for uni-valent species = ',F10.4)
 518 Format('   Activity of water                    = ',F10.4)
 519 Format('   Dissociation constant of water           = ',E10.4)
 520 Format('   Dissociation constant of HCl             = ',E10.4)
 521 Format('    Stoich. conc. of HCl(mol/kg)            = ',E10.4)
 300 Continue
     Call EJ_HCl(T,m1,m2,m3,kappa0,B2,den,Kw,Ac,Bc,aion,mu,VH2O)
 600 Continue
     CLOSE(6)
     END
C
C
C
     Subroutine Props(T,den,vis,de)
C Program calculates the density, viscosity, and dielectric constant of
water
C at the saturation pressure
     REAL T,den,vis,de,X,Y,Z
     Tk=T+273.17
     X=0.86893-6.28057e-3*Tk+1.52228e-5*Tk*Tk-1.28688e-8*Tk*Tk*Tk
```

```
      Y=4.11353-3.68247e-2*Tk+6.65911e-5*Tk*Tk-4.22098e-8*Tk*Tk*Tk
      Z=3.95620-1.28236e-2*Tk+2.61694e-5*Tk*Tk-2.07544e-8*Tk*Tk*Tk
      den=10.**X
      vis=10.**Y
      de=10.**Z
      return
      end
C
C
C
      Subroutine KwCalc(T,den,AKw)
C Program calculates the ionic product of water from the equation of
Marshall
C and Franck
      REAL T,Tk,Den,AKw,a,b,c,d,e,f,g
      a=-4.098
      b=-3245.2
      c=2.2362e5
      d=-3.984e7
      e=13.957
      f=-1262.3
      g=8.5641e5
      Tk=T+273.15
      xx=(e+f/Tk+g/(Tk*Tk))*log10(den)
      yy=a+b/Tk+c/(Tk*Tk)+d/(Tk*Tk*Tk)
      zz=xx+yy
      zz1=-zz
      AKw=10.**zz
      return
      end
C
C
C
      Subroutine
EJ_HCl(T,m1,m2,m3,kappa0,B2,den,Kw,Ac,Bc,aion,mu,VH2O)
C Subroutine calculates the liquid junction potential for an EPBRE in
contact
C with a HCl-H2O system
C
C          H+   = Species 1
C          Cl-  = Species 2
C          OH-  = Species 3
C          K+   = Species 4
C
      REAL T,Tk,m1,m2,m3,m0KCl,den,KdKCl,rm1,rm2,rm3,rm4,Kw
```

```
      REAL STX,Ac,Bc,EJ(4),EJunct,c(4,10000),LX0(4),L,R,F,ISX(10000)
      REAL
zz1,zz2,zz3,gamX(10000),ACT(4,10000),LACT(4,10000),x(10000)
      REAL
LX(4,10000),Sum(10000),TR(4,10000),SumTR1,SumTR2,SumTR3,dx
      REAL SUMY(4),dL_dx(4,10000),Y(4,10000),ahat(4),RSTX,mu,kappa
      REAL kappa0
      INTEGER Z(4),J1,J2,J5,J6,K,Nx,NN
C     Input parameters and physical constants
      Tk=T+273.15
      ax=4.5e-8
      Nx=10000
      R=1.98717
      F=23060.9
      KdKCl=10.**(-2.477+951.53/Tk+(9.307-3482.8/Tk)*log10(den)) !
Dissociation constant for KCl
C     KCl concentration and ion activities in the EPBRE
      m0KCl=0.1   ! Stoichiometric KCl concentration in the EPBRE mol/kg
C
      rm2=-KdKCl/2.+0.5*sqrt(KdKCl**2.+4.*KdKCL*m0KCl) ! K+ in the
EPBRE
      rm4=rm2                          ! Cl- in the EPBRE
      rm1=10.**(log10(Kw)/2.)               ! H+ in the EPBRE
      rm3=rm1                          ! OH- in the EPBRE
      RSTX=rm1+rm2+rm3+rm4
c      Calculate water activity (R & S p.235)
      kappa=kappa0*RSTX
      xka=kappa*aion
      sig=3.*(1.+xka-(1./(1.+xka))-4.606*log(1.+xka))/(xka**3.)
      xx1=55.51/(55.51+mu*2.*RSTX)
      yy1=VH2O*kappa*sig/4.5418e25
      aw=xx1*exp(yy1)
C
      L=1.0     ! Thickness of the liquid junction
C*    Calculate species concentrations in mol/liter
      c(1,1)=den*rm1      ! H+ in the EPBRE
      c(1,Nx)=m1*den      ! H+ in the test solution
      c(2,1)=den*rm4      ! Cl- in the EPBRE
      c(2,Nx)=m2*den      ! Cl- in the test solution
      c(3,1)=rm3*den      ! OH- in the EPBRE
      c(3,Nx)=m3*den      ! OH- in the test solution
      c(4,1)=rm2*den      ! K+ in the EPBRE
      c(4,Nx)=1.e-20      ! K+ in the test solution
C*
C*    Begin iteration on distance through the junction assuming a
```

```
C*    linearly graded junction.
C*
C*    Calculate the ionic conductances at infinite dilution as a function
C*    of temperature.
C*
      Z(1)=1
      Z(2)=-1
      Z(3)=-1
      Z(4)=1
C*
      IF(TK.GT.647.0) go to 623
C     Calculate ion conductivities at subcritical temperatures
      LX0(1)=-2759.6378+17.51518*TK-0.02844*TK*TK+1.5698e-
5*TK*TK*TK !H+
      LX0(3)=-929.1116+3.3085*TK+3.7545e-3*TK*TK-7.3268e-
6*TK*TK*TK !OH-
      LX0(4)=76.8362-2.1562*TK+9.5292e-3*TK*TK-7.7938e-6*TK*TK*TK
!K+
      LX0(2)=-150.6670-0.4938*TK+5.5471e-3*TK*TK-4.3962e-
6*TK*TK*TK !Cl-
      go to 624
  623 continue
C*    Calculate ion conductivities at supercritical temperatures
  624 continue
C*
C*
      ISX(1)=0.5*(C(1,1)+C(2,1)+C(3,1)+C(4,1))
      ISX(Nx)=0.5*(C(1,Nx)+C(2,Nx)+C(3,Nx)+C(4,Nx))
C
C       Inner(reference) boundary of the junction
        STX=sqrt(ISX(1))
        zz1=Ac*sqrt(den*ISX(1))/(1.+Bc*aion*sqrt(den*ISX(1)))
        zz2=log(1.+0.018016*mu*2.*ISX(1)/den)
        zz3=-zz1-zz2
        gamX(1)=10.**zz3
C
C       Outer boundary of the junction
C
        STX=sqrt(ISX(Nx))
        zz1=Ac*sqrt(den*ISX(Nx))/(1.+Bc*aion*sqrt(den*ISX(Nx)))
        zz2=log(1.+0.018016*mu*2.*ISX(Nx)/den)
        zz3=-zz1-zz2
        gamX(Nx)=10.**zz3
c
c
```

```
      ACT(1,1)=c(1,1)*GamX(1)
      ACT(2,1)=c(2,1)*GamX(1)
      ACT(3,1)=c(3,1)*GamX(1)
      ACT(4,1)=c(4,1)*GamX(1)
c
      ACT(1,Nx)=c(1,Nx)*GamX(Nx)
      ACT(2,Nx)=c(2,Nx)*GamX(Nx)
      ACT(3,Nx)=c(3,Nx)*GamX(Nx)
      ACT(4,Nx)=c(4,Nx)*GamX(Nx)
c
      LACT(1,1)=log(ACT(1,1))
      LACT(2,1)=log(ACT(2,1))
      LACT(3,1)=log(ACT(3,1))
      LACT(4,1)=log(ACT(4,1))
c
      LACT(1,Nx)=log(ACT(1,Nx))
      LACT(2,Nx)=log(ACT(2,Nx))
      LACT(3,Nx)=log(ACT(3,Nx))
      LACT(4,Nx)=log(ACT(4,Nx))
C
C     Assume a linearly-graded junction
C
      dx=L/(Nx-1)
      DO 130 I=1,Nx-1
      x(I)=(I-1)*dx
C     Begin iteration on each species
      DO 120 K=1,4
      ahat(K)=(c(K,Nx)-c(K,1))/L
      c(K,I)=ahat(K)*x(I)+c(K,1)
  120 CONTINUE
C
C     Calculate the ionic strength at each point in the junction.
C
      ISX(I)=0.5*(c(1,I)+c(2,I)+c(3,I)+c(4,I))  !mol/l
C
C     Calculate activities and transport numbers for species across
C     the junction.
C
        STX=sqrt(ISX(I))
        zz1=Ac*sqrt(ISX(Nx))/(1.+Bc*aion*sqrt(ISX(Nx)))
        zz2=log(1.+0.018016*mu*2.*ISX(Nx)/den)
        zz3=-zz1-zz2
        gamX(I)=10.**zz3
C
      DO 121 J1=1,4
```

```
            ACT(J1,I)=GamX(I)*c(J1,I)                ! Activity of species
        C   Correct conductances for ionic strength
            LX(J1,I)=LX0(J1)-0.5*B2*SQRT(ISX(I))/(1.+ax*kappa0*SQRT(ISX(I)))
!S.cm^2/equiv.
          121 CONTINUE
        C   Calculate total conductivity at each mesh point
            SUM(I)=(LX(1,I)*c(1,I)+LX(2,I)*c(2,I)+LX(3,I)*c(3,I)+LX(4,I)*c(4,I
           <))/1000.   ! S/cm
          130 CONTINUE
        C
            DO 299 J1=1,4
            LX(J1,NX)=LX0(J1)-0.5*B2*SQRT(ISX(NX))/(1.+ax*kappa0*
           <SQRT(ISX(NX))) !S.cm^2/equiv.
          299  continue
            SUM(nx)=(LX(1,nx)*c(1,nx)+LX(2,nx)*c(2,nx)+LX(3,nx)*c(3,nx)+
           <LX(4,nx)*c(4,nx))/1000.   ! S/cm
            DO 149 I=1,Nx
            DO 125 J5=1,4
            TR(J5,I)=LX(J5,I)*c(J5,I)/(1000.*SUM(I))    ! Transport numbers
            LACT(J5,I)=Log(ACT(J5,I))
          125 CONTINUE
          149 CONTINUE
        C
        C   Check that the sums of the transport numbers at the junction
boundaries and
        C   in the middle of the junction are zero
        C
            NN=Nx/2
            SumTR1=0.
            SumTR2=0.
            SumTR3=0.
            DO 148 J6=1,4
            SumTR1=SumTR1+TR(J6,1)
            SumTR2=SumTR2+TR(J6,NN)
            SumTR3=SumTR3+TR(J6,Nx)
          148 CONTINUE
        C
        C   Calculate the differential of ln(activity) of each species with respect to
        C   x at each location across the junction
        C
            DO 140 J2=1,4
            DO 147 I=2,Nx
            DL_DX(J2,I)=(LACT(J2,I)-LACT(J2,I-1))/dx
            Y(J2,I)=TR(J2,I)*DL_DX(J2,I)/Z(J2)
          147 CONTINUE
```

```
            SUMY(J2)=0.
            DO 176 I=1,Nx
            SUMY(J2)=SUMY(J2)+Y(J2,I)*dx
          176 CONTINUE
        C
        C    Calculate the contribution of each species to the liquid
        C    junction potential.
        C
            EJ(J2)=-(R*Tk/F)*SUMY(J2)
          140 CONTINUE
            EJunct=EJ(1)+EJ(2)+EJ(3)+EJ(4)
        C
        C    Print out the results
        C
             WRITE(*,*)
             WRITE(*,*) 'Contribution of H+ to EJ       =',EJ(1),' V'
             WRITE(*,*) 'Contribution of K+  to EJ      =',EJ(4),' V'
             WRITE(*,*) 'Contribution of OH- to EJ      =',EJ(3),' V'
             WRITE(*,*) 'Contribution of Cl- to EJ      =',EJ(2),' V'
             WRITE(*,*)
             WRITE(*,*) '  Isothermal Liquid Junction Potential =',EJunct,' V'
             WRITE(*,*)
             WRITE(*,*)
             WRITE(*,*) '        Sum of transport numbers at x=0   is',SumTR1
             WRITE(*,*) '        Sum of transport numbers at x=L/2 is',SumTR2
             WRITE(*,*) '        Sum of transport numbers at x=L   is',SumTR3
             WRITE(*,*)
             WRITE(*,*)
        c     IF (Ndec.NE.1) go to 850
        C
        C
           19  WRITE(6,595)
          595
FORMAT(5x,'&&&&&&&&&&&&&&&&&&&&&&&&&&&&&&&&&&&&&&&&&&&&&&&&&&&&&&&&
&&&&&&&&&&
            <&&&&&&&&&&')
              WRITE(6,202)
              WRITE(6,596)
          596  FORMAT(15x,'ISOTHERMAL LIQUID JUNCTION POTENTIAL
FOR THE EPBRE')
             WRITE(6,202)
             WRITE(6,597)
          597
FORMAT(5x,'&&&&&&&&&&&&&&&&&&&&&&&&&&&&&&&&&&&&&&&&&&&&&&&&&&&&&&&&
&&&&&&&&&&
```

```
     <&&&&&&&&&&')
       WRITE(6,202)
       WRITE(6,202)
       WRITE(6,505) EJ(1)
       WRITE(6,507) EJ(3)
       WRITE(6,508) EJ(4)
       WRITE(6,509) EJ(2)
       WRITE(6,202)
       WRITE(6,202)
       WRITE(6,510) EJunct
C
  505  FORMAT(15x,'Contribution of H+ to EJ       =',E10.4,' V')
  507  FORMAT(15x,'Contribution of OH- to EJ      =',E10.4,' V')
  508  FORMAT(15x,'Contribution of K+  to EJ      =',E10.4,' V')
  509  FORMAT(15x,'Contribution of Cl- to EJ      =',E10.4,' V')
  510  FORMAT(25x,'Isothermal Liquid Junction Potential =',E10.4,' V')
  202  FORMAT(' ')
       close (6)
  850 CONTINUE
       RETURN
       END

c  Copyright D.D. Macdonald, January 1,1997
```

Appendix B

Program NaOH_pH

```
C Program calculates the species concentrations in the NaOH-H2O
C system at subcritical and supercritical temperatures
C
C
C       m1 = molal concentration of H+
C       m2 =  "       "      "  OH-
C       m3 =  "       "      "  Na+
C       m4 =  "       "      "  NaOH(0)
C
C
      REAL
T,P,Tk,m0NaOH,m1,m2,m3,m4,gam1,gam0,Ac,Bc,ST,STX,kappa,sig
      REAL ST_new,aw,Kw,K1,De,Vis,kappa0,pH,Den,aion,mu,yy1,xx1
      REAL VH2O,xka,zz1,zz2,zz3,Fx,dFx,m1_new,XWW
      INTEGER I,J,Ndec0,Ndec1
C Select method of data input
      Write(*,*)'Do you wish to input data from the screen?--If "yes" ty
     <pe "1"'
      READ(*,*)Ndec0
      IF(Ndec0.EQ.1) go to 30
C Input data via the program
      T=500.00
      P=306.20
      Call Props(T,den,vis,de)
      m0NaOH=.01
      go to 40
C Input parameters from the screen
   30 Write(*,*)' Temperature in degrees centigrade ='
      Read(*,*)T
      Write(*,*)' Pressure in bars ='
      Read(*,*)P
      Write(*,*)' Density in grams/cubic centimeter ='
      Read(*,*)Den
      Write(*,*)' Stoichiometric concentration of NaOH(molal) ='
      Read(*,*)m0NaOH
      Write(*,*)' Dielectric constant ='
      Read(*,*)De
      Write(*,*)' Viscosity in poise ='
```

```
      Read(*,*)Vis
   40 Continue
      Tk=T+273.15
C Calculate the dissociation product of water
      Call KwCalc(T,Den,Kw)
      XWW=-16.4
      Kw=10.**XWW
C Dissociation constant of NaOH
      K1=10.**(-2.477+951.53/Tk+(9.307-3482.8/Tk)*log10(Den))
C Initiate the calculation
      gam0=1.
      gam1=1.
      aw=1.
      G1=1.
      Gw=1.
      z11=den/(de*Tk)
      write(*,*)'line 55'
      kappa0=50.29e8*sqrt(z11)
      Ac=1.8246e6/((de*Tk)**1.5)
      Bc=50.29e8/sqrt(de*Tk)
      B2=82.5/(vis*sqrt(de*Tk))
      aion=4.5e-8
      mu=2.
      VH2O=18.016/den
C Initialize the H+ concentration
c      write(*,*)'line 64'
      m2=-K1/2.+0.5*sqrt(K1*K1+4.*K1*m0NaOH)
      m1=Kw/m2
      ST=2.*m2+0.01*m0NaOH
C Begin iteration
      DO 100 I=1,100
        STX=sqrt(ST)
c        write(*,*)'line 71'
C        Calculate water activity (R & S p.235)
        kappa=kappa0*STX
        xka=kappa*aion
        sig=3.*(1.+xka-(1./(1.+xka))-4.606*log(1.+xka))/(xka**3.)
        xx1=55.51/(55.51+mu*2.*ST)
        yy1=VH2O*kappa*sig/4.5418e25
        aw=xx1*exp(yy1)
C        Calculate single ion activity coefficient (R & S p.229)
        zz1=Ac*sqrt(den*ST)/(1.+Bc*aion*sqrt(den*ST))
        write(*,*)'line 81'
        zz2=log(1.+0.018016*mu*2.*ST)
        zz3=-zz1-zz2
```

```
            gam1=10.**zz3
      C      Calculate activity coefficient of neutral species (R & S p.243)
            gam0=exp(0.018016*9.*2.*ST)
      C      Calculate G values from activity coefficients and the activity of
water
            G1=gam1*gam1/gam0
            Gw=gam1*gam1/aw
      C           Solve for species concentrations using Newton-Raphson
                  DO 60 J=1,100
                  Fx=m1+m1*m0NaOH/(m1+(Kw*G1/K1*Gw))-Kw/(Gw*m1)

dFx=1.+(Kw*G1/(Gw*K1))*m0NaOH/((m1+(Kw*G1/(K1*Gw)))**2.)+
           <       Kw/(Gw*m1*m1)
                  m1_new=m1-Fx/dFx
                  IF(abs((m1_new-m1)/m1_new).LT.1.e-6) go to 61
                  m1=m1_new
          60 Continue
          61 Continue
            write(*,*)'line 100  j=',j
      C       Calculate species concentrations
            m2=Kw/(Gw*m1)
            m3=m1*m0NaOH/(m1+Kw*G1/(Gw*K1))
            m4=m0NaOH*Kw*G1/(Gw*K1)/(m1+Kw*G1/(Gw*K1))
            ST_new=0.5*(m1+m2+m3)
      C       Test for convergence on ionic strength
            IF(abs((ST_new-ST)/ST_new).LT.1.e-6) go to 62
            ST=ST_new
         100 Continue
          62 Continue
            m1=m1_new
            ST=ST_new

      C Calculate pH, note that pH is defined on the molar scale
            pH=-log10(m1*gam1*den)
      C Write out the species concentrations
            Write(*,*)'*****************************************************
           <********** '
            Write(*,*)' '
            Write(*,*)'    COMPOSITION OF THE NaOH-H2O SYSTEM '
            Write(*,*)' '
            Write(*,*)'*****************************************************
           <********** '
            Write(*,*)' '
            Write(*,*)' Temperature in degrees centigrade = ',T
            Write(*,*)' Pressure in bars                  = ',P
```

```
      Write(*,*)' Density in grams/cm^3            = ',Den
      Write(*,*)' Dielectric constant              = ',De
      Write(*,*)' Viscosity in poise               = ',Vis
      Write(*,*)' Stoich. conc. of NaOH(mol/kg)    = ',m0NaOH
      Write(*,*)' '
      Write(*,*)' '
      Write(*,*)'        Concentration of H+(mol/kg)    =    ',m1
      Write(*,*)'        Concentration of OH-(mol/kg)   =    ',m2
      Write(*,*)'        Concentration of Na+(mol/kg)   =    ',m3
      Write(*,*)'        Concentration of NaOH(mol/kg)  =    ',m4
      Write(*,*)' '
      Write(*,*)' '
      Write(*,*)'                          pH(molar scale)   = ',pH
      Write(*,*)'                       Ionic strength(mol/kg) = ',ST
      Write(*,*)'     Activity coefficient for neutral species = ',gam0
      Write(*,*)'   Activity coefficient for uni-valent species = ',gam1
      Write(*,*)'                          Activity of water = ',aw
      Write(*,*)'               Dissociation constant of water = ',Kw
      Write(*,*)'               Dissociation constant of NaOH  = ',K1
      Write(*,*)' '
      Write(*,*)' '
      Write(*,*)'*************************************************
     <********** '
C Ask if results should be printed out
      Write(*,*)' Do you wish to print the results?-- If "yes", type"1"'
      READ(*,*)Ndec1
      IF(Ndec1.NE.1) go to 300
C Print out results on a printer
      OPEN(6,file='NaOH_pH.OUT',status='unknown')
      Write(6,500)
      Write(6,501)
      Write(6,502)
      Write(6,501)
      Write(6,500)
      Write(6,501)
      Write(6,501)
      Write(6,503)T
      Write(6,504)P
      Write(6,505)Den
      Write(6,506)De
      Write(6,507)Vis
      Write(6,521)m0NaOH
      Write(6,501)
      Write(6,508)m1
      Write(6,509)m2
```

```
      Write(6,510)m3
      Write(6,511)m4
      Write(6,501)
      Write(6,514)pH
      Write(6,501)
      Write(6,515)ST
      Write(6,501)
      Write(6,516)gam0
      Write(6,501)
      Write(6,517)gam1
      Write(6,501)
      Write(6,518)aw
      Write(6,501)
      Write(6,519)Kw
      Write(6,501)
      Write(6,520)K1
      Write(6,501)
      Write(6,501)
      Write(6,500)
C Format statements
  500 Format('************************************************************
     <***** ')
  501 Format(' ')
  502 Format('              COMPOSITION OF THE NaOH-H2O SYSTEM ')
  503 Format('    Temperature in degrees centigrade = ',F10.2)
  504 Format('    Pressure in bars                  = ',F10.2)
  505 Format('    Density in grams/cm^3             = ',F10.4)
  506 Format('    Dielectric constant               = ',F10.4)
  507 Format('    Viscosity in poise                = ',F10.5)
  521 Format('    Stoich. conc. of NaOH(mol/kg)     = ',E10.4)
  508 Format('          Concentration of H+(mol/kg)    =     ',E10.4)
  509 Format('          Concentration of OH-(mol/kg)   =     ',E10.4)
  510 Format('          Concentration of Na+(mol/kg)   =     ',E10.4)
  511 Format('          Concentration of NaOH(mol/kg)  =     ',E10.4)
  514 Format('                   pH(molar scale)       = ',F10.4)
  515 Format('                   Ionic strength(mol/kg) = ',F10.4)
  516 Format('    Activity coefficient for neutral species =    ',F10.4)
  517 Format('    Activity coefficient for uni-valent species = ',F10.4)
  518 Format('    Activity of water                       = ',F10.4)
  519 Format('    Dissociation product of water           = ',E10.4)
  520 Format('    Dissociation product of NaOH            = ',E10.4)
c     Write(*,*)'Do you wish to calculate the isothermal liquid junction
c     < potential?--If "yes" type "1"'
c     READ(*,*)Ndec2
c     IF(Ndec2.NE.1) go to 600
```

```
            Call EJ_NaOH(T,m1,m2,m3,kappa0,B2,den,Kw,Ac,Bc,aion,mu,VH2O)
          600 Continue
            CLOSE(6)
          300 Continue
            END
        C
        C
        C
            Subroutine Props(T,den,vis,de)
        C Program calculates the density, viscosity, and dielectric constant of
water
        C at the saturation pressure
            REAL T,den,vis,de,X,Y,Z
            Tk=T+273.17
            X=0.86893-6.28057e-3*Tk+1.52228e-5*Tk*Tk-1.28688e-8*Tk*Tk*Tk
            Y=4.11353-3.68247e-2*Tk+6.65911e-5*Tk*Tk-4.22098e-8*Tk*Tk*Tk
            Z=3.95620-1.28236e-2*Tk+2.61694e-5*Tk*Tk-2.07544e-8*Tk*Tk*Tk
            den=10.**X
            vis=10.**Y
            de=10.**Z
            return
            end
        C
        C
        C
            Subroutine KwCalc(T,Den,AKw)
        C Program calculates the ionic product of water from the equation of
Marshall
        C and Franck
            REAL T,Tk,Den,AKw,a,b,c,d,e,f,g
            a=-4.098
            b=-3245.2
            c=2.2362e5
            d=-3.984e7
            e=13.957
            f=-1262.3
            g=8.5641e5
            Tk=T+273.15
            xx=(e+f/Tk+g/(Tk*Tk))*log10(Den)
            yy=a+b/Tk+c/(Tk*Tk)+d/(Tk*Tk*Tk)
            zz=xx+yy
            zz1=-zz
            AKw=10.**zz
            return
            end
```

```
      C
      C
      C
            Subroutine
EJ_NaOH(T,m1,m3,m2,kappa0,B2,den,Kw,Ac,Bc,aion,mu,VH2O)
      C Subroutine calculates the liquid junction potential for an EPBRE in
contact
      C with a NaOH-H2O system
      C
      C           H+   = Species 1
      C           Na+  = Species 2
      C           OH-  = Species 3
      C           K+   = Species 4
      C           Cl-  = Species 5
      C
            REAL T,Tk,m1,m2,m3,m0KCl,den,KdKCl,rm1,rm2,rm3,rm4,Kw
            REAL STX,Ac,Bc,EJ(5),EJunct,c(5,10000),LX0(5),L,R,F,ISX(10000)
            REAL
zz1,zz2,zz3,gamX(10000),ACT(5,10000),LACT(5,10000),x(10000)
            REAL
LX(5,10000),Sum(10000),TR(5,10000),SumTR1,SumTR2,SumTR3,dx
            REAL SUMY(5),dL_dx(5,10000),Y(5,10000),ahat(5),RSTX,mu,kappa
            REAL kappa0
            INTEGER Z(5),J1,J2,J5,J6,K,Nx,NN
      C     Input parameters and physical constants
            Tk=T+273.15
            ax=4.5e-8
            Nx=10000
            R=1.98717
            F=23060.9
            KdKCl=10.**(-2.477+951.53/Tk+(9.307-3482.8/Tk)*log10(den)) !
Dissociation constant for KCl
      C     KCl concentration and ion activities in the EPBRE
            m0KCl=0.1   ! Stoichiometric KCl concentration in the EPBRE mol/kg
            write(*,*)'m0KCL=',m0KCl,'  KdKCl=',KdKCl
      C
            rm2=-KdKCl/2.+0.5*sqrt(KdKCl**2.+4.*KdKCL*m0KCl) ! K+ in the
EPBRE
            write(*,*)'line 289'
            rm4=rm2                              ! Cl- in the EPBRE
            rm1=10.**(log10(Kw)/2.)                    ! H+ in the EPBRE
            rm3=rm1                              ! OH- in the EPBRE
            RSTX=rm1+rm2+rm3+rm4
      c       Calculate water activity (R & S p.235)
              kappa=kappa0*RSTX
```

```
            xka=kappa*aion
            sig=3.*(1.+xka-(1./(1.+xka))-4.606*log(1.+xka))/(xka**3.)
            xx1=55.51/(55.51+mu*2.*RSTX)
            yy1=VH2O*kappa*sig/4.5418e25
            aw=xx1*exp(yy1)
      C
           L=1.0     ! Thickness of the liquid junction
      C*    Calculate species concentrations in mol/liter
           c(1,1)=den*rm1      ! H+ in the EPBRE
           c(1,Nx)=m1*den      ! H+ in the test solution
           c(2,1)=1.e-8        ! Na+ in the EPBRE
           c(2,Nx)=m3*den      ! Na+ in the test solution
           c(3,1)=rm3*den      ! OH- in the EPBRE
           c(3,Nx)=m2*den      ! OH- in the test solution
           c(4,1)=rm2*den      ! K+ in the EPBRE
           c(4,Nx)=1.e-8       ! K+ in the test solution
           c(5,1)=rm4*den      ! Cl- in the EPBRE
           c(5,Nx)=1.e-8       ! Cl- in the test solution
      C*
      C*    Begin iteration on distance through the junction assuming a
      C*    linearly graded junction.
      C*
      C*    Calculate the ionic conductances at infinite dilution as a function
      C*    of temperature.
      C*
           Z(1)=1
           Z(2)=1
           Z(3)=-1
           Z(4)=1
           Z(5)=-1
      C*
           IF(TK.GT.647.0) go to 623
      C     Calculate ion conductivities at subcritical temperatures
           LX0(1)=-2759.6378+17.51518*TK-0.02844*TK*TK+1.5698e-
5*TK*TK*TK !H+
           LX0(2)=98.2830-1.9122*TK+7.4673e-3*TK*TK-5.2925e-6*TK*TK*TK
!Na+
           LX0(3)=-929.1116+3.3085*TK+3.7545e-3*TK*TK-7.3268e-
6*TK*TK*TK !OH-
           LX0(4)=76.8362-2.1562*TK+9.5292e-3*TK*TK-7.7938e-6*TK*TK*TK
!K+
           LX0(5)=-150.6670-0.4938*TK+5.5471e-3*TK*TK-4.3962e-
6*TK*TK*TK !Cl-
           go to 624
         623 continue
```

```
C*    Calculate ion conductivities at supercritical temperatures
  624 continue
C*
C*
      ISX(1)=0.5*(C(1,1)+C(2,1)+C(3,1)+C(4,1)+C(5,1))
      ISX(Nx)=0.5*(C(1,Nx)+C(2,Nx)+C(3,Nx)+C(4,Nx)+C(5,Nx))
C
C       Inner(reference) boundary of the junction
        STX=sqrt(ISX(1))
        write(*,*)'line 345'
        zz1=Ac*sqrt(den*ISX(1))/(1.+Bc*aion*sqrt(den*ISX(1)))
        write(*,*)'line 347'
        zz2=log(1.+0.018016*mu*2.*ISX(1)/den)
        zz3=-zz1-zz2
        gamX(1)=10.**zz3
C
C       Outer boundary of the junction
C
        STX=sqrt(ISX(Nx))
        zz1=Ac*sqrt(den*ISX(Nx))/(1.+Bc*aion*sqrt(den*ISX(Nx)))
        write(*,*)'line 356'
        zz2=log(1.+0.018016*mu*2.*ISX(Nx)/den)
        zz3=-zz1-zz2
        gamX(Nx)=10.**zz3
c
c
      ACT(1,1)=c(1,1)*GamX(1)
      ACT(2,1)=c(2,1)*GamX(1)
      ACT(3,1)=c(3,1)*GamX(1)
      ACT(4,1)=c(4,1)*GamX(1)
      ACT(5,1)=c(5,1)*GamX(1)
c
      ACT(1,Nx)=c(1,Nx)*GamX(Nx)
      ACT(2,Nx)=c(2,Nx)*GamX(Nx)
      ACT(3,Nx)=c(3,Nx)*GamX(Nx)
      ACT(4,Nx)=c(4,Nx)*GamX(Nx)
      ACT(5,Nx)=c(5,Nx)*GamX(Nx)
c
      LACT(1,1)=log(ACT(1,1))
      LACT(2,1)=log(ACT(2,1))
      LACT(3,1)=log(ACT(3,1))
      LACT(4,1)=log(ACT(4,1))
      LACT(5,1)=log(ACT(5,1))
c
      LACT(1,Nx)=log(ACT(1,Nx))
```

```
      LACT(2,Nx)=log(ACT(2,Nx))
      LACT(3,Nx)=log(ACT(3,Nx))
      LACT(4,Nx)=log(ACT(4,Nx))
      LACT(5,Nx)=log(ACT(5,Nx))
C
C     Assume a linearly-graded junction
C
      dx=L/(Nx-1)
      DO 130 I=1,Nx-1
      x(I)=(I-1)*dx
C     Begin iteration on each species
      DO 120 K=1,5
      ahat(K)=(c(K,Nx)-c(K,1))/L
      c(K,I)=ahat(K)*x(I)+c(K,1)
  120 CONTINUE
C
C     Calculate the ionic strength at each point in the junction.
C
      ISX(I)=0.5*(c(1,I)+c(2,I)+c(3,I)+c(4,I)+c(5,I))  !mol/l
C
C     Calculate activities and transport numbers for species across
C     the junction.
C
        STX=sqrt(ISX(I))
        zz1=Ac*sqrt(ISX(Nx))/(1.+Bc*aion*sqrt(ISX(Nx)))
        write(*,*)'line 406'
        zz2=log(1.+0.018016*mu*2.*ISX(Nx)/den)
        zz3=-zz1-zz2
        gamX(I)=10.**zz3
C
      DO 121 J1=1,5
      ACT(J1,I)=GamX(I)*c(J1,I)                ! Activity of species
C     Correct conductances for ionic strength
      LX(J1,I)=LX0(J1)-0.5*B2*SQRT(ISX(I))/(1.+ax*kappa0*SQRT(ISX(I)))
!S.cm^2/equiv.
      write(*,*)'line 415'
  121 CONTINUE
C     Calculate total conductivity at each mesh point
c      write(*,*)'LX0 LX(1,I)  c(1,I) ',LX0(1),LX(1,I),c(1,I)
      SUM(I)=(LX(1,I)*c(1,I)+LX(2,I)*c(2,I)+LX(3,I)*c(3,I)+LX(4,I)*c(4,I
     <)+LX(5,I)*c(5,I))/1000.   ! S/cm
  130 CONTINUE
C
      DO 299 J1=1,5
      LX(J1,NX)=LX0(J1)-0.5*B2*SQRT(ISX(NX))/(1.+ax*kappa0*
```

```
     <SQRT(ISX(NX))) !S.cm^2/equiv.
      write(*,*)'line 426'
  299  continue
      SUM(nx)=(LX(1,nx)*c(1,nx)+LX(2,nx)*c(2,nx)+LX(3,nx)*c(3,nx)+
     <LX(4,nx)*c(4,nx)+LX(5,nx)*c(5,nx))/1000.   ! S/cm
      DO 149 I=1,Nx
      DO 125 J5=1,5
      TR(J5,I)=LX(J5,I)*c(J5,I)/(1000.*SUM(I))    ! Transport numbers
      LACT(J5,I)=Log(ACT(J5,I))
  125 CONTINUE
  149 CONTINUE
C
C    Check that the sums of the transport numbers at the junction
boundaries and
C    in the middle of the junction are zero
C
      NN=Nx/2
      SumTR1=0.
      SumTR2=0.
      SumTR3=0.
      DO 148 J6=1,5
      SumTR1=SumTR1+TR(J6,1)
      SumTR2=SumTR2+TR(J6,NN)
      SumTR3=SumTR3+TR(J6,Nx)
  148 CONTINUE
C
C    Calculate the differential of ln(activity) of each species with respect to
C    x at each location across the junction
C
      DO 140 J2=1,5
      DO 147 I=2,Nx
      DL_DX(J2,I)=(LACT(J2,I)-LACT(J2,I-1))/dx
      Y(J2,I)=TR(J2,I)*DL_DX(J2,I)/Z(J2)
  147 CONTINUE
      SUMY(J2)=0.
      DO 176 I=1,Nx
      SUMY(J2)=SUMY(J2)+Y(J2,I)*dx
  176 CONTINUE
C
C    Calculate the contribution of each species to the liquid
C    junction potential.
C
      EJ(J2)=-(R*Tk/F)*SUMY(J2)
  140 CONTINUE
      EJunct=EJ(1)+EJ(2)+EJ(3)+EJ(4)+EJ(5)
```

```
C
C   Print out the results
C
      WRITE(*,*)
      WRITE(*,*) 'Contribution of H+ to EJ       =',EJ(1),' V'
      WRITE(*,*) 'Contribution of Na+ to EJ      =',EJ(2),' V'
      WRITE(*,*) 'Contribution of K+  to EJ      =',EJ(4),' V'
      WRITE(*,*) 'Contribution of OH- to EJ      =',EJ(3),' V'
      WRITE(*,*) 'Contribution of Cl- to EJ      =',EJ(5),' V'
      WRITE(*,*)
      WRITE(*,*) '  Isothermal Liquid Junction Potential =',EJunct,' V'
      WRITE(*,*)
      WRITE(*,*)
      WRITE(*,*) '        Sum of transport numbers at x=0   is',SumTR1
      WRITE(*,*) '        Sum of transport numbers at x=L/2 is',SumTR2
      WRITE(*,*) '        Sum of transport numbers at x=L   is',SumTR3
      WRITE(*,*)
      WRITE(*,*)
c     IF (Ndec.NE.1) go to 850
C
C
  19  WRITE(6,595)
 595
FORMAT(5x,'&&&&&&&&&&&&&&&&&&&&&&&&&&&&&&&&&&&&&&&&&&&&&&&&&&&&&&&&
&&&&&&&&&&
     <&&&&&&&&&&')
      WRITE(6,202)
      WRITE(6,596)
 596  FORMAT(15x,'ISOTHERMAL LIQUID JUNCTION POTENTIAL
FOR THE EPBRE')
      WRITE(6,202)
      WRITE(6,597)
 597
FORMAT(5x,'&&&&&&&&&&&&&&&&&&&&&&&&&&&&&&&&&&&&&&&&&&&&&&&&&&&&&&&&
&&&&&&&&&&
     <&&&&&&&&&&')
      WRITE(6,202)
      WRITE(6,202)
      WRITE(6,505) EJ(1)
      WRITE(6,506) EJ(2)
      WRITE(6,507) EJ(3)
      WRITE(6,508) EJ(4)
      WRITE(6,509) EJ(5)
      WRITE(6,202)
      WRITE(6,202)
```

```
      WRITE(6,510) EJunct
C
  505  FORMAT(15x,'Contribution of H+ to EJ       =',E10.4,' V')
  506  FORMAT(15x,'Contribution of Na+ to EJ      =',E10.4,' V')
  507  FORMAT(15x,'Contribution of OH- to EJ      =',E10.4,' V')
  508  FORMAT(15x,'Contribution of K+  to EJ      =',E10.4,' V')
  509  FORMAT(15x,'Contribution of Cl- to EJ      =',E10.4,' V')
  510  FORMAT(25x,'Isothermal Liquid Junction Potential =',E10.4,' V')
  202  FORMAT(' ')
     close (6)
  850 CONTINUE
     RETURN
     END

c  Copyright D.D. Macdonald, January 1,1997
```

VITA

Xueyong Guan

Xueyong Guan was born in Urumqi city, China. Xueyong received his bachelor's degree in mechanical engineering from University of Petroleum, China in June 1998.

Xueyong joined the Department of Mechanical and Nuclear Engineering at the Pennsylvania State University as a graduate assistant in the fall of 2001. He received his master's degree in mechanical engineering in the fall of 2003. Dr. Fan-Bill Cheung, professor of Mechanical and Nuclear Engineering, was his advisor of the master's thesis work. The topic of his master's thesis is "A One-Dimensional Lagrangian/Eulerian Two-Phase Nucleating Flow Model".

Xueyong joined the Department of Materials Science and Engineering at the Pennsylvania State University in the fall of 2003. Since then, he has been working on the project of "Novel Corrosion Monitoring and Control Technologies for Super Critical Aqueous Systems". Dr. Digby Dr. Macdonald, distinguished professor in Materials Science and Engineering, is his Ph.D thesis advisor.